Capillary Effects of Nanoporous Networks on Aerospace Autoclave-grade Prepreg Composites Enabling Vacuum-bag-only Manufacturing

by

Travis J. Hank

Submitted to the Department Aeronautics and Astronautics
in partial fulfillment of the requirements for the degree of

Master of Science in Aeronautics and Astronautics

at the

MASSACHUSETTS INSTITUTE OF TECHNOLOGY

June 2021

Author .....
Department Aeronautics and Astronautics
May 24, 2021

Certified by .....
Brian L. Wardle
Professor of Aeronautics and Astronautics, and Mechanical Engineering
Thesis Supervisor

Accepted by .....
Zoltan Spakovszky
Chairman, Department Graduate Committee

Capillary Effects of Nanoporous Networks on Aerospace Autoclave-grade Prepreg Composites Enabling Vacuum-bag-only Manufacturing

by

Travis J. Hank

Submitted to the Department Aeronautics and Astronautics
on May 24, 2021, in partial fulfillment of the
requirements for the degree of
Master of Science in Aeronautics and Astronautics

Abstract

The use of carbon fiber reinforced polymer (CFRP) composite systems has grown in the aerospace industry due to their high mass-specific stiffness and strength and other properties. Yet, many advanced aerospace-grade CFRPs require autoclave pressure vessels to thermally process composites, which has numerous drawbacks such as high capital costs, hours-long heating and cooling cycles, high energy use, and bottlenecks due to fixed size. This work investigates various nanomaterial systems with nanoscale porosity, termed nanoporous network (NPN) materials, which are applied to each ply-ply interface in the composite prepreg laminates to remove voids by encouraging resin infusion through capillary effects. This removes the need for applied autoclave pressure and enables vacuum-bag-only (VBO) curing of autoclave-grade composites using either conductive or convective heating under vacuum. Aligned carbon nanotubes (A-CNTs) have been successfully utilized as textured NPNs with aligned capillaries, but alternative, particularly scaled and lower-cost, NPN materials are of interest. Commercially-available electrospun polymer nanofiber (EPN) films with different fiber diameters, film thickness, and polymer material are investigated extensively and a bespoke-commercial polyimide (PI) aerogel is preliminarily investigated. EPN NPN interlayers are able to create void-free laminates as revealed by micro-computed tomography (μCT) on flat aerospace-grade CFRP laminates using unidirectional epoxy-based prepreg plies. The VBO cured EPN NPN laminates are also found to have the same interlaminer shear strength as the autoclave-cured baseline laminates. It is found that polymer (polyimide) aerogels with a given porosity of 96 vol% are also a viable NPN. L-shape geometries with autoclave-grade laminates are preliminary examined with the investigation revealing void elimination, including in the problematic curved section using EPN NPN interlayers when cured under VBO conditions. Investigations using interlaminar NPNs to reduce voids in laminates that contain woven-woven and unidirectional-woven prepreg interfaces reveal significant void reductions, but not elimination, utilizing various NPNs, such that continuing

challenges exist for full void elimination. Future work includes parametric studies of various NPN materials to further increase the breadth of NPNs available as well as quantifying the precise capillary pressures needed in different prepreg systems to eliminate interlaminar voids.

Thesis Supervisor: Brian L. Wardle
Title: Professor of Aeronautics and Astronautics, and Mechanical Engineering

Acknowledgments

I could not have completed these six years, first and foremost, without the grace and power of God. He has been my rock and foundation, and I would like to thank all those who have helped me become spiritually strong. Over my past six years, I have made many good friends, colleagues, and peers. Everyone from the Maseeh dining cooking staff to my current academic advisor have aided my growth as a person and always challenged me to be my best. Whether on the baseball field or in the lab, there have always been people who took a risk and gave me a chance to show what I had to offer. I have tried to fill every minute with 60 seconds worth of distance run. Some highlights include winning the NEWMAC conference my Sr. year and pitching in the NCAA tournament, building a tin-can radar, a lasercom system, a model STOL aircraft, helping develop a lunar tower prototype, participating in the MIT Gordon Engineering Leadership Program, pulling all nighters studying with friends, and Friday night COVID get togethers. Thank you to my parents, John and Caryn Hank, as well as my sister Carling S. for always encouraging me. For this particular work, it could not have been done without Prof. Brian Wardle who accepted me into necstlab but also worked with me on revisions to this document, as well as Jeonyoon Lee who has mentored me since I was an undergraduate student. I am greatly appreciative of them both as well as all my labmates, teammates, and fellow friends. I will cherish all the adventures undertaken, laughter had, learnings received, and encouragements given. Thank you all who have made this experience so special.

Contents

List of Figures **9**

List of Tables **19**

List of Abbreviations **20**

1 Introduction **23**

1.1 Motivation 26

1.2 Thesis Outline 28

2 Background **29**

2.1 Autoclave and Alternative Curing Methods 29

2.2 Voids in Composites 36

2.3 Void Removal Utilizing Aligned Carbon Nanotubes (A-CNTs) as a Nanoporous Network (NPN) 39

2.4 Electrospun Polymer Nanofiber (EPN) Films 40

2.5 Polymer Aerogel Material 42

2.6 L-shape Composites 43

3 Objectives and General Approach **47**

3.1 Objectives 47

3.2 General Approach 48

4 Vacuum-bag-only (VBO) Composite Manufacturing of Unidirectional Autoclave-grade Prepreg Using Capillary Effects of Nanoporous Networks (NPNs) **51**

4.1 Background . . . 52
4.2 Materials and Methods . . . 55
4.2.1 General Composite Manufacturing Process . . . 55
4.2.2 Polymer Nanofiber Diameter Analysis . . . 59
4.2.3 µCT Imaging and Void Analysis . . . 59
4.2.4 Short Beam Shear (SBS) Testing . . . 61
4.3 Electrospun Polymer Nanofiber (EPN) NPN Films for VBO Curing . 64
4.4 Polyimide Aerogel NPN Films for VBO Curing . . . 70
4.5 Capillary Wetting from NPN Materials . . . 75
4.6 NPN Interlayers Acting as Porous Void Evacuation Channels . . . 78
4.7 Conclusions . . . 78

5 Preliminary Investigations into Integrating NPNs in Geometrically Complex L-shaped Composites and Woven Fiber Prepeg to Enable VBO Curing of Autoclave-grade Prepreg 81

5.1 Materials and Methods . . . 82
5.1.1 L-shape Layup . . . 82
5.1.2 Aligned and Patterned CNT Synthesis and Transfer . . . 84
5.1.3 Extended Cure Cycle . . . 88
5.2 NPN Integration into Geometric Complex L-shaped Composites for Vacuum-bag-only Curing of Autoclave-grade Prepreg . . . 91
5.3 Preliminary Investigations into Autoclave-grade Woven Prepreg with NPN Interlaminar Integration for VBO Curing . . . 97
5.3.1 NPN Integration at Unidirectional-Woven Ply Interfaces . . . 100
5.3.2 NPN Integration at Woven-Woven Ply Interfaces . . . 106
5.4 Conclusions . . . 110

6 Conclusions and Recommendations 113

6.1 Summary of Thesis Contributions . . . 115
6.2 Future Work . . . 117

Bibliography **119**

List of Figures

1-1 Growth of carbon fiber composites in aerospace applications as percent of aircraft mass vs. time. The more recent adoption curve of carbon nanotubes is perceived [1]. 24

1-2 Diagram of a unidirectional carbon fiber reinforced polymer ply consisting of fiber and matrix material. 24

1-3 Ashby charts plotting material strength and stiffness (Young's modulus) vs density. The design guidelines are used for minimum mass design with the (upper left quadrant being advantaged) [2]. 25

1-4 Schematic of a carbon microfiber reinforced plastics composite laminate consisting of stacked plies to form a laminate. Here, the two plies are unidirectional or a 90°orientation on a 90°orientation. The plies are then stacked. The interlaminar voids in the laminate in white can be observed in the interface between the two plies. 27

2-1 Example of an autoclave. Side view of an Econoclave® 12×40. The diameter is 12 feet (3.66 m) and it has a length of 40 feet (12.19 m) [13]. 30

2-2 Comparison of autoclave and out-of-autoclave, sometimes called oven or vacuum-bag-only (VBO) curing [8]. 31

2-3 Out-of-autoclave (OoA) prepreg. EVaC is from the original source and refers to engineered vacuum channel [21]. 32

2-4 Out-of-autoclave (OoA) consolidation of two plies. The three steps show layup, debulking in a vacuum hold, and the heated cure [3]. . . 33

2-5 Composite laminate manufacturing costs when cured with autoclave, thermal and microwave oven prepreg (PP) with thermal and microwave oven vacuum infusion (inf) processes. The thermal oven prepreg is OoA prepreg [17]. 34

2-6 Synchrotron radiation computed tomography (SRCT) high resolution scan of a composite showing voids, fibers and matrix material [33]. The scale bar is 50 µm. 37

2-7 Void formation of epoxy matrices under temperature, pressure, and humidity conditions [35]. 38

2-8 Aligned carbon nanotube (A-CNT) NPN materials enable VBO curing of autoclave-grade prepreg with: a) autoclave comparable void-free laminates and b) no reduction of short-beam (SBS) strength [39]. . . 40

2-9 EPN films on a prepreg: a) initial layup and b) after a few minutes for due to resin infiltration [43]. 42

2-10 Common complex geometries, T,I,Z,L, and hat shaped stiffeners with corner fillers [58]. 43

2-11 L-shape manufacturing defects: a) fiber wrinkling and delamination, b) micro and macro voids in between plies, c) corner thickening and resin accumulation and d) corner thinning [8]. 45

2-12 Diagrams of friction dominated L-shape manufacturing with no slip between plies and only the first ply considered: a) female mould, c) male mould; diagrams of pressure dominated scenarios with slippage and conformation of plies and the whole corner considered: b) female mould, and d) male mould [63]. 45

4-1 Ply orientation and layup schematic of 16-ply quasi-isotropic laminate with $[0/90/\pm 45]_{2S}$ orientation. 56

4-2 Vacuum bag layup diagram showing material and stacking sequence. . 57

4-3 Hexply 8552 manufacturer recommended cure cycle (MRCC) [73] (black), and VBO cure cycle used (orange) used in this work for NPN studies. The temperature profile follows the MRCC, but with -1 bar vacuum and no applied pressure (orange dashed lines) throughout the cure. . 58

4-4 Polymer nanofiber diameter measurement figures showing i) ImageJ fiber diameter segmentation method [74] and ii) segmentations of polyamide (PA) fibers. The corresponding SEM image is provided followed by the thresholded image and resulting fiber diameter histogram. Polyamide XD10 (PA XD10) nanofibers with manufacturer specified fiber diameter of 230 nm are shown in a-c. Polyamide 66 (PA 66) nanofibers with a manufacturer specified diameter of 150 nm are shown in d-f. The measured PA XD10 nanofiber diameter was 248 nm with a standard error of ±0.92 nm. The measured PA 66 nanofiber diameter was 153 nm with a standard error of ±0.32 nm. 60

4-5 µCT setup inside Zeiss Xradia 520 Versa for scanning composite samples at MIT ISN. 61

4-6 Process of segmenting image for void percentage analysis in ImageJ. The µCT slices are imported and auto contrast is applied. A mean blur filter of 3 pixels is applied to help better differentiate the voids from the individual fibers. The image is thresholded to draw contrast between the voids (black) and the composite (white). Particle analysis is completed on thresholded voids. This exemplary specimen is a 16 ply quasi-isotropic layup with IM7/8552 with the 20 µm PI aerogel in the middle 5 interfaces. 62

4-7 Short-beam strength mechanical testing: a) sample dimensional setup following ASTM D2344, and b) Zwick/Roell Z010 sample setup at MIT ISN. 63

4-8 SEM scans of polyamide nanofibers. SEM images of: a) 1.5 gsm 8 µm PA XD10 and b) 4.5 gsm 23 µm PA 66. The top image is taken at a 90° angle to show the thickness. The middle and bottom images are top down views. The micrometer measured the 1.5 gsm PA XD10 at 8 µm and the 4.5 gsm PA 66 at 23 µm. 65

4-9 IM7/8552 layup images of: a) prebagging manufacturing set up, and b) midlayup laminate. The white film is the 1.5 gsm 8 µm PA XD10 NPN nanofibers and the underneath black square is a UD IM7/8552 ply at 90°. c) Diagram of laminate layup with the gold lines representing the 4.5 gsm 23 µm PA 66 NPN interlayers. d) Representative µCT slices of the cured samples. The hot plate cured specimen without NPN interlayers had a void content percentage of 1.62 vol% compared to no measured voids when the NPN was applied. In the specimen with NPN interlayers applied to only middle seven interfaces, those interfaces are void-free while voids are observed in the non-NPN interfaces. 67

4-10 Representative µCT scans comparing: a) a hot plate cured specimen without NPN, and b) a hot plate cured specimen with 1.5 gsm 8 µm PA XD10 in all interlaminar regions. 68

4-11 Short-beam strength comparison with various cure methods with and without PA NPNs displaying: a) average values, standard error, and b) representative short beam shear test load-force displacement curves, where displacement is shifted for clarity. Autoclave cure data was previously reported in [77]. 69

4-12 SEM and optical observations of: a) 20 µm thick PI aerogel observed with sample mounted at 90°, and 20 µm PI aerogel porous structure observed top down via b) SEM, and c) optical microscope. 70

4-13 Heat assisted transfer process for the 20 µm thick PI aerogel from backing film to prepreg. The prepreg is then stacked directly to form a laminate with NPN at desired interfaces. 71

4-14 µCT image of sample with 20 µm PI aerogel NPN applied in middle five interlaminar interfaces. No voids are present in the interfaces where the PI aerogel interlayer is incorporated. The average void content of the top and bottom sections (non-NPN regions) is 0.76 vol%. 72

4-15 SEM of sample with 20 µm PI aerogel NPN in middle five interlaminar interfaces. No voids are present in the middle five interfaces. In the one interface where no NPN was applied, a void can be seen. 72

4-16 Representative optical microscopy images of hot plate cured specimens in a vacuum-bag-only environment. Specimens without any NPN show interfaces of 1-2 µm (a,b). A resin-rich region in image b) is observed, similar to the thickness of autoclave-cured IM7/8552 UD laminate material [78]. Specimens with 20 µm thick PI aerogel NPN (c,d) and 1.5 gsm 8 µm PA XD10 NPN (e,f) interlayers placed in all interlaminar regions have an interlaminar thickness of 5-7 µm. 73

4-17 Representative µCT image of of sample with the uncompressed 200 µm PI aerogel NPN all interfaces. No interlaminar voids are present but intralaminer voids are seen throughout the specimen. The intralaminer voids can be seen in the call out. The overall void content percentage is measured to be 0.11 vol%. 74

4-18 Illustration displaying the interlaminar void pressure interface with and without an NPN interlayer and the pressure forces defining the void boundary. The NPN enables capillary-driven polymer wetting into the interface, leading to void elimination and resin infiltration [10]. 77

5-1 Diagram of L-shape mold dimensions. Image modified from [83]. . . . 83

5-2 L-shape mold layup: a) layup diagram showing material and material stacking sequence, b) image of cure setup in oven prior to curing. . . 84

5-3 Ply and laminate diagrams for L-shape curing: a) ply dimensions, b) first ply laid up in L-shape mold, and c) L-shape geometry laminate stacking sequence. 85

5-4 CNT synthesis furnace and 50.8 mm (2 in) diameter quartz tube. Tube is black due to carbon deposits built up over time. 86

5-5 SEM image at 45° inclination of aligned carbon nanotube (A-CNT) array [10]. 86

5-6 Patterning of Si wafer: a) Si wafer is spin-coated with a positive photoresist polymer (orange). A positive photomask (black) is placed on top. (b) UV light is introduced weakening the photo resist. c) A photo resist developer removes the photo resist from the unmasked area of the wafer. d) The photomask is removed. e) E-beam deposits 0.1 nm Fe/Al_2O_3 catalyst layer for A-CNT growth. f) Photoresist removed leaving desired catalyst and support pattern on wafer. Image modified from [87]. 87

5-7 A-CNT post growth processing and imaging: i) CNT height measurement locations. ii) CNT transfer from wafer. Image 1 is of a ply interface before CNTs are applied. Image 2 shows the wafer post patterned 14 µm CNT transfer. The green color is the wafer and the black is the CNTs. Remnants of CNTs can be seen especially in the areas of the weave where there is no direct fiber contact with the wafer. Image 3 shows 14 µm tall CNTs post transfer on the woven prepreg. Image 4 shows 65 µm tall non patterned aligned CNTs post-transfer to the prepreg. Notice the matte black coloring from the complete transfer of CNTs due to the CNTs height. iii) Patterned CNTs under (a,c) light and b) dark microscopy. c) CNT pattern shows some non uniformity due to the ability of the CNT forests to delaminate from the wafer and shift position. 89

5-8 Hexply 8552 manufacturer recommended cure cycle (MRCC) for both UD and woven fabric materials [73], (black), and extended VBO cure cycle for some NPN studies in this work, where first temperature hold (solid blue line) is doubled to 120 minutes with -1 bar vacuum and no applied pressure (standard dashed blue line) throughout the cure. . . 90

5-9 L-shape composite optical images after curing: a) top down view, b) side profile. 92

5-10 Approximate L-shape µCT scan points: in the midpoint of the curved and flat regions and midway through the laminate width. 93

5-11 Representative µCT scans of a L-shape specimen with 4.5 gsm 23 µm PA 66 in the middle 5 interfaces cured without the 1 mm thick rubber caul plate; a) The flat area showed no voids in the NPN regions similar to flat plate results in Chapter 4; b) The curved area showed both interlaminar and intralaminer voids in the NPN region. 94

5-12 Flat section of L-shape specimen cured with 1 mm thick rubber caul plate; a) No NPNs were placed in the interlaminar regions and void content of 1.13 vol% was observed; b) 4.5 gsm 23 µm PA 66 interlayers were placed in all interlaminar regions (ply-ply interfaces) and void content of 0.00 vol% was observed. 94

5-13 Curved section of L-shape specimen cured with 1 mm thick rubber caul plate: a) No NPNs were placed in the interlaminar regions and void content of 1.67 vol% was observed; b) 4.5 gsm 23 µm PA 66 interlayers were placed in all interlaminar regions (ply-ply interfaces) and void content of 0.00 vol% was observed. Two rare scattered interlaminar voids were observed $\sim$ 5 µm in diameter along the center line, however, the contribution to void content percentage was less than 0.01 vol%. . 95

5-14 Void content percentage of L-shape samples. 95

5-15 Representative microscopy images of the flat region of L-shape specimens: a) specimen without any NPN shows interlaminar and intralaminer voids; b) specimen with 4.5 gsm 23 µm PA 66 interlayers is void-free. There is a 10-15 µm increase in interlaminar thickness which can be easily seen in the middle interlaminar region. 96

5-16 Representative microscopy images of the curved region of L-shape specimens: a) specimen without any NPN shows interlaminar and intralaminer voids; b) specimen with 4.5 gsm 23 µm PA 66 interlayers is void-free. There is a 10-15 µm increase in interlaminar thickness which can be easily seen in the middle interlaminar region 96

5-17 Diagram comparing: a) unidirectional ply and b) woven ply [6]. . . . 98

5-18 Diagram showing the different prepreg morphologies and interfaces of specimens tested. 98

5-19 IM7/8552 woven prepreg characteristics: a) optical image of woven fabric ply; b) optical microscopy image of woven ply. The glossy area is the preimpreginated resin and the gap between the fibers tows as seen in the inset is one of the regions where voids still persist even after the integration of NPN. 99

5-20 Void content of 8-ply IM7/8552 UD-woven fabric $[0^{UD}/0^{Fabric}]_{2S}$ laminates cured with various methods and NPN interlayers. 101

5-21 Representative µCT images of an 8-ply IM7/8552 hybrid laminates alternating between woven and unidirectional prepeg plies, $[0^{UD}/0^{Fabric}]_{2S}$, cured via hot plate with various NPNs at all ply interfaces showing: a) the baseline containing no NPN layers with a large elongated voids and an overall void content percentage of 3.62 vol%; b) 230 µm aligned CNT NPN with a void percentage of 2.03 vol%; (c-d) 80 µm patterned CNT NPN with a void percentage of 0.02 vol%; (e-f) 70 µm aligned CNT NPN with an extended cure cycle with a void percentage of 0.27 vol%. While most slices of the of the 80 µm patterned CNT and 70 µm aligned CNT NPN with an extended cure can be represented by c) and e) respectively, d) and f) show that the specimens are clearly not void-free and contains rare but large voids. 102

5-22 Identified void prone areas. Interweave void prone area (orange) occurs in areas where there are gaps between tows. Corner voids occur in the corner region of the elliptical tows and can generally follow a tow along its length. 103

5-23 Representative images of void locations in UD-woven laminate interfaces: i) A diagram showing warp (orange) and weft (blue) fiber tows and how interweave voids appear on the slices as they progress (a to c) in a µCT scan where the weft fiber tows disappear. Due to the weave pattern the weft tows have the opposite slope when they reappear; and ii) Voids are shown in the µCT images of a UD-woven laminate with 230 µm CNT NPN interlayers. The red circles are corner voids. The interweave void progression can be seen in the green boxed woven ply. An orange guideline drawn to enable tracking of the weave slope flip (a to d). 104

5-24 Cross sectional optical microscopy of interlaminar regions and resin-rich regions in samples of Woven-UD interfaces with 70 µm A-CNT interlayers: CNTs and interlaminar thickness of $\sim$ 20 µm, b) a large resin-rich interface where there is some evidence of no CNTs, c) corner region where there no CNTs are observed, d) CNTs in the interlaminar region follow the bottom ply and do not integrate into the corner region where there are no observed CNTs. The lack of CNTs in d) the corner region and b) the interweave resin-rich region is important as those areas are typically where voids have been found with µCT scans. . . . 105

5-25 Void content of 8-ply IM7/8552 woven fabric $[0]_{4S}$ laminates cured with various methods and NPN interlayers. 107

5-26 Representative µCT images of 8-ply IM7/8552 woven laminates, $[0^{Fabric}]_{4S}$, cured via hot plate with various NPNs at all ply interfaces showing: a) the baseline containing no NPN layers with a void percentage of 5.61 vol%; b) 140 µm aligned CNT NPN with a void percentage of 2.91 vol%; c) 4.5 gsm 23 µm PA 66 with a void percentage of 3.67 vol%. . 108

5-27 Void content of IM7/8552 woven fabric 8-ply $[0]_{4S}$ laminate (green) with 3 layers of 4.5gsm 23 µm PA 66 in each interface and 4-ply $[0]_{2S}$ laminate (purple) with 5 layers of 4.5gsm 23 µm PA 66 in each interlaminar region. The void content percentage of the 5 NPN layered 4-ply laminate is higher than the 3 NPN layered 8-ply laminate at 4.27 vol% and 1.65 vol% respectively. 109
5-28 Void content percentage comparison of 8-ply $[0]_{4S}$ with 3 layers of 4.5 gsm 23 µm PA 66 in each interface and 4-ply $[0]_{2S}$ with 5 layers of 4.5 gsm 23 µm PA 66 in each interface. 109

List of Tables

4.1 Table of values for short-beam strength and standard error of samples cured with various methods and NPN interlayers. Autoclave cure data was previously reported in [77]. 69

5.1 Table of void content for 8-ply IM7/8552 UD-woven fabric $[0^{UD}/0^{Fabric}]_{2S}$ laminates cured with various methods and NPN interlayers. 101

5.2 Void content of 8-ply IM7/8552 woven laminate fabric $[0]_{4S}$ laminates cured with various methods and NPN interlayers. 107

List of Abbreviations

A-CNT ..... Aligned carbon nanotube

CFRP ..... Carbon fiber reinforced polymer

D_f ..... (Nano)fiber diameter

EPN ..... Electrospun polymer nanofiber film

EVaC ..... Engineered vacuum channel

FRP ..... Fiber reinforced polymer

GNPT ..... Guaranteed nonporous Teflon

ILSS ..... Interlaminar shear strength

K ..... Permeability tensor

MRCC ..... Manufacturer recommended cure cycle

n ..... Number of moles of gas

NDE ..... Non-destructive evaluation

NPN ..... Nanoporous network

OoA ..... Out-of-autoclave

P ..... Pressure

$\mathbf{P}_m$ ..... Maximum load during short beam shear test

$\mathbf{P}_{NPN}$ ..... Capillary pressure from NPN

$\mathbf{P}_r$ ..... Pressure of the resin

$\mathbf{P}_v$ ..... Pressure of the gas in the entrapped void

PA ..... Polyamide

PET ..... Polyethylene terephthalate

PI ..... Polyimide

Prepreg ..... Pre-impregnated fibers in a partially cured polymer matrix

r ..... Universal gas constant

SBS ..... Short beam shear

SE ..... Standard error

SEM ..... Scanning electron microscope

SRCT ..... Synchrotron radiation computed tomography

T ..... Temperature

$\mathbf{t}_{sbs}$ ..... Short beam shear specimen thickness

UD ..... Unidirectional prepreg

V ..... Volume

$\mathbf{V}_{flow}$ ..... Flow velocity vector

VBO ..... Vacuum-bag-only

$\mathbf{w}_{sbs}$ ..... Short beam shear specimen width

XD10 ..... Xylylenesebacamide

$\Delta\mathbf{P}$ ..... Pressure differential at void boundary

ϵ ..... Porosity

σ ..... Resin surface tension

σ^{sbs} ..... Short-beam strength

θ ..... Contact angle between the resin and the nanofiber film

µCT ..... X-ray micro-computed tomography

μ_v ..... Dynamic viscosity

∇P_f ..... Pressure gradient at front of the flow

Chapter 1

Introduction

The world has at times been defined by the materials used by its people whether it be stone, or bronze, or iron. New material systems enable tools and abilities which enhance the capabilities of each society. Likewise, the aerospace field, though relatively young, has too undergone changes in the material systems deployed. In 1903, the Wright brothers' Flyer was primarily made out of spruce wood and in the mid to late 20th century metals such as aluminum, titanium, and steel were used extensively. In the 21st century, composite materials are used increasingly in widespread application with the Boeing 787, as an example, being 50% composite material by weight as seen in Figure 1-1. Advanced composites, and in particular laminated carbon fiber reinforced polymers (CFRPs), present many advantages over more traditional materials such as aluminum. CFRPs are made from a high tensile strength fiber made of carbon and a polymer matrix. The fibers can be preimpregnated with the resin system to form sheets of material called prepreg. These individual sheets or plies are stacked into laminates as seen in Figure 1-2. The primary advantage of CFRPs is their high strength to density ratio. Figure 1-3 shows Ashby charts plotting strength vs density and stiffness vs density (upper left quadrant is advantaged). Note that technical ceramics, despite being stiff, do not compare in strength to composites (except in compression) and are therefore disadvantaged to composites. One can see that the CFRPs are more advantaged compared to the metal grouping for a given guideline representing a more optimal material for use. Additional advantages for CFRPs

include being able to manufacture parts with complex geometries without the need for extensive machining or fasteners, advantaged thermal expansion properties, corrosion resistance, and the ability to absorb vibrations. These properties have driven composite adoption in cases requiring strong and lightweight load bearing material systems.

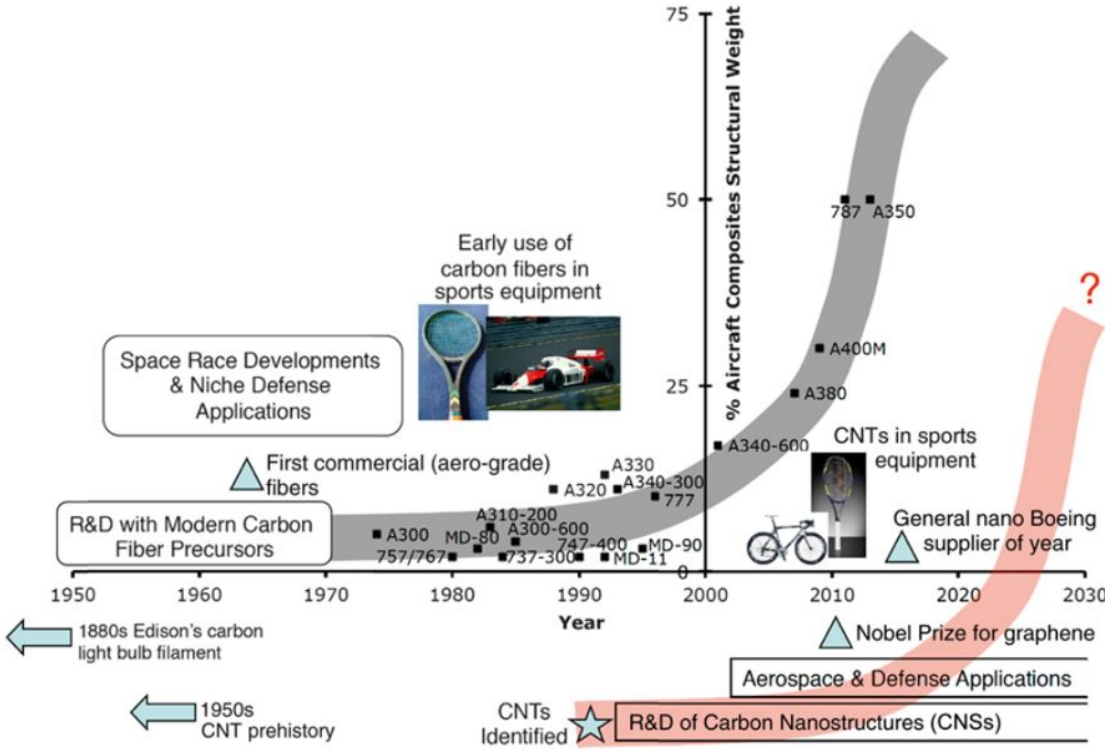

Figure 1-1: Growth of carbon fiber composites in aerospace applications as percent of aircraft mass vs. time. The more recent adoption curve of carbon nanotubes is perceived [1].

Figure 1-2: Diagram of a unidirectional carbon fiber reinforced polymer ply consisting of fiber and matrix material.

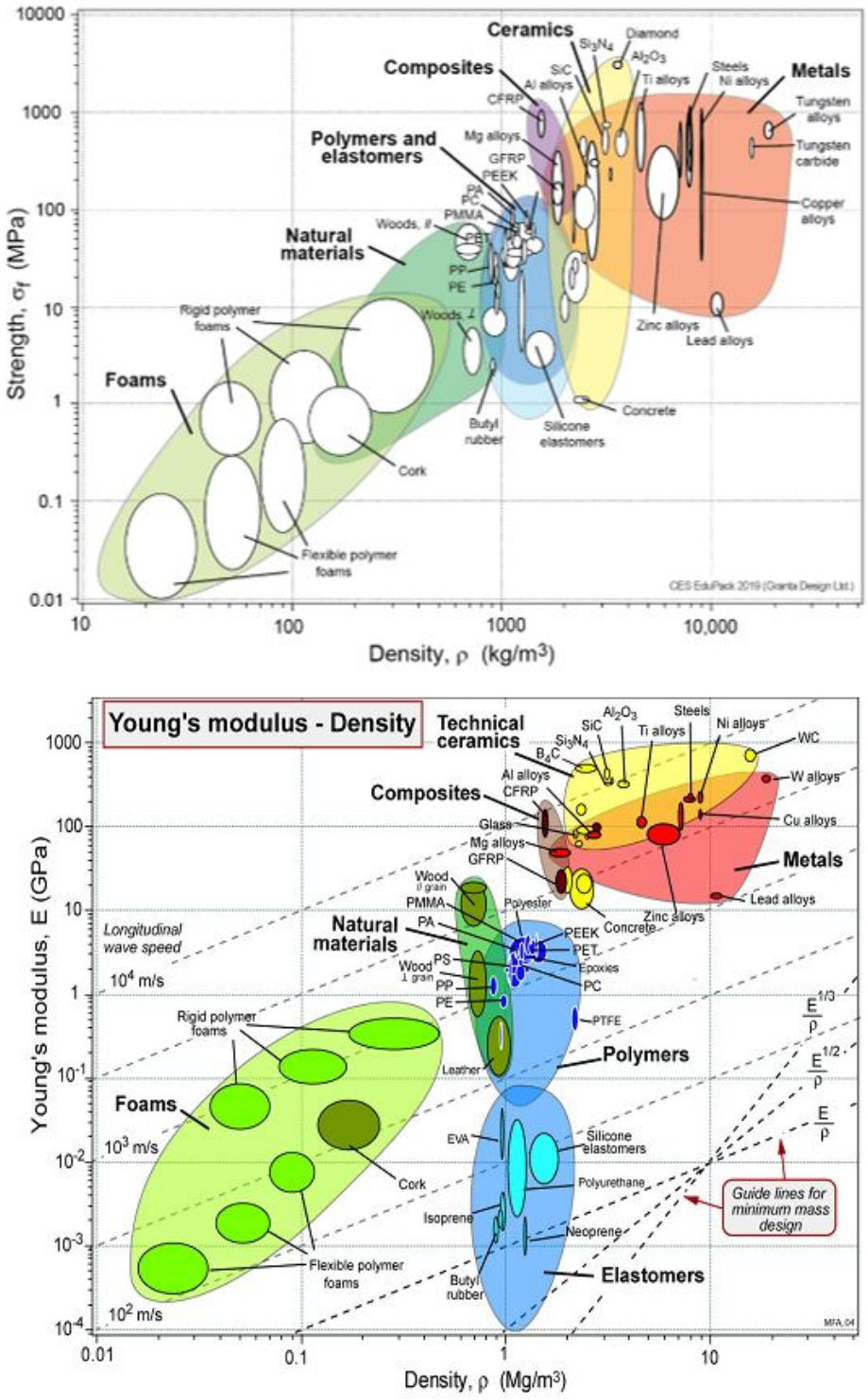

Figure 1-3: Ashby charts plotting material strength and stiffness (Young's modulus) vs density. The design guidelines are used for minimum mass design with the (upper left quadrant being advantaged) [2].

1.1 Motivation

The use of composite materials has grown in industries as diverse as wind energy, aerospace, automobile, medical, and civil engineering [1, 3, 4]. Void-free composites are a key goal in high grade composite manufacturing as voids can cause a severe drop in mechanical properties [5]. Voids weaken the structure and void-initiated cracks can lead to a reduction in service life. As such, significant time and effort is spent on manufacturing parts with a minimal to no void content and verifying this fact, e.g., through non-destructive evaluation (NDE) techniques such ultrasonic testing. Interlaminar voids are particularly problematic and are illustrated in Figure 1-4. Defective parts that have voids often must be scrapped and are deemed unusable. To reduce void quantity, commonly, an autoclave (heated pressure vessel) is used [6]. Autoclave based manufacturing techniques are extremely capital intensive, have limited production rates and part size, have slow cycle times, and require high labor and energy intensity [7, 4, 8]. As composites have expanded their use in industry and make up a larger percentage of the product, cost has become a more influential factor [3].

Driven by manufacturing challenges, there has been development of a prepreg material system fittingly called Out-of-Autoclave (OoA) prepreg where the prepreg morphology or other characteristics are modified, such as leaving dry fiber channels in the prepreg for gas evacuation of the material system [3]. These materials are designed to cure in an oven without applied pressure, but still utilize pulled vacuum in a vacuum-bag-only (VBO) cure, and are envisioned to overcome the cost and manufacturing challenges of traditional autoclave approaches. However, OoA prepreg systems have many drawbacks. The cycle times may actually be longer due to the time spent debulking or setting up the edge-breathing that is required for low void content [9]. There are also surface quality challenges for sandwich structures such as honeycomb composite structures. These material systems require specific material and environmental parameters and are very sensitive to deviations from ideal conditions with entrapped voids being the consequence. Furthermore, the matrix material rheology

is often altered [3].

The motivation for this thesis was to ascertain a system that would remove interlaminar voids without external pressure while utilizing standard previously certified aerospace-grade autoclave prepreg. Various nanomaterial systems with nanoscale porosity, termed nanoporous network (NPN) materials, are applied to each ply-ply interface to remove voids by encouraging resin infusion. Aligned carbon nanotube (A-CNT) systems have been utilized as textured NPNs with aligned capillaries for interlaminar void removal in aerospace-grade CFRP autoclave prepreg laminates [10], but more affordable and scalable NPN materials are of interest. This work aims to expand material systems of the nanoporous networks (NPN) as well as their application into different prepreg systems. In particular there is focus on enhancing composite manufacturing with new commercializable and scalable NPN materials. Preliminary work is also done in the utilization of NPNs in more complex geometries.

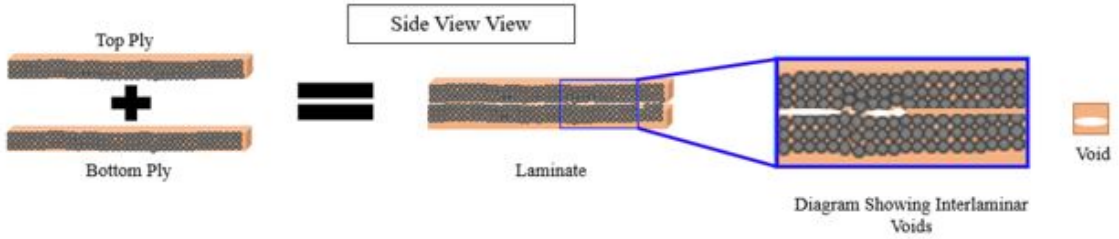

Figure 1-4: Schematic of a carbon microfiber reinforced plastics composite laminate consisting of stacked plies to form a laminate. Here, the two plies are unidirectional or a 90°orientation on a 90°orientation. The plies are then stacked. The interlaminar voids in the laminate in white can be observed in the interface between the two plies.

1.2 Thesis Outline

Chapter 2 will present an overview of nano-engineered hierarchical composites and background information covering prepreg laminate processing with different fiber systems, and manufacturing laminate processes. It will also cover the use of NPNs as void reducers, and the challenges complex composite geometries have.

Chapter 3 outlines the general objective of this thesis while expanding upon the approach employed towards investigation of void reduction through the utilization of newly identified NPN materials.

Chapter 4 focuses on utilizing the capillary effects of two different NPN material systems: electrospun polymer polyamide (PA) nanofibers (EPN films) and a bespoke polyimide (PI) aerogel. It covers the results exhibiting void elimination, a discussion on interlaminar thickness, and short-beam strength results of the specimens made with EPN films as well as the implications of the results.

Chapter 5 focuses on preliminary investigations on void removal in complex geometries with EPN films and investigating NPNs in woven-woven and unidirectional-woven prepreg layups with a variety of NPN systems including aligned carbon nanotubes (A-CNTs), patterned A-CNTs, and the EPN films.

Chapter 6 gives the overall conclusions and implications drawn from the work presented and future directions to be explored.

Chapter 2

Background

Composite material is a broad term. However, in this document, the type of composites of concern are aerospace-grade advanced composites comprised of carbon fibers in a (thermoset) polymer matrix, known as carbon fiber reinforced polymers (CFRPs). As introduced in Chapter 1, such composites have grown in usage across a variety of industries, especially aerospace, due to their advantaged mass-specific properties. CFRPs are susceptible to more complex failure modes compared to homogeneous materials as failure in composites can reflect fiber dominated failure, matrix dominated failure or interfacial dominated failure between the two constituents [11]. The objective of this chapter is to give a background in composite curing utilizing both autoclave curing methods and non-autoclave methods, typical manufacturing defects, in particular voids, the utilization of capillary effects for void removal, an introduction to two different polymer nanoporous network (NPN) materials of interest in this thesis, and challenges with L-shape or complex geometry parts .

2.1 Autoclave and Alternative Curing Methods

In the aerospace industry, the traditional manufacturing technique of composites has been the utilization of autoclaves, or large pressure vessels (depicted in Figure 2-1), to cure prepreg which consists of fibers that are preimpregnated with a partially-cured polymer, typically epoxy, resin system. This traditional system has been well

documented, and its high usage has enabled knowledge gain through experience. It is the *de facto* standard for competing processes, as the end autoclave cured product has high fiber volume fractions, low defect (voids and others) rates and the best reproducibility [12]. The use of prepreg simplifies manufacturing as a resin infiltration step is not needed. Autoclave curing has some important drawbacks, however, as it requires high capital investment, high energy use, long manufacturing times due to limitations on heating, cooling, and pressurizing large volumes of gas, and is fixed in size. This presents high barriers of entry and limits rapid scaling due to the specialized nature of the equipment. The fixed autoclave size limits part sizes and requires high utilization rates, especially for small part sizes, for sustainable autoclave production. As composites gain widespread adoption, non-autoclave grade methods that produce aerospace grade composites parts are increasing in usage [3].

Figure 2-1: Example of an autoclave. Side view of an Econoclave® 12×40. The diameter is 12 feet (3.66 m) and it has a length of 40 feet (12.19 m) [13].

Various alternative methods of manufacture have been investigated to try and circumvent the autoclave with numerous heat sources (microwave, induction heating, joule heating, lasers, hot presses, blankets, etc. [14, 15, 16] as well as prepreg modifications. In particular, a prepreg system termed out-of-autoclave (OoA) has shown that it is viable to produce parts using only vacuum bag consolidation without the applied pressure that an autoclave provides. This allows for a significant reduction in

operation and acquisition costs, enabling lower cost cure set ups and can increasing the number of composite manufacturers, particularly smaller ones [3]. The challenge for OoA prepregs, however, has been its propensity to have voids (particularly in the already low-performance interlaminar regions between the plies) in the laminate and disputes over the true cost saving of utilizing these materials in part due to their longer preparation time and higher material costs [17]. The comparison of autoclave manufacturing and out of autoclave manufacturing can be seen in Figure 2-2.

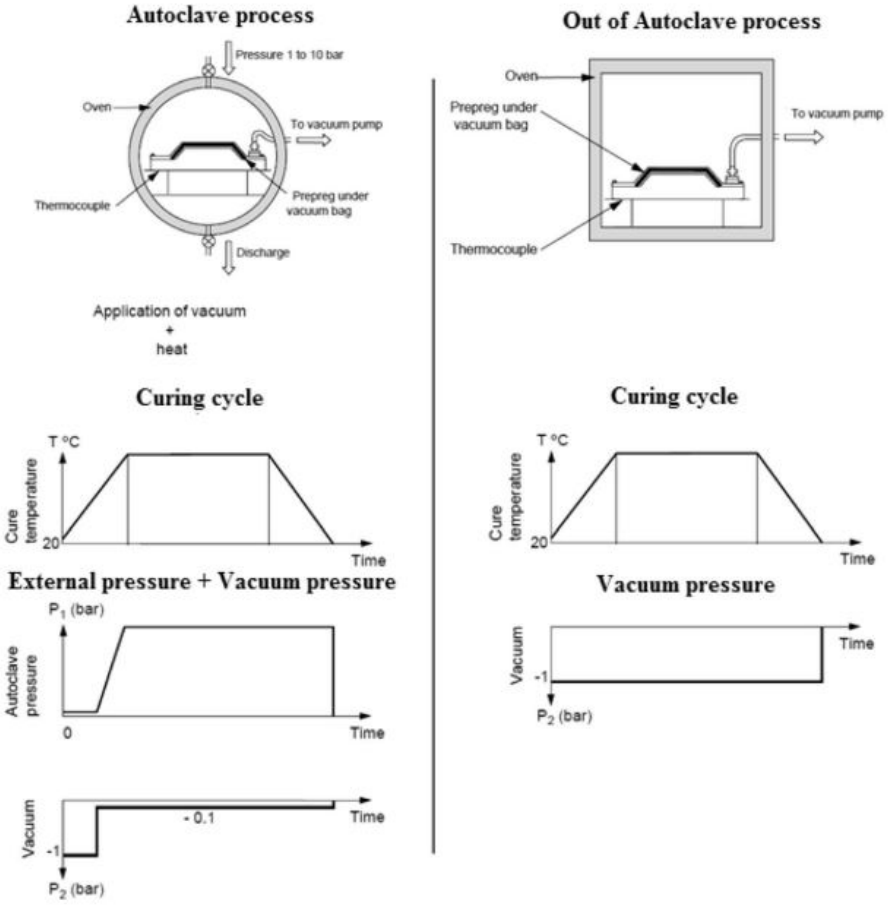

Figure 2-2: Comparison of autoclave and out-of-autoclave, sometimes called oven or vacuum-bag-only (VBO) curing [8].

While there has been recent research to understand, fundamentally, OoA materials, much of the research has been done in industry on the OoA material system and not available publicly for competitive reasons [3]. A key technology utilized in OoA prepreg is the use of engineered vacuum channels of dry fibers next to regions of

resin-heavy impregnated fibers as seen in Figure 2-3. The dry fibers enable gas to exit the laminate by moving along these dry zones towards the edges of the laminate while vacuum is pulled [18]. When the temperature is increased, the resin flows into the dry fiber regions and ideally fully engulfs the dry fibers allowing for no residual voids after curing. Breathable edges are extremely important when using OoA material as air transport occurs in-plane and an impediment in the vacuum channel would hinder air evacuation [18]. High vacuum is also pulled throughout the cure with a minimum of 28 in Hg to encourage air evacuation [3]. Other manufacturing changes from an autoclave cure procedure include an initial debulking step lasting from a few hours to more than 15 depending on part size (thicker and larger part sizes require longer debulk times) to encourage gas evacuation, and a modified cure cycle [19]. µCT images showed that voids decreased with the debulking time and that the dry fiber regions were infiltrated with resin as the material is heated [20]. As the dry regions were infiltrated with resin, the in-plane permeability decreased supporting the theory that the dry fiber regions dictate the prepreg's in plane permeability.

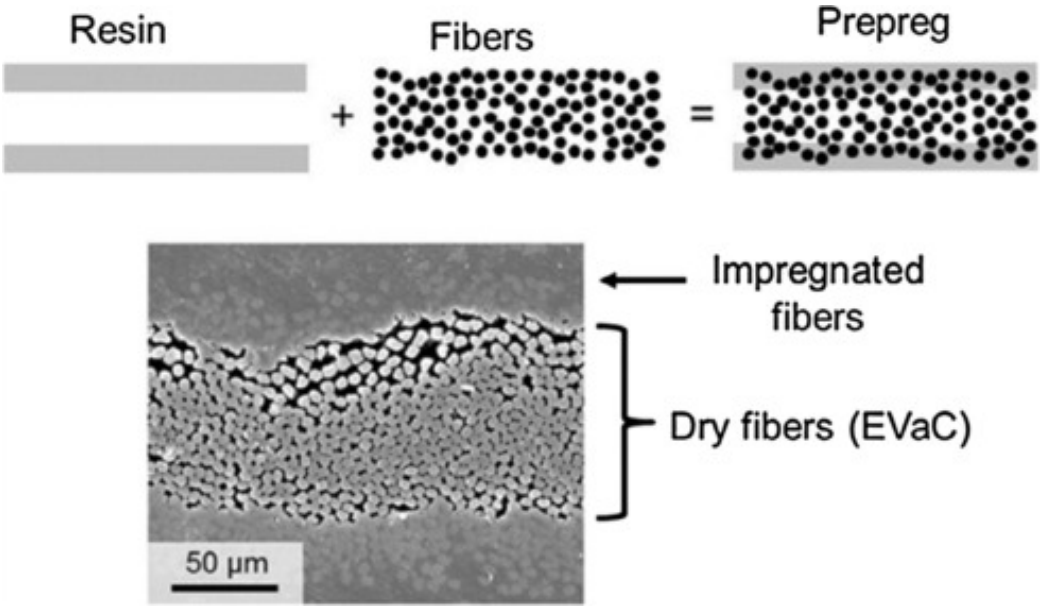

Figure 2-3: Out-of-autoclave (OoA) prepreg. EVaC is from the original source and refers to engineered vacuum channel [21].

New resin systems were developed for the OoA prepregs unique needs. The resin needs to be highly viscous during the debulking phase which can last on the order of

hours or even days, as resin infiltration of dry regions could seal the vacuum pathways, but as temperature increases, resin viscosity needs to rapidly decrease to ensure fiber infiltration. The rheology alteration led to new resins to be developed. When autoclave resin Hexply 8552 (epoxy) was compared to various OoA resins, (MTM 45-1 and 5320), it was found to be less viscous in the 80°–140°C range. However, the OoA resins due to their higher reactivity and higher viscosities, only had 60–120 min of flow time compared to 500 min for the 8552 autoclave resin, suggesting that full prepreg impregnation occurs at the onset of cure for the OoA material [22, 23].

Due to the lack of applied pressure, which is used for consolidation of the laminate, fiber volume fraction of VBO cured specimens tend to be reduced (i.e., there is more polymer matrix) and the laminate is slightly thicker compared to if the same material was cured in an autoclave [3]. The consolidation phase can be seen in Figure 2-4 with Δh representing the change in thickness that occurs during consolidation between two plies occurring on a macro scale between plies and around the resin, and on a micro scale in the tows between the individual fibers. The consolidation for OoA prepreg systems is higher than autoclave grade prepreg systems due to the engineered dry channels in the plies and lack of external pressure. If there was additional applied pressure, Δh would be larger as the plies would have less of an interlaminar region [3].

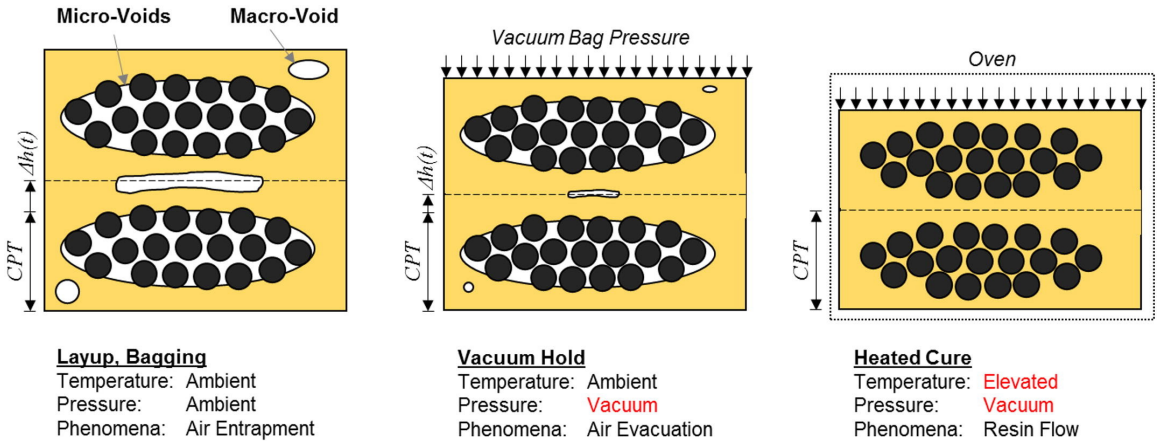

Figure 2-4: Out-of-autoclave (OoA) consolidation of two plies. The three steps show layup, debulking in a vacuum hold, and the heated cure [3].

The economics of VBO curing was shown to reduce part costs by 6%, driven by the reduction of energy and capital costs compared to autoclave curing as seen in Figure 2-5. [17]. This is partially offset by higher material costs. Additional benefits include curing larger parts more easily, which would reduce assembly costs and post-cure machining. Additionally, cure cycles can be faster and for parts where there is a sensitive skin layer, pressure-induced (from the autoclave) defects such as face sheet dimpling can be reduced [24].

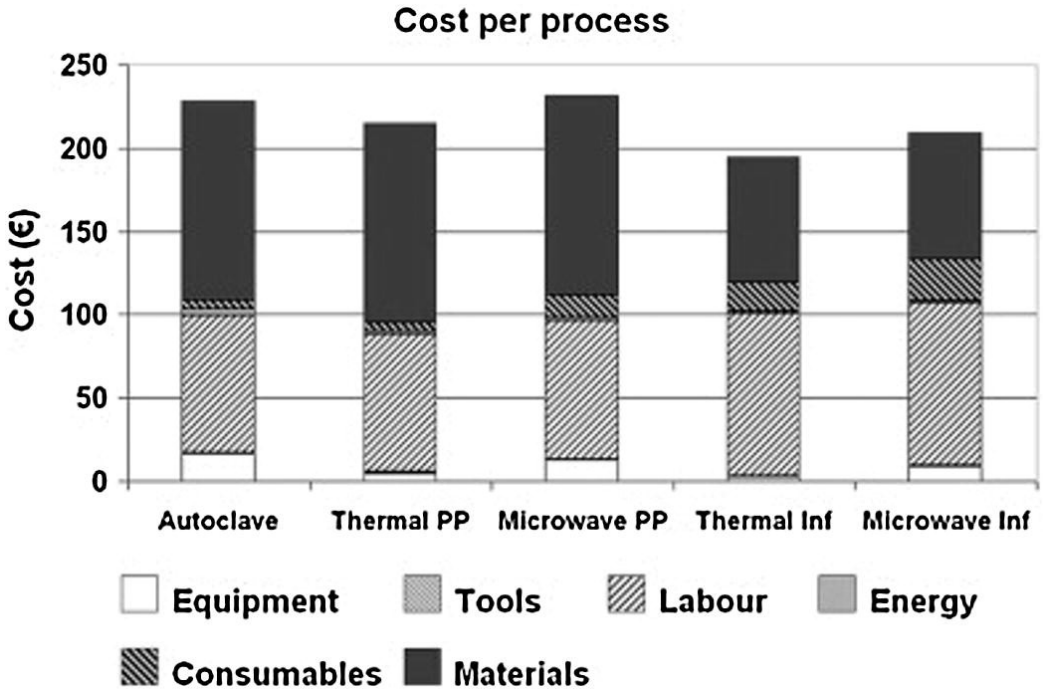

Figure 2-5: Composite laminate manufacturing costs when cured with autoclave, thermal and microwave oven prepreg (PP) with thermal and microwave oven vacuum infusion (inf) processes. The thermal oven prepreg is OoA prepreg [17].

Defects in composite manufacturing, particularly voids, under VBO conditions, tend to come from two sources: the presence of entrapped air or released volatiles (gas-induced voids) or the failure of the dry fibers to be fully infiltrated by the resin (flow-induced voids). Modeling of gas induced voids show that the evacuation of voids decreases linearly with dry fiber permeability, but increases quadratically with part size [25]. Gas-induced voids are evacuated primarily through the in-plane permeability, enhanced by the dry fiber regions in OoA prepreg, as the transverse plane or

thickness permeability is four orders of magnitude larger. With an increase in plies, the air flow in the transverse plane becomes near zero, in part because as additional plies are added, the likelihood of complete overlap of dry fibers decreases through the thickness. Additionally, unlike in autoclave cured prepreg, increased humidity has a large effect on void content as gas pressure within moisture-induced voids can be greater than the resin pressure without the autoclave to apply pressure during manufacturing. These conditions of larger part sizes and humidity effects can be offset by increased debulking time where vacuum is pulled, and/or increased vacuum pressure applied to ensure higher levels of air and volatile evacuation in VBO cures [25, 26].

Flow induced voids often occur due to partial impregnation of the dry fiber pathways and are due to the fiber and matrix properties as opposed to manufacturing error in vacuum bagging or otherwise. A main driving factor is long out time where the prepreg material is left at room temperature or if the laminate is cured at lower temperatures. In these cases, voids occur as viscosity is higher than expected which hinders resin flow into the dry fiber region [23].

Woven fabrics have additional difficulties. In order to make certain the dry pathways are contiguous for void evacuation, the entire tow cross section should to be unimpregnated. If not, the entrapped air may not be able to fully evacuate [7]. Both woven and unidirectional VBO prepreg systems have been shown to have mechanical properties of near equivalence to autoclave-cured specimens [27]. However, in a study done with IM7/8552 and IM7/MTM45 representing autoclave and out of autoclave material systems respectively, when there was out time, drops in drape and tack were observed with the MTM45 followed by a decrease in mechanical properties and an increase in void content. This out time sensitivity corresponds to the importance of resin properties, particularly viscosity, to void percentage of OoA prepregs and their effects on the dry fiber evacuation channels. When there was no out time effects, mechanical performance of VBO and autoclave cured specimens was similar [28].

VBO curing is a promising cure methodology especially with OoA prepreg material. It has many benefits as it does not require large costly autoclaves. However, there are higher material costs and due to it not being an established method there

is a lack of diverse set of certifiable materials at the current time, and both time and capital will be required to attempt to certify OoA prepregs. Additionally, OoA prepreg systems have a propensity for voids due to their high dependence on resin properties, especially viscosity. This can be mitigated with extended debulking, but debulking on tooling is a limiting factor for cycle time.

2.2 Voids in Composites

Defects created during the manufacturing of composites are a core source of divergence of composite performance from the expected value. Common defects that occur during the manufacturing process are fiber misalignment or tow distortions (formed around the corner of complex geometries), fiber waviness, broken fibers, interlaminar delamination, incomplete matrix material cure, voids, and machining damage. These manufacturing defects are different from damage, as damage typically is incurred under a loading condition or during operation [29]. Voids, or areas of the manufactured composite part that lacks either fiber or matrix, are studied in depth due to their prevalence to occur over a wide range of manufacturing methods and their large effect on mechanical properties and failure mechanisms. The study of voids continues to be an active field of research due to a current lack of understanding on void formation and its continued relevance. Recently, there have been studies of voids in prepreg manufacturing, especially as OoA and automated prepreg laying has increased in prevalence due to lower manufacturing time and costs. In both these technologies, voids are a frequent defect [29, 30].

As resin impregnation for prepreg material (forming intralaminar voids) occurs at the supplier, void formation during this stage is typically not studied. Instead, research has centered on the final void percentage of a part and its relationship to the manufacturing procedure [29]. Interlaminar voids, which are formed due to air entrapped between plies during layup, are a large challenge. While voids in prepreg laminates can also occur due to volatiles being released from the matrix material or moisture content found in the matrix materials [31, 32], modern resins are designed

to have very low moisture percentages and volatile content leading to confined air being the core void formation method. The factors that can influence the entrapment of air at ply-ply junctions (the interlaminar region) include ply orientation, ply morphology, laminate thickness, composite and tool shape, bagging procedure and layup environment [29]. Examples of voids in a can be seen as in Figure 2-6 as taken by synchrotron radiation computed tomography (SRCT).

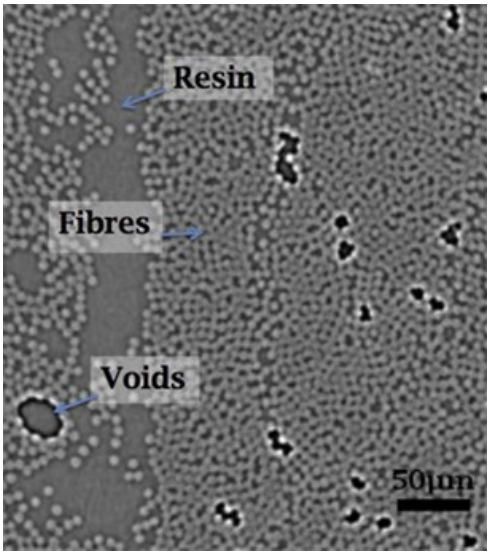

Figure 2-6: Synchrotron radiation computed tomography (SRCT) high resolution scan of a composite showing voids, fibers and matrix material [33]. The scale bar is 50 µm.

In an autoclave cure, the voids created during the layup are removed or dissolved under the applied pressure with the high pressure also suppressing volatile emissions. A void, once entrapped in a laminate, if not vacated, can grow or shrink in size depending on the temperature and pressure [34]. Kardos et al tried to model the void size as a function of temperature, pressure, and humidity which can be seen in Figure 2-7 [35]. Their basic model was built on to include the important effect of the surface pressure of the resin which would reduce void growth at high temperatures and other models were additionally developed to include micromechanical effects, staged curing, and non-Fickian (Dual-Fick) behavior of the epoxy resin [36]. The process of void formation and size is not completely understood. This is especially true for cylindrical type voids as the models proposed have been primarily for spherical voids.

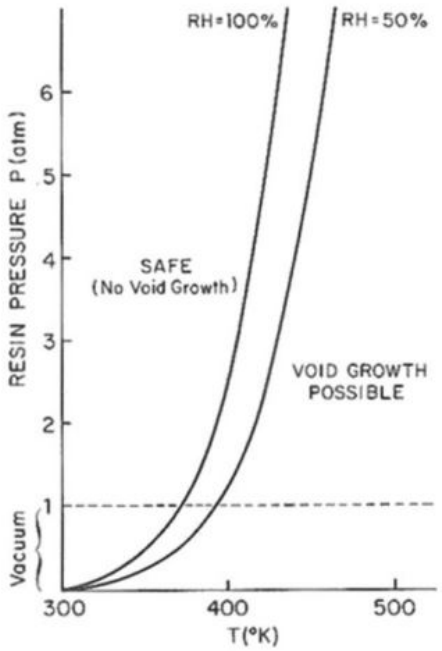

Figure 2-7: Void formation of epoxy matrices under temperature, pressure, and humidity conditions [35].

In autoclave prepreg systems, voids are primarily evacuated along the interlaminar regions. This is because there is very low air permeability though the thickness of the prepreg. The low air permeability hinders intralaminar vacuum-driven void evacuation. The cure cycle parameters also alter the distribution, size, and shape of the voids. In an experiment by Shim et al, autoclave-grade CFRP prepreg cured without applied vacuum and pressure had the highest void content. When pressure was added without vacuum, large interlaminar void percentage still occurred, but it was reduced slightly compared to the no vacuum and no pressure specimens, reinforcing the autoclave's laminate consolidating role [37]. When prepreg was cured without vacuum pressure, void content could be decreased by increasing the applied pressure during cure, though never eliminating interlaminar voids completely. An increase in autoclave pressure helps with consolidation and suppresses entrapped air volume growth of voids [38]. Autoclave prepreg is widely used for high fiber volume content and high mechanical performance. Voids are an often-found manufacturing defect that can have a detrimental effect on the performance of the manufactured part. Applied

pressure of the autoclave is traditionally necessary for void free composites. Applied pressure, temperature, and vacuum pressure need to be optimized together to create void free or reduced voids in samples.

2.3 Void Removal Utilizing Aligned Carbon Nanotubes (A-CNTs) as a Nanoporous Network (NPN)

In the article, "Void-Free Layered Polymeric Architectures via Capillary-Action of Nanoporous Films," [39] A-CNTs were shown to enable VBO curing of autoclave-grade unidirectional prepreg CFRP composites. The capillary pressure of the A-CNTs based nanoporous network (NPN) film replaced the applied autoclave pressure allowing VBO cured laminates to be cured with void content percentage of <0.1 vol% similar to autoclave cured specimens. The A-CNT NPN film encouraged resin flow into the interlaminar region. This capillary driven resin wetting was an enabling force for the void elimination. Short beam shear (SBS) tests were performed, and the mechanical performance of the NPN + VBO cured specimen was not statistically different when compared to the autoclave-cured specimen, which is a concern with OoA material systems and processes. The specimen cured in the VBO environment without the CNT NPN interlayers had a void content percentage of 1.65 vol% and a decrease in short-beam strength. Figure 2-8 shows the effects of the A-CNTs when cured under VBO conditions with and without the A-CNTs interlayers as well a baseline conventionally cured autoclave grade specimen. Another hypothesized void reduction mechanism is the conformability of the NPN to achieve a uniform ply-ply interface. The interlaminar voids can become trapped due to the irregular interface which prevents voids from being evacuated along the axial direction of the fibers. The A-CNTs conformed to both sides of the plies ensuring there to be a uniform contact area, perhaps leading to the reduction of voids due to strong capillary effects as well as a hypothesized void extraction pathway [39].

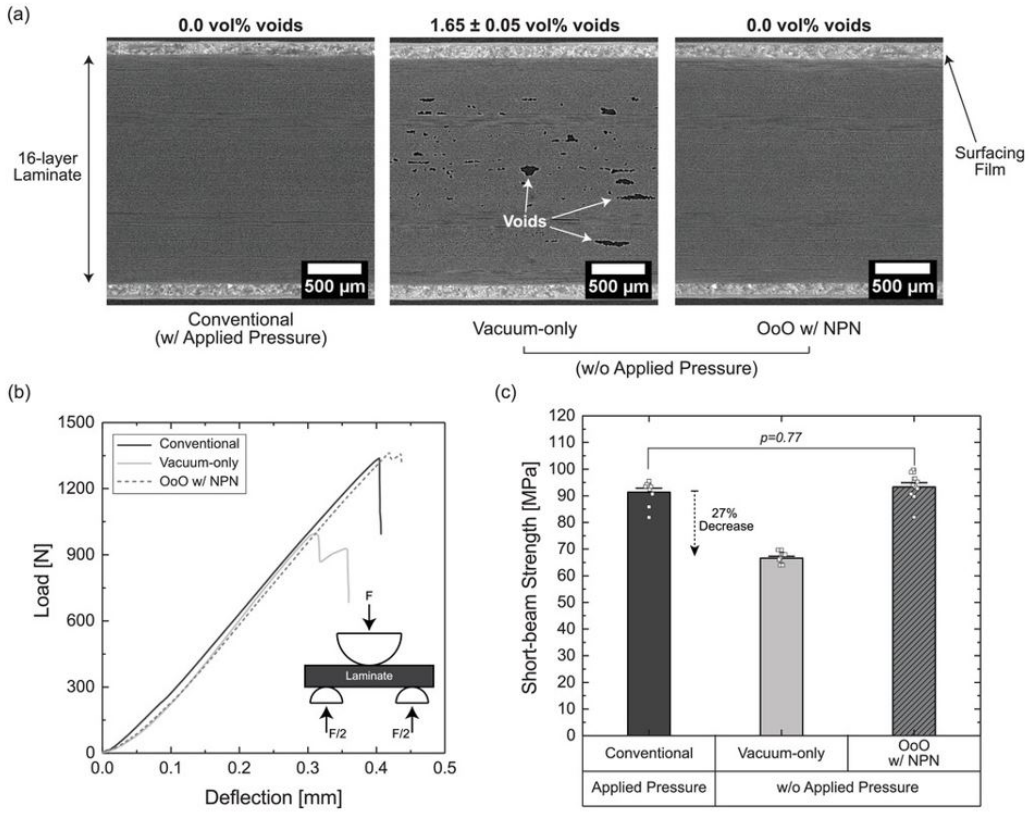

Figure 2-8: Aligned carbon nanotube (A-CNT) NPN materials enable VBO curing of autoclave-grade prepreg with: a) autoclave comparable void-free laminates and b) no reduction of short-beam (SBS) strength [39].

2.4 Electrospun Polymer Nanofiber (EPN) Films

Electrospun polymer nanofibers (EPNs) are a material class that has a multitude of industrial usages from biomedical applications, such as tissue engineering, to functional structural materials such as filtration or composite reinforcement [40, 41]. The nanofiber mats or films are manufactured by a high voltage electric force drawing charged threads of polymer solution. The high voltage is applied to the liquid droplet, charging it, and electrostatic forces stretch the droplet counteracting the surface tension. The liquid dries as it is deposited on the surface. This process enables nanometer-scale polymer fibers to be created. The fibers, when collected on a surface, form veils, mats, or films [42]. The fiber morphological properties can be tuned by the polymer characteristics including surface tension and viscosity, the pro-

cess parameters including voltage, federate capillary diameter, and shape, as well as environmental conditions including pressure, temperature, and humidity [42, 41, 43]. The thickness of the film is altered by how fast the deposit surface is removed. Thermoplastic materials are typically used as there is a good bond between the fibers and matrix for composite applications which facilitates improved fracture toughness. When utilizing thermoset resins for the EPN, there is less improvement in fracture toughness [43, 44, 45]. A popular EPN used is polyamide (PA) which is known commercially as Nylon. Polyamide is inexpensive, has relatively good mechanical properties in bulk and as individual nanofibers, a high melting temperature (compared to thermoset matrix cure temperatures), and is easily dissolved in a wide range of solvents [43]. By having the melting temperature higher than cure temperature, when the CFRP laminate cures, the nanofibers in the EPN film maintain their shape and therefore can be used for reinforcement.

EPN films are used for mechanical reinforcement of glass and carbon reinforced polymer composites. The EPN films are used due to their ability to be manufactured in thin film only a few microns thick, their low density, their high porosity enabling-resin infiltration, and low volume. The low volume enables low interlaminar thickness changes of only a few percent, as the material is additionally compressed when pressure is applied to the laminate during curing, helping minimize the interlaminar thickness. Additionally, the high surface area promotes good bonding [43, 46].

EPNs, when placed in the interlaminar region as an interlayer have been shown to improve mechanical properties including Mode I, Mode II interlaminar fracture toughness, compression after impact fatigue resistance, and vibrational damping. 1.5 gsm polyamide 66 was shown to improve Mode II critical strain energy release rate by 29% [47].

Thermosetting resins like epoxy tend to be brittle materials with little resistance to crack propagation. During delamination failure modes, cracks propagate through the matrix material. Two options to help address this are toughening the matrix with the addition of particles and inserting nanofiber mats as in the ply-ply interlayer. The nanofiber mat was seen to encourage nanofiber bridging [48], resin reinforcement

[49], and crack path modification [50] Toughening particles increase resin viscosity which can increase void content when curing in vacuum-bag-only conditions with OoA prepreg systems, but are a more common technology as they are included in the surface in CFRP prepreg in several aerospace autoclave CFRP systems in production of primary structures.

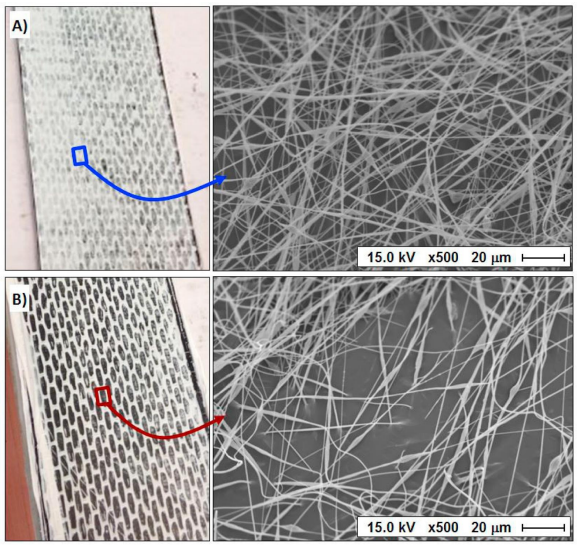

Figure 2-9: EPN films on a prepreg: a) initial layup and b) after a few minutes for due to resin infiltration [43].

2.5 Polymer Aerogel Material

Aerogels are a class of micro porous solids where the dispersed phase is a gas. They have ultra low densities, large surface areas, high porosity, low values of thermal conductivity and form three dimensional solid networks that can be highly cross linked. They are often formed by super critical drying to avoid structural collapse during manufacturing and have an air volume of 80-99% [51, 52]. Their large surface areas and nanoporosity (pores are 1-100 nm) make them good candidates as NPNs for polymer composites. Aerogels can be made out of a variety of materials including CNTs, graphene, polymers, chalcogenide, silica, etc. Traditional silica aerogel nanocomposites have been attempted [53, 54]. However, their properties were lost when polymer was mixed into the aerogel. When a carbon aerogel was integrated into the matrix

system of a CFRP laminate, modulus, strength, and interfacial properties increased. Mode I tests with a carbon 0.1 wt% aerogel showed delamination fraction energy increase from 265 J m^{-2} to 346 J m^{-2}. The delamination fracture energy caused by Mode II loading was increased from 655 J m^{-2} for the unmodified laminate to 1088 J m^{-2} for laminate modified with 0.5 wt% aerogel [55]. Aerogels form three dimensional hierarchical morphologies with large surface areas, porosities, and have ultra-low densities with some demonstrated reinforcement properties. Polymer aerogels will be explored in this thesis.

2.6 L-shape Composites

Composites can typically be categorized into three categories: flat panels, sandwich structures and complex geometries. Complex geometries are commonly used as stiffeners or to attach composite flat panels together. Stiffer cross sections come in various shapes. L, T, J, and hat shaped are most common and can be seen in Figure 2-10. Manufacturing defects, in particular fiber wrinkling leading to void formation, are common in these types of parts around the curved section [38, 56, 57]. When the part is put under load the complex section then develops a high stress concentration around the defect which leads to the laminate's failure. This reduces service life and leads to a decrease in the mechanical properties. The elimination of such manufacturing defects in the complex section leads to higher and longer performance before laminate failure [8].

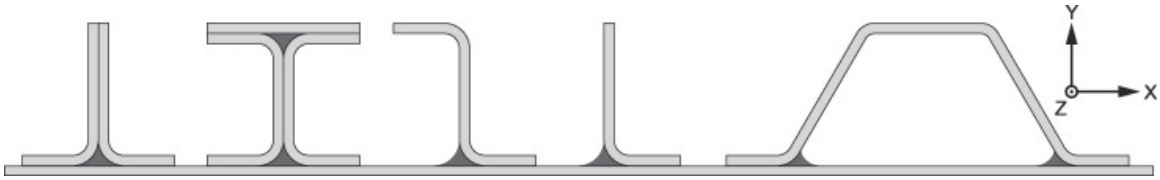

Figure 2-10: Common complex geometries, T,I,Z,L, and hat shaped stiffeners with corner fillers [58].

Interlaminar fiber wrinkling is the most prevalent manufacturing defect which directly influences the to interlaminar voids. This occurs along sharp curvatures of

complex composites and in laminates that include 90° plies as these transverse plies have little resistance to the deviatoric stresses from the mold geometry curvature or the pressure intensifier. Resin accumulation in the corners occurs in complex shaped laminated when laid up in a female mold as the corner is a low-pressure region which can cause low compaction and resin flow to that region causing corner thickening (see Figure 2-11) [59, 8]. To ensure a more uniform pressure distribution a caul sheet or a rubber pressure intensifier is often used [60, 61]. The amount of thickening changes based on layup orientation as well as mold geometry. A higher radius to thickness ratio corresponds to higher thickness variation [62]. There are two main drivers of corner thickening or thinning. The first is pressure and the second is friction (or lack of friction which is beneficial to corner quality) [63] and they impact compaction as seen in Figure 2-12. To reduce thickness variation and defects and thick laminates, ply-by-ply debulking every 3-5 plies is seen as critical to reduce void content [64]. Drapability or mold conformability is also an important factor. Laminates made with unidirectional (UD) prepreg have a tendency for fiber wrinkling due to low drapability. Therefore, plain and satin woven fabric has been seen as the more suitable prepreg system [65].

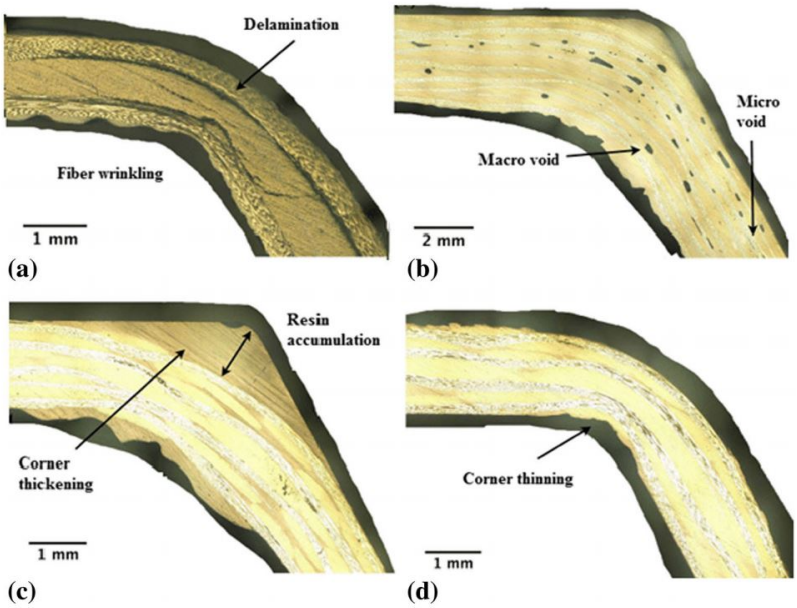

Figure 2-11: L-shape manufacturing defects: a) fiber wrinkling and delamination, b) micro and macro voids in between plies, c) corner thickening and resin accumulation and d) corner thinning [8].

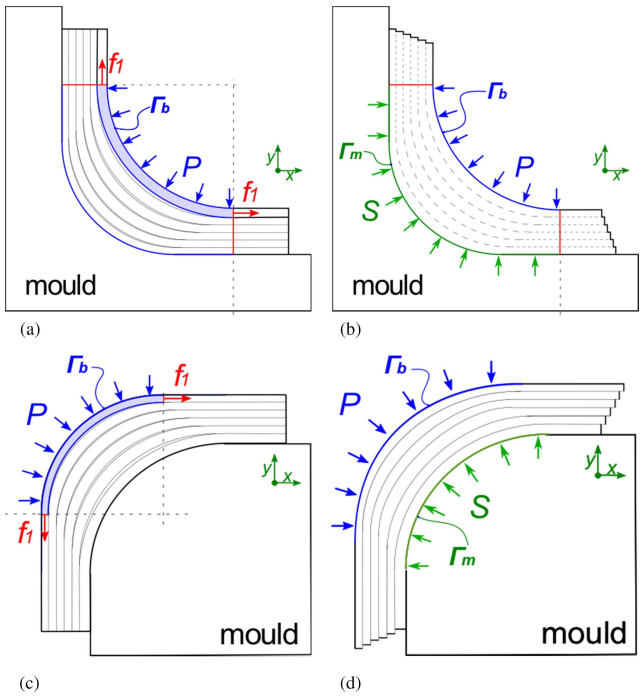

Figure 2-12: Diagrams of friction dominated L-shape manufacturing with no slip between plies and only the first ply considered: a) female mould, c) male mould; diagrams of pressure dominated scenarios with slippage and conformation of plies and the whole corner considered: b) female mould, and d) male mould [63].

Chapter 3

Objectives and General Approach

Chapter 2 discussed the challenges of autoclave manufacturing and the reasons why composites have specific requirements for void content due to the voids' negative effects on composite mechanical performance. Two different commercial NPN systems are explored for autoclave-prepreg CFRP in flat coupons, and preliminary studies completed into NPN application in complex (non-flat) geometries and different prepreg morphologies.

3.1 Objectives

The overarching objective of this work is to demonstrate next-generation composite manufacturing techniques for the creation of aerospace-grade advanced composite architectures. This is broken down into four discrete goals:

1. Identify and demonstrate a variety of commercial (and therefore scalable) NPN material systems (see Chapter 4)

2. Demonstrate the removal and elimination of voids in composite laminates made up of traditional autoclave unidirectional (UD) prepreg systems using commercial NPNs. These samples are made of autoclave-grade prepreg yet manufactured in a vacuum-bag-only (VBO) cure with

vacuum and temperature but without the use of an autoclave for pressure (see Chapter 4)

3. Confirm that there is no composite strength or quality degradation of the composite by using these NPN material systems (see Chapter 4), including evaluation the interlaminar region to make sure there is not a large interlaminar increase which would reduce the fiber volume fraction of the composite, void assessment and measuring the interlaminar shear strength as is is the most critical mechanical property to maintain for this NPN technology (see Chapter 4)

4. Expand the applicability of NPNs to woven prepreg morphologies and geometries enabling complex shapes to enhance the applicability of the NPN technology (see Chapter 5)

3.2 General Approach

The general approach employed is as follows:

• Obtain or manufacture NPN material systems. Commercially obtained NPN systems include a polyimide (PI) polymer aerogel and polyamide (PA) electrospun polymer nanofiber (EPN) films. Manufactured NPN systems include vertically aligned CNTs grown in a uniform forest pattern and in a grid like pattern to various heights via chemical vapor deposition (CVD)

• Characterization of the NPN material systems, typically via optical microscopy and/or scanning electron microscopy (SEM)

• Manufacture of specimens by layup including the transfer of the NPN layer to the prepreg. Layup and curing are done according to the manufacturer's recommendations except for the additional interply layers of NPN material and lack of applied pressure (i.e., VBO curing). Flat

samples were cured conductively on a hot plate under vacuum while complex geometry samples were cured convectively in an oven under vacuum.

• Assessment of laminate quality is completed via optical and scanning electron microscopy of polished cross-sections. Voids are assessed primarily via X-ray micro-computed tomography (μCT) with a focus on the interlaminar region. Interlaminar shear strength is evaluated by short beam shear (SBS) testing.

Details of each experiment can be found in the following chapters.

Chapter 4

Vacuum-bag-only (VBO) Composite Manufacturing of Unidirectional Autoclave-grade Prepreg Using Capillary Effects of Nanoporous Networks (NPNs)

While traditionally aerospace-grade composites are cured with capital- and operational-intensive thermal pressure vessels or autoclaves [17], a next generation processing technique, where voids are evacuated from a composite laminate, not by external pressure but by capillary pressure, is presented utilizing polymer based nanoporous networks (NPNs). The technique enables conduction or convection vacuum-bag-only (VBO) curing of traditional autoclave-grade prepreg material systems, and as discussed in Chapter 2, has been demonstrated using a conduction cure with aligned carbon nanotubes (A-CNTs) as an NPN in a lab scale environment [10]. Utilizing autoclave-grade prepreg systems enables a diverse selection of certified and widely studied materials to be manufactured in vacuum-bag-only conditions. These traditional materials do not contain morphology or polymer rheology modifications that

comprise out-of-autoclave (OoA) prepeg systems [3], which are limited in the number of certified materials due to the additional testing required that costs millions of dollars and spans 15-20 years to complete [66]. This chapter demonstrates a technique utilizing two NPN material systems: commercial electrospun polymer nanofiber (EPN) films with polyamide (PA) nanofibers and a bespoke polyimide (PI) aerogel, both having commercial scale capabilities. These polymer-based NPN systems have different morphologies and manufacturing techniques. The EPN material group utilizes two different polyamide variants: common PA 66 (Nylon 66), and PA XD10 (Lexter®), the latter of which is a thermoplastic bio-inspired polyamide resin developed by Mitsubishi Gas and Chemical Company. The XD10 resin, 8000 variant, has a melting point of 190°C, a bending modulus of 3.2 GPa, bending strength of 136 MPa, density of 1.13 g/cm^3, and saturated water gain of 2.4% [67, 68]. µCT images show interlaminar void elimination when the NPN systems are applied to the interlaminar region as an interlayer while an autoclave-grade prepreg laminate is cured under VBO conditions. Presented is the manufacturing process of the NPN applied composites, SEM images and characterization of the NPN, void content of the cured composites, mechanical testing of specimens made with the electrospun polyamide NPNs, and an interlaminar region thickness analysis. Results are compared to laminates cured via VBO without NPN interlayers and to autoclave-processed composites as a baseline for the same material system. The alternative-NPN polymer materials and the NPN approach shows great capability as the NPN material system can be transferred directly to a prepreg before layup, or likely applied in an automated layup capable manner, thereby enabling practical autoclave-less curing of autoclave-grade prepreg.

4.1 Background

Diverse industries including aerospace, wind, solar, automobile, and civil have been utilizing the lightweight but strong material performance of advanced fiber reinforced polymer (FRP) composites in large and small structures [7, 3, 10]. A keystone manufacturing technique for carbon fiber FRPs (CFRPs) has been the utilization of a

material system designated as a prepreg, in which continuous fibers (carbon, glass, etc.) are pre-impregnated with a resin (thermoset or thermoplastic) to form a layer of, typically, between 0.1 and 0.3 mm thick. These layers are then cut to the desired shape and laid up or stacked on one another, after rotating the orientation of the fibers as needed, to achieve a laminate with desired properties. Prepreg is often used due to the high fiber volumes, reproducibility, and low void content of the laminates [12]. The standard prepreg is autoclave-grade, meaning it is engineered to be cured under vacuum at up to -0.1 MPa (-1 bar), with applied pressure of 0.5-1.4 MPa (5-14 bar) in an autoclave, with the most common being 0.7 MPa (7 bar). The applied vacuum causes an atmospheric pressure of 0.1 MPa (1 bar) to be applied on the laminate [5, 69]. This manufacturing technique obtains repeatable high quality laminates as the applied pressure, in combination with the part under vacuum, removes the entrapped voids or air pockets that form during the prepreg and layup processes while suppressing new voids from developing [3]. For aerospace applications, a void allowance of around 1% is considered acceptable, with autoclave-processed composites typically generating voids that are immeasurably small given common techniques such as ultrasonic C-scan. In other commercial applications, a void percentage of 3-5% can be acceptable [70]. Voids can lead to severe degradation of composite part performance and lifespan. Specifically, they degrade the composite's polymer matrix dominated properties such as interlaminar shear, transverse tensile strength, and fatigue resistance [29]. While the void percentage specifications appear to be minimal at first glance, composites have strict requirements as the effects of voids can be significant. Only a 1-3% increase in void content can decrease the mechanical properties by up to 20% [71]. Voids act as crack initiation sites and can allow moisture penetration [29, 11]. While providing the highest-quality and repeatable laminates, autoclave manufacturing has some major commercial drawbacks. In particular, the autoclave pressure vessels require high capital cost, long heating and cooling cycles limiting cycle frequency, high energy use, inert gas (often nitrogen) to pressurize, and are size-fixed, which limits maximum part size and run efficiencies when not filled [3]. Due to these drawbacks, there has been research on alternative methods to man-

ufacture high quality composites without an autoclave, in a VBO cure, where only vacuum is applied with no external pressure. The most common of these currently is the OoA prepreg material system that is engineered to be cured without a pressure vessel.

OoA prepreg materials have their resin chemistry altered to prevent gas from being released during curing (out-gassing) and are engineered to have partially impregnated microstructures to become "breathable" with both dry and resin rich areas. The dry fiber regions, which act as void extraction channels, are next to resin-rich regions [3]. The extraction channels increase the in-plane permeability and the dry fiber pockets enable the entrapped air voids to be extracted through these channels to the laminate edge. The voids are then evacuated from the vacuum bag by the vacuum pump. The dry regions become impregnated with resin as the resin flows from the resin-rich regions. This OoA prepreg technology allows the composite to be cured without additional pressure, enabling VBO oven curing, which enables lower manufacturing cost due to lower capital and operational costs [17]. However, OoA prepreg systems have some key drawbacks. In particular, the morphology changes with the addition of the dry fiber void extraction channels and the altered resin chemistry [3]. Additionally, the OoA prepreg often requires an extended debulking step where the laminate is subjected to vacuum pressure. This can last up to 16 hours and may need to be done every laid ply (i.e., ply-by-ply debulking) depending on the laminate and material system [9]. These changes increase the layup processing time due to the extra debulking steps while limiting the variety of certified materials for aerospace use due to resin and morphology modifications which require lengthy certification testing. Here is presented the ability to cure composites without an autoclave, without the morphology changes, extra debulking steps, or resin modifications that OoA materials have, and rather utilizing autoclave-grade prepreg, which has a diverse selection of already certified material options with aerogel and EPN polymers. The NPN materials have porosities of 80% or above for void evacuation channels. Implementing the NPN at all ply interfaces enables a void evacuation channel to be a maximum of half a ply thickness away from any point in the laminate. As the resin's viscosity decreases

with an increase in temperature during curing, the capillary pressure caused by the NPN encourages resin infiltration into the NPN in the interlaminar region. Due to the NPN's compressible nature, the NPN-comprised interlayer shrinks in thickness during manufacture and cure of the composite.

4.2 Materials and Methods

The effects of the integration of two NPN material systems, electrospun PA nanofibers and a PI aerogel, into a laminate's interlaminar regions are analyzed. The composite void content is found using X-ray micro-computed tomography (µCT), while the interlaminar region thickness is analyzed primarily by optical microscopy but also secondarily by scanning electron microscope (SEM) and µCT. Composite interlaminar shear strength is tested via short beam shear testing. Interlaminar region thickness is documented for comparison to non-NPN processed samples. The engineering goal would be to achieve void-free laminates integrating novel commercially available non-porous material systems, with autoclave-grade prepreg cured without applied pressure, that have similar properties and performance similar to A-CNT NPNs [72, 39].

4.2.1 General Composite Manufacturing Process

The work presented in this chapter utilizes unidirectional (UD) IM7/8552 which is an aerospace-grade carbon fiber prepreg designed to be cured with applied pressure under vacuum. It has a nominal cured ply thickness of 0.131 mm. The target fiber volume fraction is 57.7 vol% with a fiber density of 1.77 g/cm^3 [73]. Driven by the short beam shear standard, ASTM D2344, which utilizes a nominal 2 mm thickness, a 16-ply quasi-isotropic layup of $[0/90/\pm 45]_{2S}$ was used, giving a nominal thickness of 2.10 mm. The stacking sequence is seen in Figure 4-1.

The plies were cut to the desired specimen dimension. The first ply had its protective film removed and placed on a sheet of peel ply material in its desired orientation. A roller was then used to push firmly against the material before the backing sheet was removed. When an interface is to receive a NPN interlayer, the

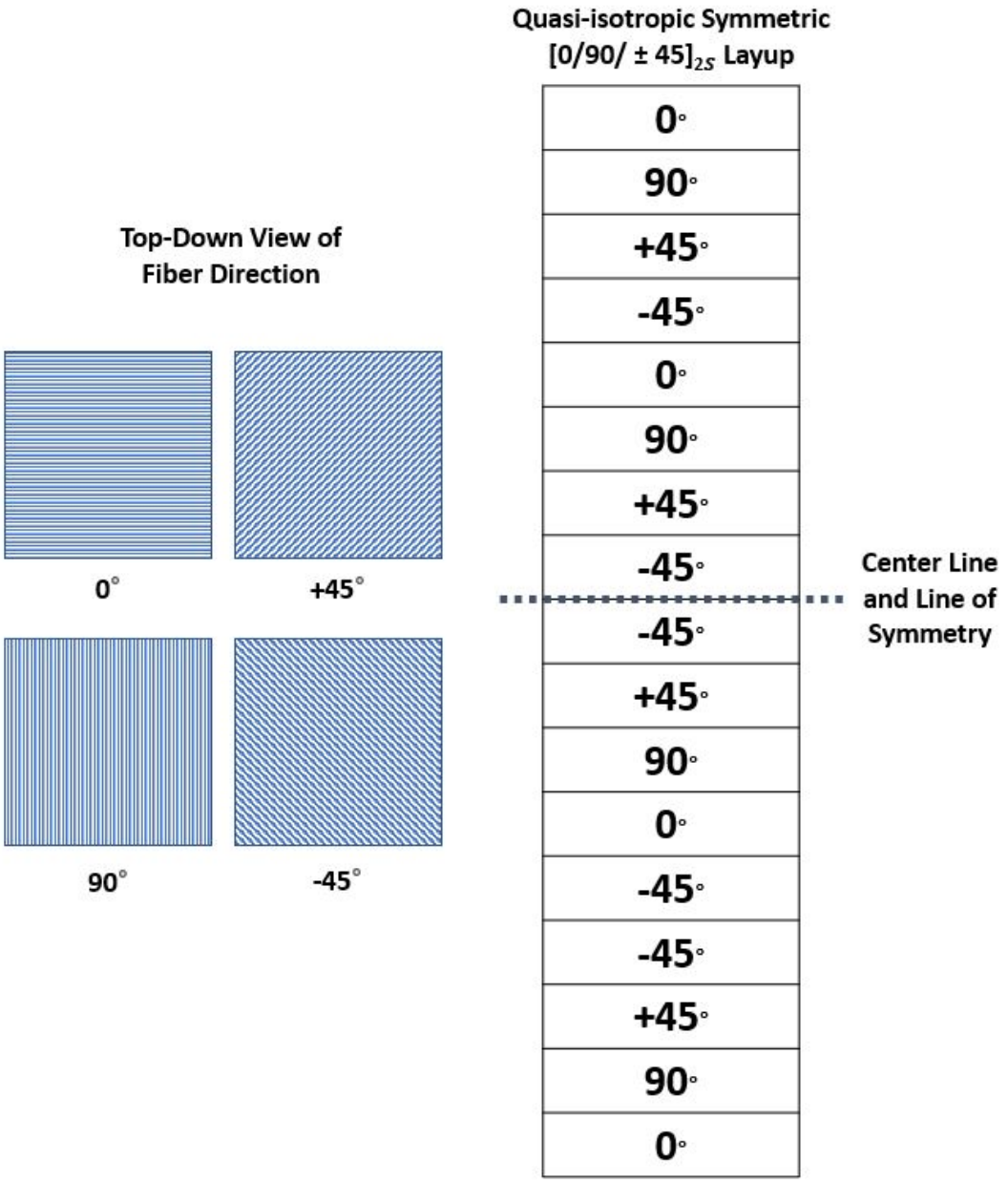

Figure 4-1: Ply orientation and layup schematic of 16-ply quasi-isotropic laminate with $[0/90/\pm 45]_{2S}$ orientation.

NPN was applied following the developed method: the NPN was cut larger than the specimen by 5 mm on each side, placed on the laminate, rolled firmly, and its backing paper removed. The oversized cut of NPN ensures full edge to edge coverage of the laminate. The process was repeated, ply-on-ply or ply-on-NPN, as determined by the stacking sequence and the desired NPN locations. After the last ply was placed, the edges were trimmed to ensure breathability (a common practice for OoA prepreg as well) and bagging materials were added to complete the vacuum bag layup process.

The bagging materials used include: guaranteed nonporous Teflon (GNPT) film (Airtech Release Ease 234 TFNP), breather (Airtech Release Ease 234 TFNP), 1 mm thick aluminum caul plate, 2.5 mm thick fiberglass plate, and a 2.25 mm tall cork dam. GNPT film was utilized as a base layer to prevent any resin that would bleed through the peel ply from attaching to either the hot plate or the caul plate. A caul plate on the laminate and an additional fiberglass plate (placed on top of the caul plate to make certain the bagging stacking sequence was higher than the cork dam) ensured that an even atmosphere pressure was exerted on the laminate (due to the setup being under vacuum). The cork dam prevents a pinching of laminate edges so as to make edges breathable while preventing resin bleed and the breather ensures vacuum is pulled from across the whole bag layup area, preventing a pinch in the bag from occurring, which would limit a uniform vacuum pull of the bagged area. These additional materials were added according to Figure 4-2 based on manufacturer recommendations [73].

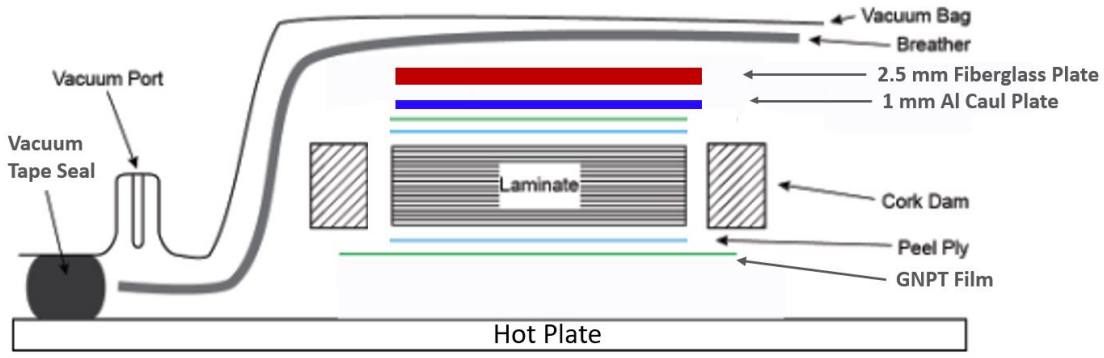

Figure 4-2: Vacuum bag layup diagram showing material and stacking sequence.

A programmable hot plate (Torey Pines EchoTherm HS60A) was utilized as the thermal element for the flat plate VBO curing. The sample underwent a 180-minute (3 hr.) debulk at room temperature before the VBO cure cycle shown in Figure 4-3. The cure cycle was ramp to temperature of 110°C at 2°C per minute with a hold time of 60 minute (1 hr.), ramp to a post cure temperature of 180°C at 2°C per minute with a hold of 120 minute (2 hr.), and then cool at 2-5°C per minute. Vacuum of -1 bar was pulled throughout the cure with no applied pressure. The VBO cure cycle can be seen in Figure 4-3 compared to the autoclave cure- manufacturer recommended cure cycle (MRCC).

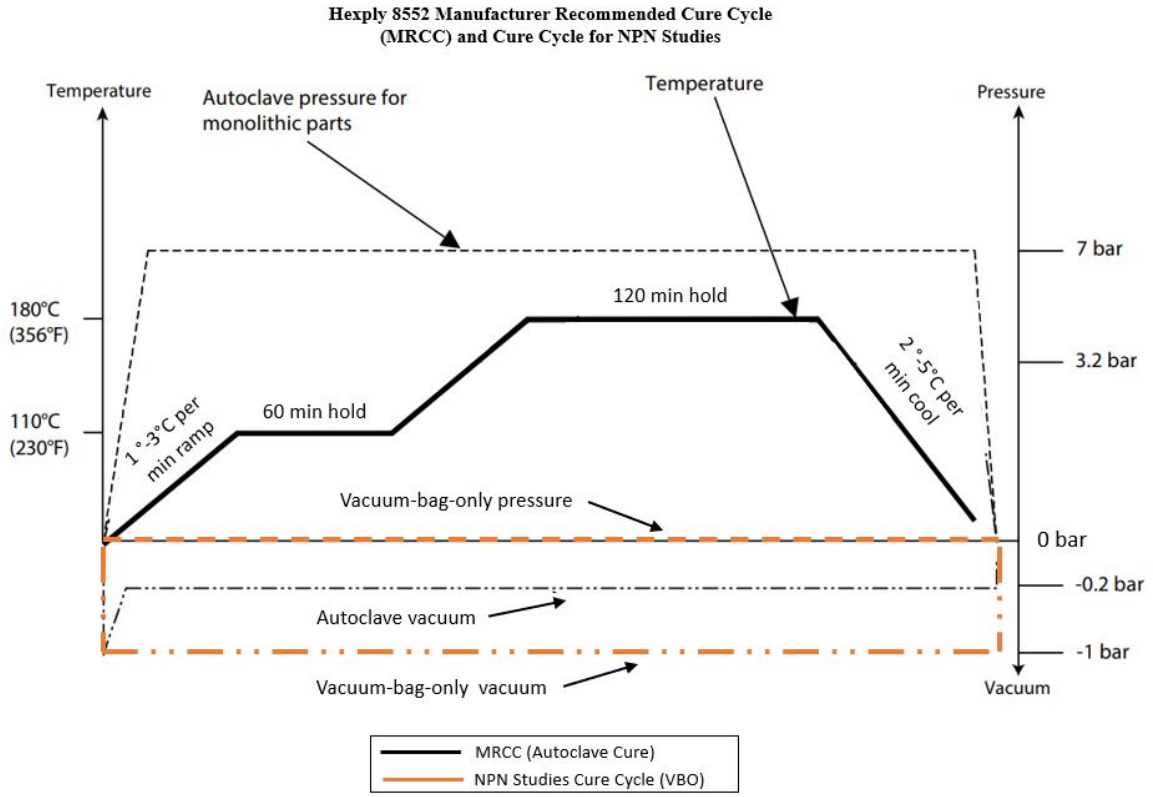

Figure 4-3: Hexply 8552 manufacturer recommended cure cycle (MRCC) [73] (black), and VBO cure cycle used (orange) used in this work for NPN studies. The temperature profile follows the MRCC, but with -1 bar vacuum and no applied pressure (orange dashed lines) throughout the cure.

4.2.2 Polymer Nanofiber Diameter Analysis

The electrospun nanofibers' diameters were analyzed using taken top-down SEM images of the nanofibers and the open-source software ImageJ, utilizing the DiameterJ toolbox [74]. The diagram, showing the open-source code method of fiber diameter measurement, is presented in Figure 4-4i followed by the process of image segmentation and then the histogram of the fibers diameters. The PA XD10 nanofibers with manufacturer specified nanofiber diameter of 230 nm was found to have diameter of 248 nm with a standard error of ± 0.92 nm. The PA 66 nanofibers with a manufacturer specified diameter of 150 nm was measured to have a diameter 153 nm with a standard error of ± 0.32 nm and depicted in Figure 4-4ii.

4.2.3 µCT Imaging and Void Analysis

Void content is important as it effects the strength and fatigue performance of composites [71]. High resolution µCT imaging is a method of imaging the 3D location, size, and quantity of voids distributed throughout a sample. The non-destructive nature of this technique enables imaging of samples before mechanical tests are performed, enabling the correlation between mechanical properties and void percentage. µCT was conducted at the Institute for Soldier Nanotechnology (ISN) at MIT. The scans utilized the Zeiss Xradia Versa High-Resolution 3D X-ray Imaging System as seen in Figure 4-5. The tungsten source was set to an X-ray energy of 80 kV and 7 W with no filter applied (apart from the ambient air). The scan isotropic pixel size is between 1.25 and 1.5 µm, giving a resolution of 4-5 µm. The specimens were rotated 360 degrees with 3201 projections taken per scan with the exposure time varying between 2.4-4.5 seconds depending on the sample thickness. The images were reconstructed utilizing the manufacture's reconstruction software and exported as 2D slices in .tiff format. The reconstructed slices were imported into ImageJ where void analysis was performed.

Void percentage analysis was conducted in ImageJ. The procedure is seen in Figure 4-6 and is as follows: 1) The 2D µCT slices are imported and auto contrast is applied.

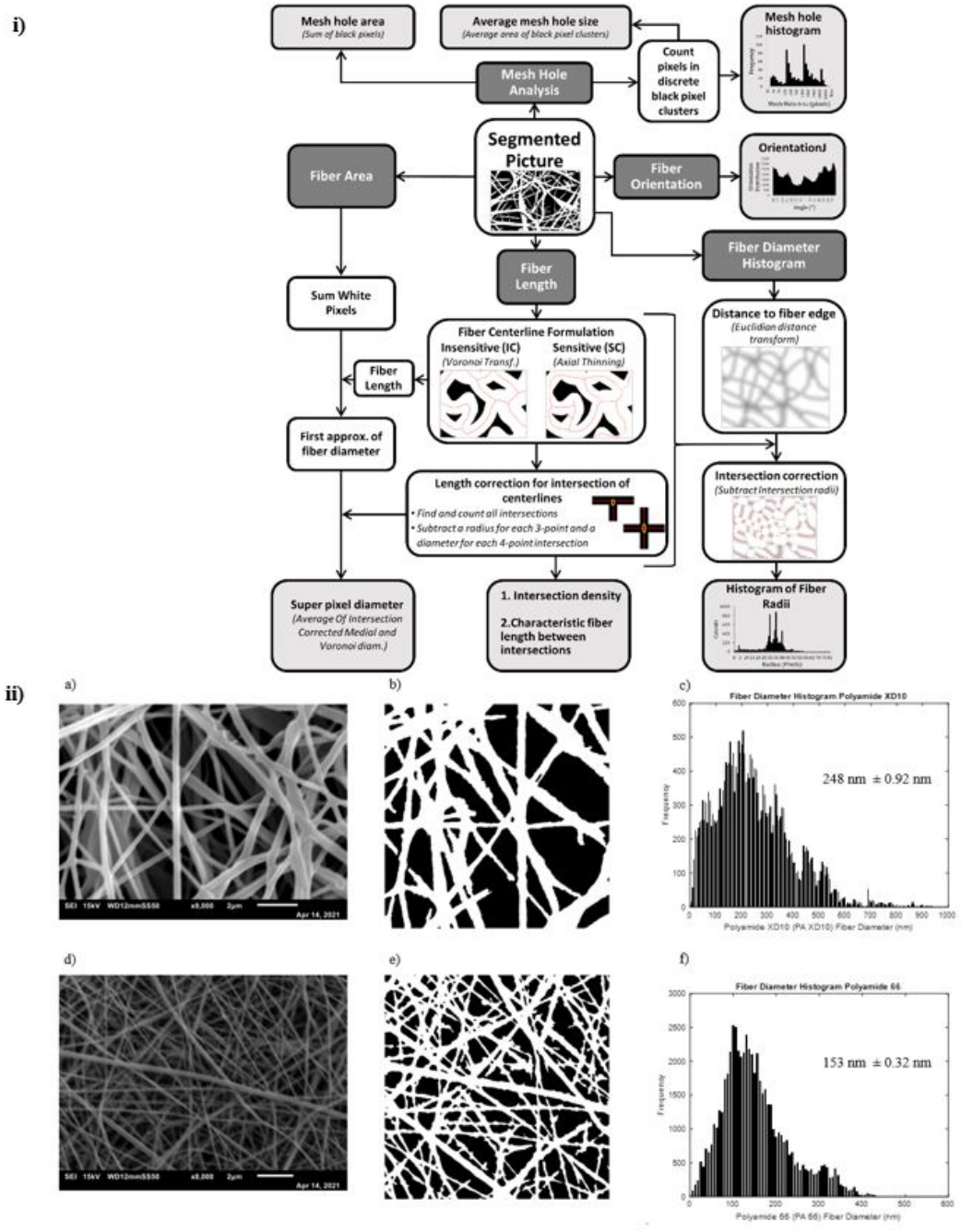

Figure 4-4: Polymer nanofiber diameter measurement figures showing i) ImageJ fiber diameter segmentation method [74] and ii) segmentations of polyamide (PA) fibers. The corresponding SEM image is provided followed by the thresholded image and resulting fiber diameter histogram. Polyamide XD10 (PA XD10) nanofibers with manufacturer specified fiber diameter of 230 nm are shown in a-c. Polyamide 66 (PA 66) nanofibers with a manufacturer specified diameter of 150 nm are shown in d-f. The measured PA XD10 nanofiber diameter was 248 nm with a standard error of ±0.92 nm. The measured PA 66 nanofiber diameter was 153 nm with a standard error of ±0.32 nm.

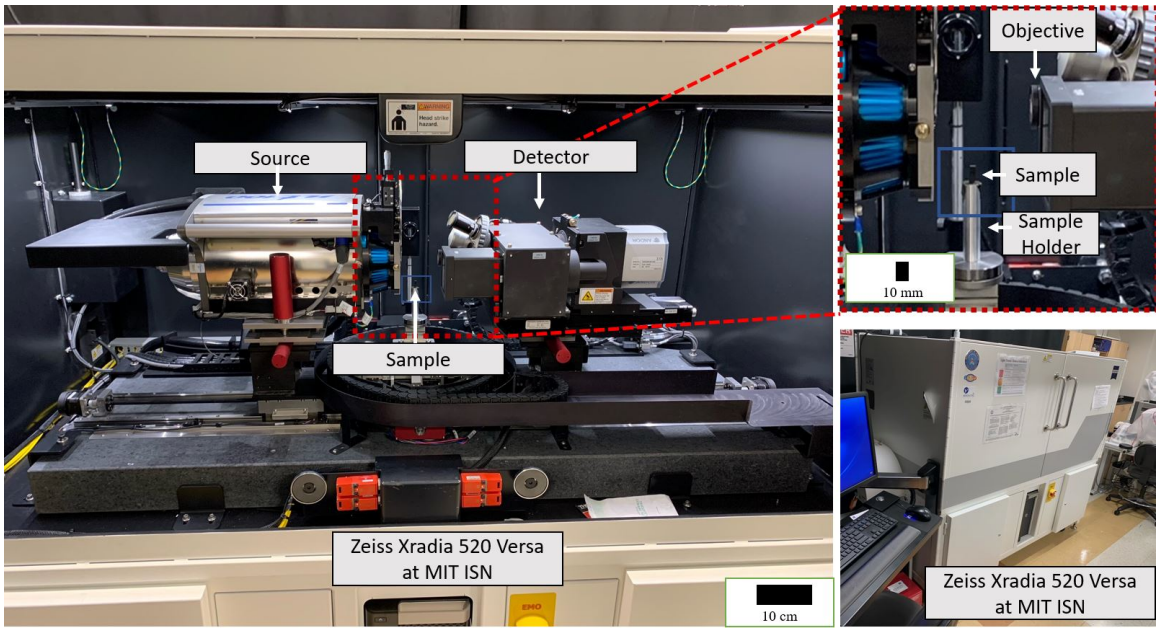

Figure 4-5: µCT setup inside Zeiss Xradia 520 Versa for scanning composite samples at MIT ISN.

2) The slices are despeckled and a mean blur filter of 3 pixels is applied to help better differentiate the voids from the individual fibers. 3) The images are thresholded to draw contrast between the voids (black) and the composite (white). 4) The images are cropped to remove the edge effects at the top and bottom of the scan images. 5) ImageJ's particle analysis tool is used to obtain void content percentage. A void content percentage of each 2D slice is found, and the mean and standard error (SE) are calculated from the whole volume.

4.2.4 Short Beam Shear (SBS) Testing

SBS testing is utilized for material performance comparison under shear like conditions and measures interlaminar shear strength (ILSS). ASTM D2344 was followed to obtain short-beam strength, a common measure of ILSS, of the specimens. The specimens' dimensions were nominally 12 mm × 4 mm × 2 mm (length × width × thickness). The specimens were cut from a 16-ply IM7/8552 laminate that was 15 cm × 15 cm (6 in × 6 in before edges were trimmed) composite laminate laid up as $[0/90/\pm 45]_{2S}$. A two-degree ply offset was used in the center, where two plies

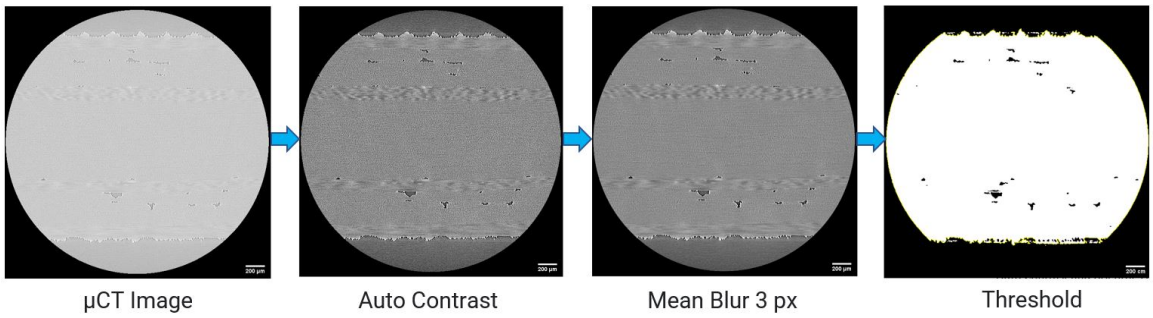

Figure 4-6: Process of segmenting image for void percentage analysis in ImageJ. The µCT slices are imported and auto contrast is applied. A mean blur filter of 3 pixels is applied to help better differentiate the voids from the individual fibers. The image is thresholded to draw contrast between the voids (black) and the composite (white). Particle analysis is completed on thresholded voids. This exemplary specimen is a 16 ply quasi-isotropic layup with IM7/8552 with the 20 µm PI aerogel in the middle 5 interfaces.

of the same orientation met, to limit the nesting of the carbon fibers of these two plies, which otherwise can give a non-conservative value of strength and contribute negatively to specimen-to-specimen variation/error. The samples were cut from the large laminate with a diamond coated band saw before being polished on a Struers TegraPol-21 grinder polisher. The short beam shear samples were polished at 320, 400, 500, 800, and 1200 American grit sandpaper (P400, P800, P1200, P2400, P1000 European grit) to remove rough edges and small cracks that might have occurred during the cutting of the laminate, or uneven surfaces. A three-point bend steel fixture with a loading nose diameter of 6 mm, support rods with diameters of 3 mm, and a span of four times the laminate thickness (nominally 8 mm) followed the ASTM D2344 standard. The loading nose was lowered at a rate of 1 mm per minute utilizing a mechanical testing machine (Zwick/Roell Z010). Figure 4-7 displays the specimen dimensions and mechanical testing set up. The thickness (t_{sbs}) and width (w_{sbs}) of each specimen was measured with a digital micrometer before being loaded on the test set-up. The maximum load observed during the test (P_m) was recorded. Short-beam strength (σ^{sbs}) was calculated following Equation 4.1:

It must be noted that SBS presents shear like values and not necessarily pure interlaminar shear due to different failure modes such as irregular interlaminar shear,

$$\sigma^{sbs} = 0.75 \times \frac{P_m}{t_{sbs} \times w_{sbs}} \tag{4.1}$$

tension, plastic deformation, and compression. More complex methodologies such as the Iosipescu shear test or v-notched rail shear test should be utilized for pure shear strength values. However, SBS is commonly used as a benchmarking tool for shear strength comparison [75].

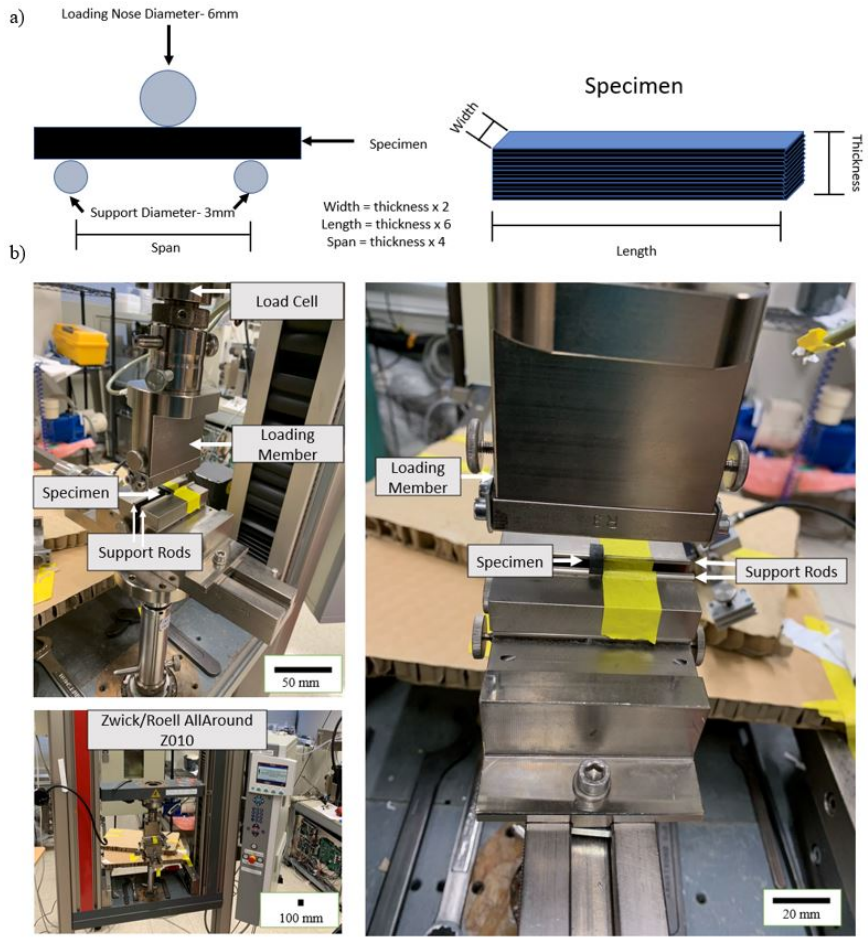

Figure 4-7: Short-beam strength mechanical testing: a) sample dimensional setup following ASTM D2344, and b) Zwick/Roell Z010 sample setup at MIT ISN.

4.3 Electrospun Polymer Nanofiber (EPN) NPN Films for VBO Curing

The polyamide nanofibers are manufactured by NanoLayr (formally known as Revolution Fibres until May 2021). The polyamide 66 (Nylon 66) came from the Xantu.Layr XLA Series, and the polyamide XD10 (poly-xylylenesebacamide, XD10, known as Lexter®) came from the Xantu.Layr XLB Series. Both materials have a manufacturer given porosity of 80 vol% [76]. The nanofibers form non-woven mats or films of continuous polymer nanofibers. The polyamide 66 (PA 66) nanofiber film and the polyamide XD10 (PA XD10) film have manufacturer stated nanofiber diameters of 150 nm and 230 nm respectively. The films, likewise, had measured nanofiber diameters of 153 nm and 248 nm (Figure 4-4), similar to the manufacturer's stated fiber diameter. SEM images were taken utilizing a JEOL JSM-6010LA machine under 15 kV. Before imaging, both the aerogel and the nanofibers were gold (Au) coated using a SC 7640 sputter with a discharge voltage of 2200 V for 90 seconds for a target thickness of 12 nm. The thickness of the PA 66 at 4.5 gsm was 120 µm and the thickness of the PA XD10 at 1.5 gsm was 9 µm as measured by SEM. The SEM images showing thickness are pictured in Figure 4-8. Additionally, the thickness was measured by a micrometer (Mitutoyo 293-344-30 Digimatic Micrometer). The measured PA 66 at 4.5 gsm nanofiber mat was 23 µm and 1.5 gsm PA XD10 nanofiber mat was 8 µm. As the SEM image for the PA 66 at 4.5 gsm had out of focus areas as seen in Figure 4-8 with an in focus area of ∼20 µm, it is concluded that the 120 µm area is due to edge effects (both from the specimen preparation and the SEM focus) and not the true representation. As such, the thicknesses was determined to be 8 µm and 23 µm following the micrometer reading and is used throughout this thesis.

16-ply quasi-isotropic specimens were first manufactured with a planar area of 2.54 cm × 2.54 cm (1 in × 1 in) according to Section 4.2.1 in three different variations. The first variation had no NPN in any of the ply interfaces, the second had 4.5 gsm 23 µm PA 66 NPN at only the middle seven interfaces, and the third had the 4.5 gsm 23 µm PA 66 NPN at all 15 interfaces. The specimens were scanned with the µCT.

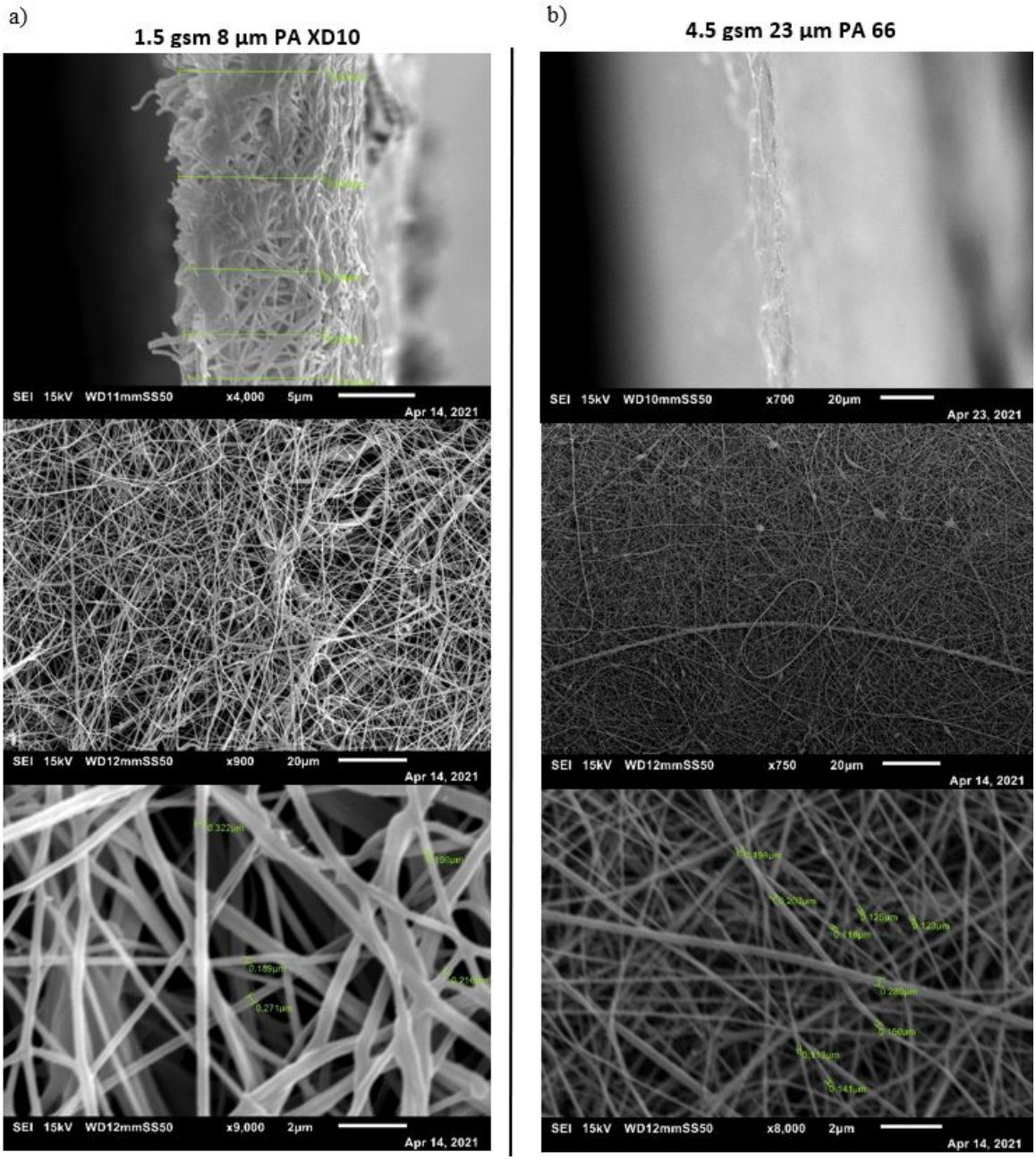

Figure 4-8: SEM scans of polyamide nanofibers. SEM images of: a) 1.5 gsm 8 µm PA XD10 and b) 4.5 gsm 23 µm PA 66. The top image is taken at a 90° angle to show the thickness. The middle and bottom images are top down views. The micrometer measured the 1.5 gsm PA XD10 at 8 µm and the 4.5 gsm PA 66 at 23 µm.

In the interfaces where the 4.5 gsm 23 µm PA 66 NPN was inserted, there were no interlaminar voids as seen in Figure 4-9. In the regions that had no NPN interlayer, there were interlaminar voids. The void elimination can be observed in the specimen with only the middle seven interlaminar regions having the NPN, where the regions without NPN interlayers clearly have voids. Comparing the hot plate cure with 4.5 gsm 23 µm PA 66 NPN in all interlaminar regions to the hot plate cure without NPN, the void percentage is 0.0 vol% compared to 1.62 vol%. Complete void removal was also obtained when utilizing the 1.5 gsm 8 µm thick PA XD10 nanofiber NPN in all interlaminar regions as seen in Figure 4-10.

Next, 15.24 cm × 15.24 cm (6 in × 6 in) samples were manufactured according to Section 4.2.1 with NPN at all interfaces and µCT scan was completed to assess voids at an isotropic voxel size of of 1.3 µm. SBS testing was completed according to Section 4.2.4 following the ASTM D2344 standard. The results can be seen in Figure 4-11. In all cases, failure occurred via plastic deformation around the loading nose followed by interlaminar shear failure. Following ASTM D2344, this was the valid mode of failure. The short-beam strength of the baseline (i.e., autoclave-cured specimens without NPN) was 96.8 MPa (SE = 1.35) [77] and the sample hot plate cured without NPN was 82.3 MPa (SE = 2.68). The hot plate cured sample with 4.5 gsm 23 µm PA 66 NPN in all interlaminar regions had a short-beam strength of 104.1 MPa (SE = 1.14) and the hot plate cured sample with 1.5 gsm 8 µm PA XD10 NPN in the interlaminar region had a short-beam strength of 97.6 MPa (SE = 1.51), increases of 7.5% and 0.7% respectively over the autoclave cured baseline. While the short-beam strength of the 1.5 gsm 8 µm PA XD10 is above that of the baseline, it falls within the standard error. Therefore, it can be concluded that there is no significant difference between the two specimens. The hot plate cure with 4.5 gsm 23 µm PA 66 in all interfaces with a 104.1 MPa short-beam strength is 7.5% higher than the baseline outside the standard error. Large interlaminar regions reduce the fiber volume fraction, a key metric in composite strength. As such an objective was to minimize the interlaminar thickness. The specimens that were hot plate cured without NPN in the interlaminar region had an interlaminar region thickness of 1-

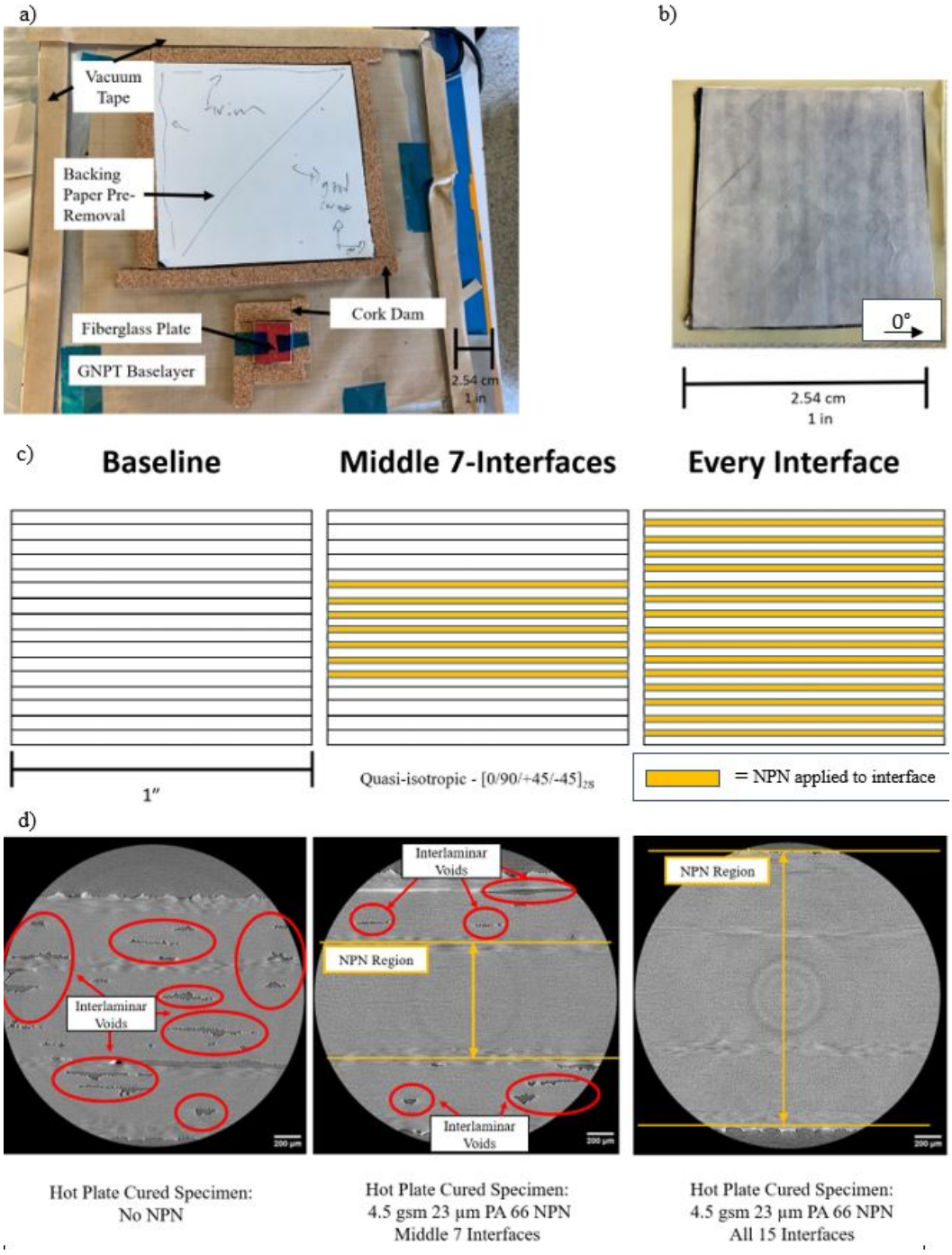

Figure 4-9: IM7/8552 layup images of: a) prebagging manufacturing set up, and b) midlayup laminate. The white film is the 1.5 gsm 8 µm PA XD10 NPN nanofibers and the underneath black square is a UD IM7/8552 ply at 90°. c) Diagram of laminate layup with the gold lines representing the 4.5 gsm 23 µm PA 66 NPN interlayers. d) Representative µCT slices of the cured samples. The hot plate cured specimen without NPN interlayers had a void content percentage of 1.62 vol% compared to no measured voids when the NPN was applied. In the specimen with NPN interlayers applied to only middle seven interfaces, those interfaces are void-free while voids are observed in the non-NPN interfaces.

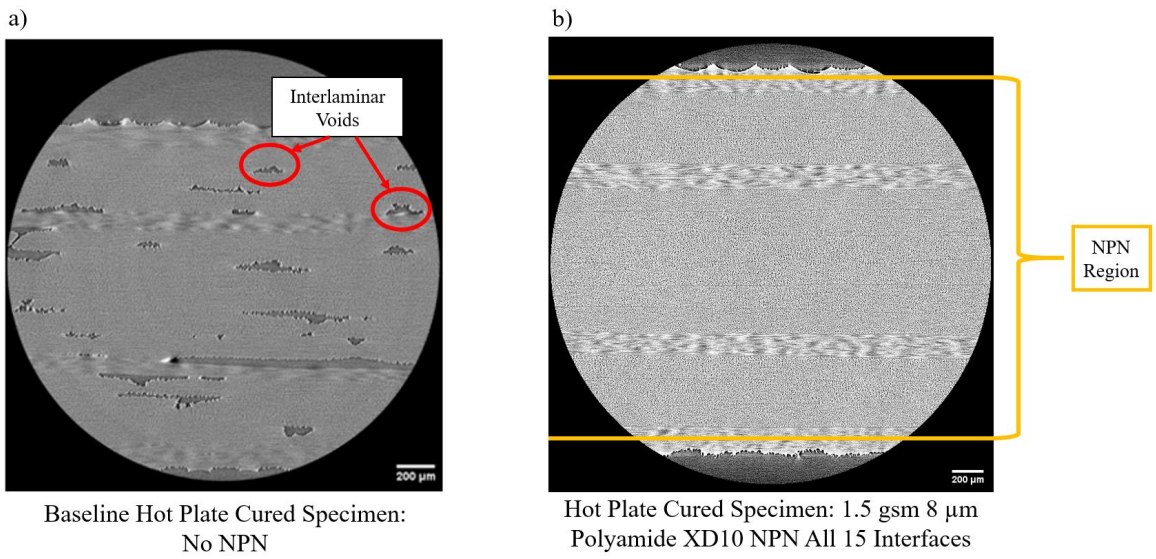

Figure 4-10: Representative µCT scans comparing: a) a hot plate cured specimen without NPN, and b) a hot plate cured specimen with 1.5 gsm 8 µm PA XD10 in all interlaminar regions.

2 µm, while specimens with 1.5 gsm 8 µm PA XD10 and 4.5 gsm 23 µm PA 66 had interlaminar regions of 5-7 µm and 10-15 µm respectively. The high values of short-beam strength is thought to be from the increased resin-rich interlaminar region with thermoplastic filler especially in the 4.5 gsm 23 µm PA 66 case. A comparison of the interlaminar thicknesses of specimens made without NPN and 1.5 gsm 8 µm PA XD10 interlayers can be seen in Figure 4-16. Table 4.1 additionally compares the short-beam strength values with previous autoclave cured samples made with IM7/8552 with aligned CNTs and buckled CNTs as reinforcing interlayers [77].

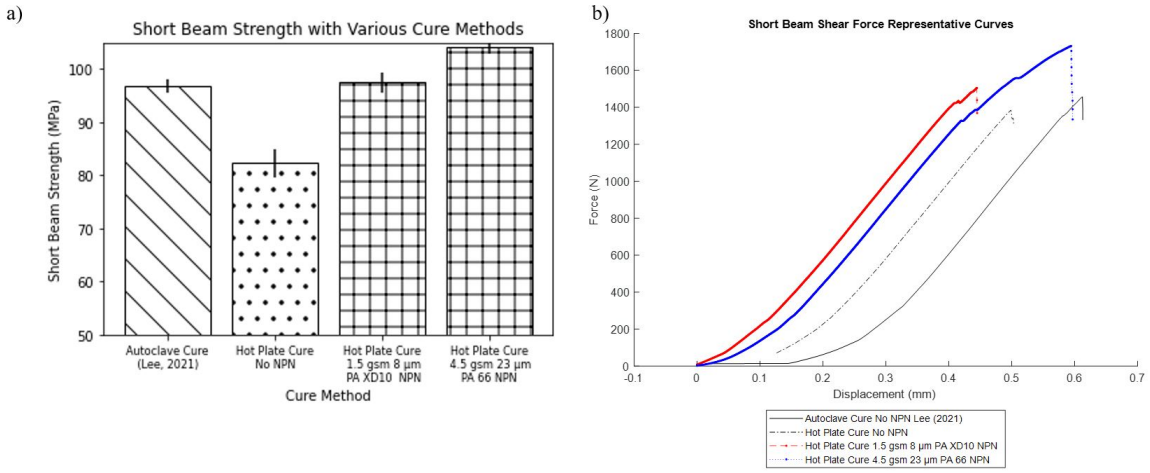

Figure 4-11: Short-beam strength comparison with various cure methods with and without PA NPNs displaying: a) average values, standard error, and b) representative short beam shear test load-force displacement curves, where displacement is shifted for clarity. Autoclave cure data was previously reported in [77].

Table 4.1: Table of values for short-beam strength and standard error of samples cured with various methods and NPN interlayers. Autoclave cure data was previously reported in [77].

Manufacturing Method	**Short-beam Strength (MPa)**	**Standard Error (+/-)**	**Percent Difference from Autoclave Cured No NPN**
Autoclave Cured No NPN	96.8	1.35	N/A
Hot Plate Cured No NPN	82.3	2.68	-15.0%
Hot Plate Cured 1.5 gsm 8 µm PA XD10 NPN	97.6	1.51	None
Hot Plate Cured 4.5 gsm 23 µm PA 66 NPN	104.1	1.14	+7.54%
Autoclave Cured 20 µm Tall Aligned Carbon Nanotube NPN	100.9	1.39	+4.24%
Autoclave Cured 10 µm Tall Buckled Carbon Nanotube NPN	104.0	2.24	+7.43%

4.4 Polyimide Aerogel NPN Films for VBO Curing

A bespoke PI aerogel was obtained from Aerogel Technologies LLC with a stated manufacturer porosity of 96%. The measured thickness of 20 µm and pores can be observed in SEM and optical images in Figure 4-12.

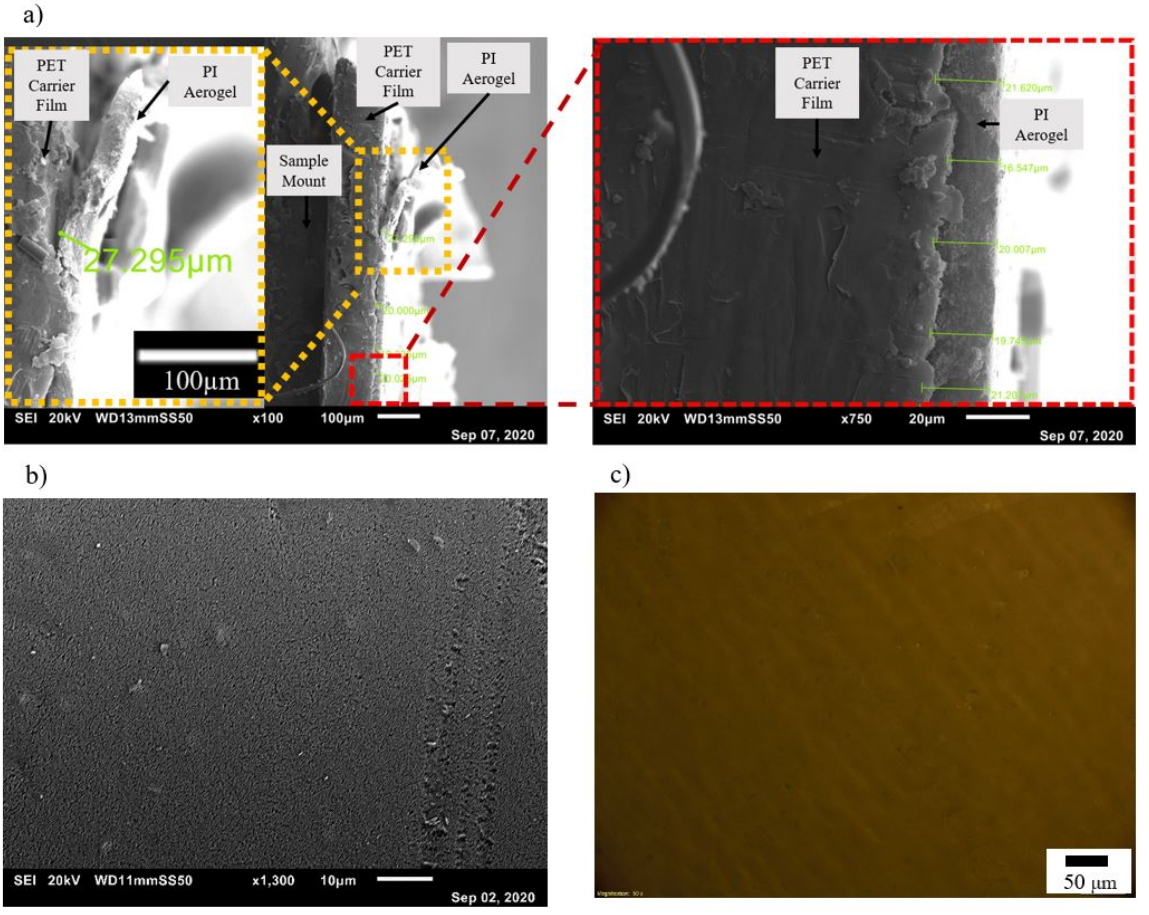

Figure 4-12: SEM and optical observations of: a) 20 µm thick PI aerogel observed with sample mounted at 90°, and 20 µm PI aerogel porous structure observed top down via b) SEM, and c) optical microscope.

The laminate manufacturing procedure was the same as in Section 4.2.1. However, due to strong adherence of the aerogel to the polyethylene terephthalate (PET) backing film, a heat-assisted method was used for application of the NPN to the prepreg. The prepreg plies were placed on a hot plate set to 30°C for 3 minutes which increased their tack. The warmed plies were then placed face down on the aerogel. After 1 minute of resting the plies were removed. The heat-assisted transfer process

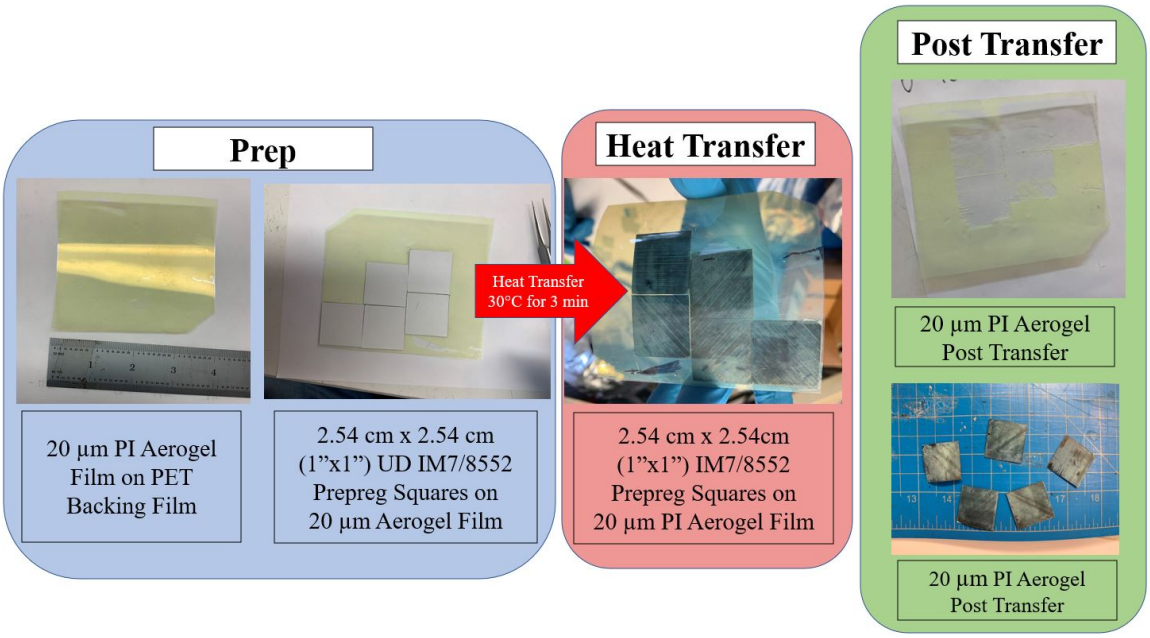

Figure 4-13: Heat assisted transfer process for the 20 µm thick PI aerogel from backing film to prepreg. The prepreg is then stacked directly to form a laminate with NPN at desired interfaces.

is presented in Figure 4-13. This pre-applied the aerogel to the plies' interfaces. The plies were then stacked up according to the $[0/90/\pm 45]_{2S}$ stacking sequence. The sample only had the 20 µm thick PI aerogel NPN in the middle five interfaces out of fifteen interfaces.

The laminate was cured under vacuum on a hot plate following the same cure cycle and bagging procedure as documented in Section 4.2.1. In the µCT scan, there were zero voids (void percentage of 0.0 vol%) in the region where the NPN was applied as seen in Figure 4-14 while there were voids (void percentage of 0.76 vol%) in the interlaminar regions where there were no NPN layers. An SEM image of the middle interfaces is shown in Figure 4-15. In that image, a void can be seen in the non-NPN interface.

Interlaminar thickness was compared via microscopy as seen in Figure 4-16. The specimens with 20 µm thick aerogel NPN interlayers, which were hot plate cured in VBO conditions had an interlaminar region of 5-7 µm thick. Similarly cured specimens without NPN in the interlaminar region had an interlaminar thickness of 1-2 µm.

PI aerogel with 200 µm thickness was also obtained from Aerogel Technologies.

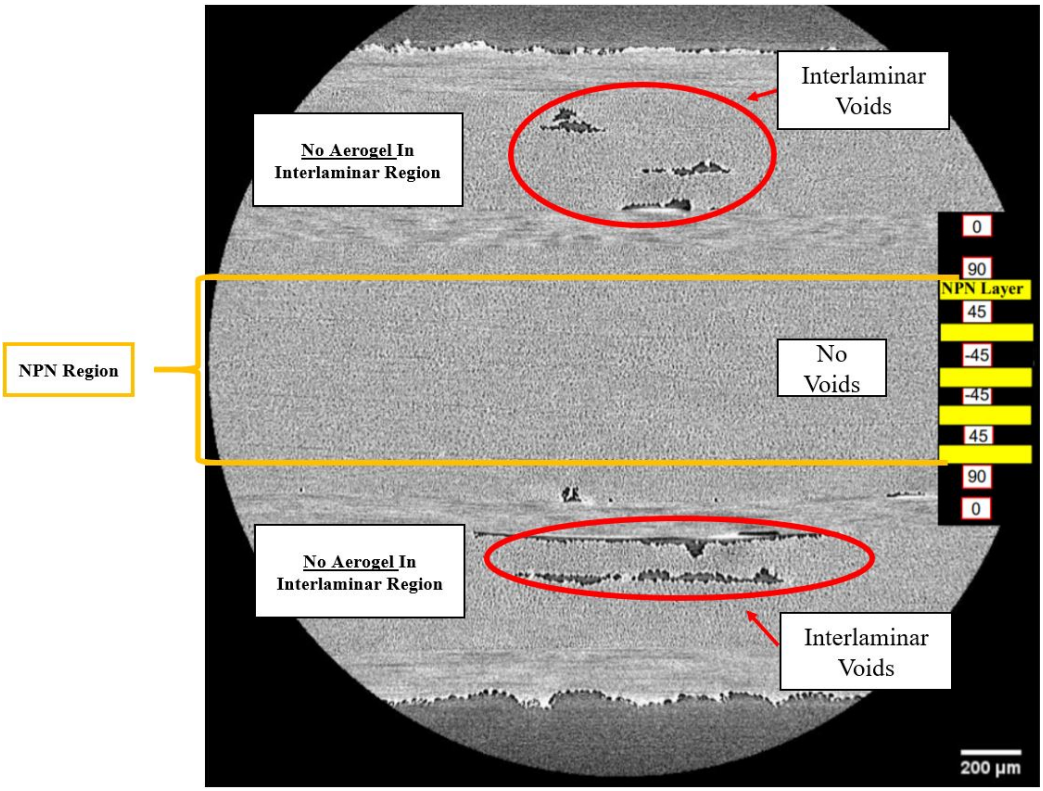

Figure 4-14: µCT image of sample with 20 µm PI aerogel NPN applied in middle five interlaminar interfaces. No voids are present in the interfaces where the PI aerogel interlayer is incorporated. The average void content of the top and bottom sections (non-NPN regions) is 0.76 vol%.

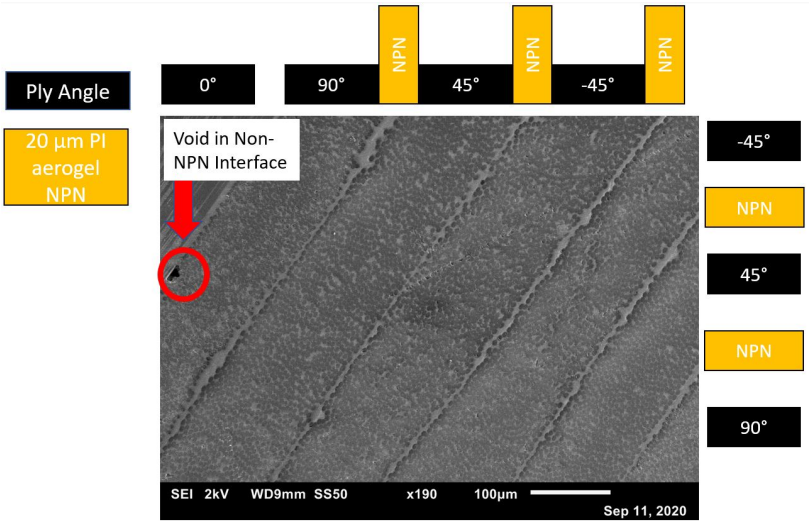

Figure 4-15: SEM of sample with 20 µm PI aerogel NPN in middle five interlaminar interfaces. No voids are present in the middle five interfaces. In the one interface where no NPN was applied, a void can be seen.

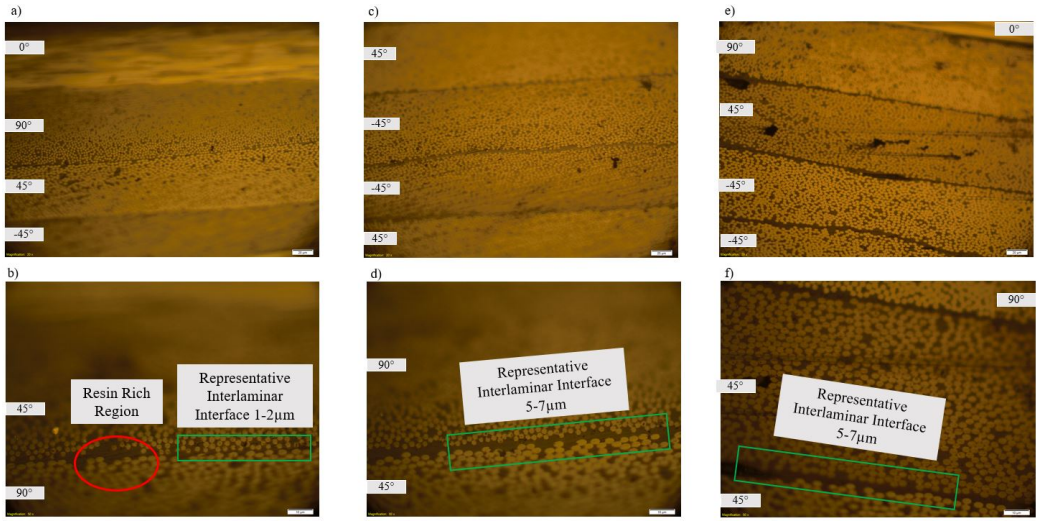

Figure 4-16: Representative optical microscopy images of hot plate cured specimens in a vacuum-bag-only environment. Specimens without any NPN show interfaces of 1-2 µm (a,b). A resin-rich region in image b) is observed, similar to the thickness of autoclave-cured IM7/8552 UD laminate material [78]. Specimens with 20 µm thick PI aerogel NPN (c,d) and 1.5 gsm 8 µm PA XD10 NPN (e,f) interlayers placed in all interlaminar regions have an interlaminar thickness of 5-7 µm.

The laminate manufacturing procedure was the same as in Section 4.2.1 with a stacking sequence of $[0/90/\pm45]_{2S}$ with the NPN applied on all interfaces. The µCT image is seen in Figure 4-17. While interlaminar voids were eliminated, intralaminar voids emerged. It is thought that this is due to the large interlaminar thickness of 40 µm. As resin is drawn from the pre-impregnated plies into the large (thick) interlaminar region, not enough resin remains in the plies. The resin flow into the PI aerogel NPN in the interlaminar region is thought to lead to intralaminer voids due to the now intraply dry fibers. Another sample was prepared with the 200 µm PI aerogel, but first it was compressed down to 50 µm by placing a layer of GNPT over the film and firmly pressing down with roller in order to see if a pre-compressed sample would have a thinner interlaminar region. Intralaminar voids appeared in that specimen also and the interlaminar region remained at ∼40 µm thick. The interlaminar region thickness of the non-compressed 200 µm thick PI aerogel NPN specimen being 40 µm thick (see Figure 4-17) and equal to the pre-compressed aerogel NPN specimen indicates internal compression either happens under vacuum or during the layup as each ply

is added. The void content percentage of both the uncompressed and compressed sample was an overall 0.11 vol%.

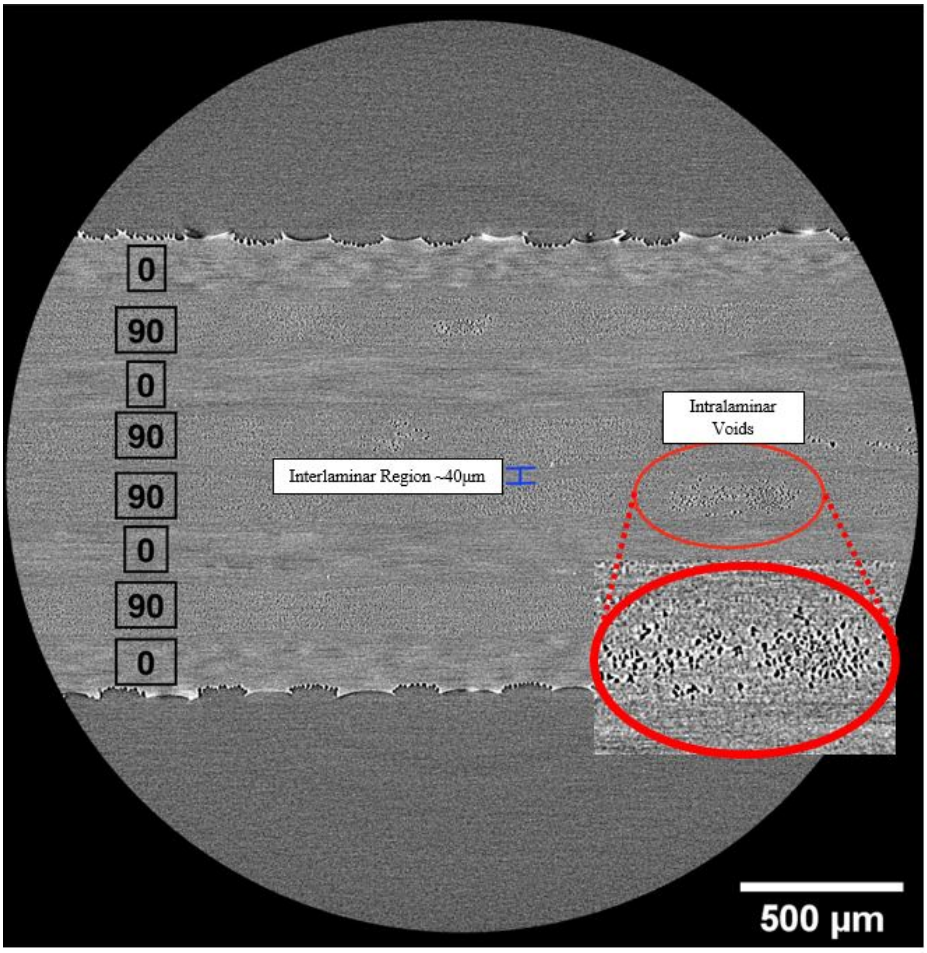

Figure 4-17: Representative µCT image of of sample with the uncompressed 200 µm PI aerogel NPN all interfaces. No interlaminar voids are present but intralaminer voids are seen throughout the specimen. The intralaminer voids can be seen in the call out. The overall void content percentage is measured to be 0.11 vol%.

4.5 Capillary Wetting from NPN Materials

The void elimination is obtained, in part, due to the capillary pressure applied by the NPN material. While polymer resins are not Newtonian fluids, the resin flow velocity is little when compared to the resin infusion [79]. The low shear rate of resin flow during composite curing allows the process to be studied as Newtonian flow, following a similar procedure to Lee [10] in a previous study. Darcy's law of capillary pressure, Equation 4.2, applies at the microscopic level to define the pressure at the interface between the resin and the gas. V_{flow} is flow velocity vector; $\mathbf{K}$ is the permeability tensor; μ_v is dynamic viscosity; and ∇P_f is the pressure gradient at front of the flow:

$$V_{flow} = \frac{\mathbf{K}}{\mu_v} \nabla P_f \tag{4.2}$$

The pressure gradient predicts the front of the flow. Figure 4-18 shows voids trapped with and without NPN in the interlaminar region which occurs during the laminate layup due to entrapped air and non-smooth surfaces. The interface contours are defined by the pressure of the gas in the entrapped void and the pressure of the resin, P_v and P_r respectively. The pressure gradient is defined as $\Delta P = P_r - P_v$. If the laminate is cured in an autoclave under vacuum, a P_r of 0.72 MPa is used as it is the difference between the external applied pressure of 0.7 MPa and partial vacuum of -0.02 MPa (-.2 bar). P_v is assumed to be 0.1 MPa (1 bar), the pressure the laminate was laid up in. In an autoclave cure, the ΔP is 0.62 MPa and void growth does not occur. Additionally, as the resin is heated and liquifies, the gas can diffuse into the resin system collapsing the voids. In a VBO cure with no applied pressure, the ΔP becomes -.08 MPa which is less than zero. In this case, the void can be expected to grow (expanding in volume and increasing the composite void percentage) according to the ideal gas law, Equation 4.3, reducing the P_v until $\Delta P = 0$. P is pressure, V is volume, n is number of moles, R is the universal gas constant, and T is temperature.

$$PV = nRT \tag{4.3}$$

The void pressure gradient with NPN included is described in Equation 4.4, where ΔP is the void pressure gradient, P_r is resin pressure, P_{NPN} is the capillary pressure of the NPN due to its pores, and P_v is void pressure.

$$\Delta P = [P_r + P_{NPN}] - P_v \tag{4.4}$$

Figure 4-18 shows that with the integration of the NPN, ΔP= P_r + P_{NPN} - P_v. P_{NPN} can be calculated by with the modeling assumption of 1D resin flow [80].

$$P_{NPN} = \frac{2 \times (1 - \epsilon)}{D_f \times \epsilon} \times \sigma \times cos(\theta) \tag{4.5}$$

A pre-factor of 2 was used in Equation 4.5 due to the nominal orthogonality of the electrospun fiber film to the resin system rather than pre-factor of 4 which would be used if the nanofibers ran parallel to the flow field. P_{NPN} is NPN pressure, ϵ is porosity, D_f is fiber diameter, σ is resin surface tension, and θ is the contact angle between the resin and the nanofiber system. With a PA 66 NPN fiber diameter of 150 nm, a porosity of 80 vol%, both given by the manufacturer [76] and an assumed resin surface tension of 35 mJ m^{-2} and $\theta = 20°$ [10], the capillary pressure from the NPN is estimated to be 0.11 MPa. The NPN capillary pressure, combined with the full vacuum pressure, creates a positive ΔP leading to void collapse. In this simplified model, when cured under full vacuum, only a minimal additional capillary pressure is needed with the contact angle $\theta < 90°$ being the determining factor, as P_{NPN} has to be only greater than zero and assumed positive values for other variables for a positive ΔP. However, more investigations need to be done to determine the minimum capillary pressure to obtain void removal and full wetting if the interlaminar region. If cured under partial vacuum, NPN traits such as fiber diameter, contact angle,

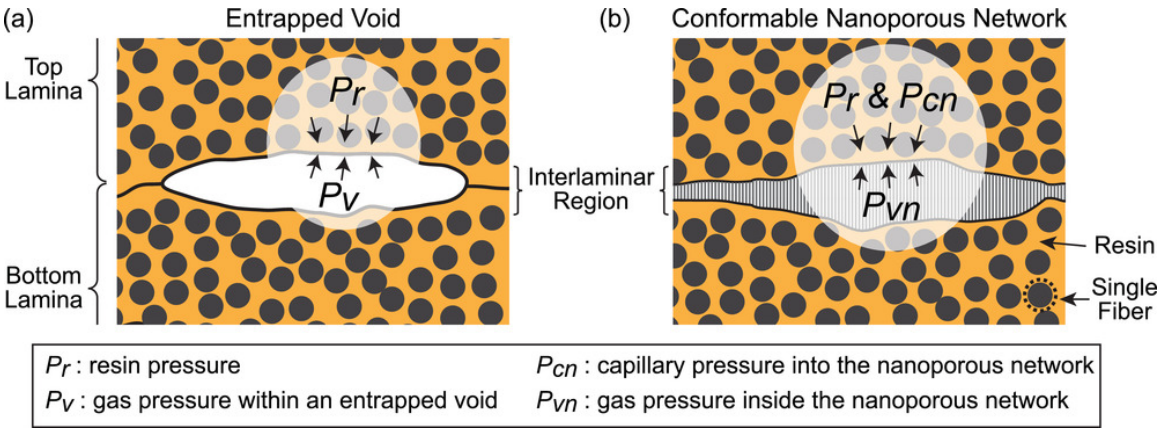

Figure 4-18: Illustration displaying the interlaminar void pressure interface with and without an NPN interlayer and the pressure forces defining the void boundary. The NPN enables capillary-driven polymer wetting into the interface, leading to void elimination and resin infiltration [10].

porosity, etc. have more governing effects. The capillary pressure of the PA XD10 nanofibers decreases to 0.07 MPa due to the increased fiber diameter of 230 nm but still leading to a positive ΔP.

In the case of no applied NPN in a vacuum-bag only-cure, the same Equation 4.5 can be used for intralaminar voids where the fiber diameter changes to 5.2 µm and porosity to 0.4 (based on fiber volume fraction). The pressure from the fibers would be 0.018 MPa. Due to the higher permeability of the carbon fibers, the void pressure is assumed to be zero. This leads to a positive pressure of 0.118 MPa as the resin pressure remains at 0.1 MPa. The 1D pressure modeling shows how intralaminar voids can be removed and helps explain why there are interlaminar voids but no intralaminar voids in hot plate cured laminates when no interlaminar NPN is added and helps explain why the interlaminar voids are more of a challenge than intralaminar voids in vacuum-bag-only cures and how the addition of NPN materials can enable VBO curing.

4.6 NPN Interlayers Acting as Porous Void Evacuation Channels

OoA prepreg systems are engineered to have alternating regions of dry fibers and resin-rich areas in-plane to the ply to enable VBO curing [3, 81]. These pathways facilitate air evacuation before resin flows into the dry fiber area and, as the cure progresses, resin flows into these dry fiber areas. Lee found that A-CNT NPNs can remove interlaminar morphology variations due to the A-CNTs compliance and eliminate interlaminar voids in autoclave-grade prepreg cured VBO due to the capillary effects of the A-CNT NPNs [39]. Polymer NPN systems act with an alike mechanism. Compared to the OoA prepreg the breathable pathway when NPNs are inserted into the interlinear region, is larger in area, the size of the whole laminate area, and the pathway is out of plane as it is an interlayer. The furthest a breathable pathway is to the NPN layer is half a ply thickness. For IM7/8552 UD prepreg, that is 0.0655 mm or 65 µm. NPNs presented here and previously are highly porous (80-99 vol%), enabling the evacuation of volatiles, entrapped air, and moisture before the resin impregnates the interlaminar region. As this void evacuation pathway is nearby all areas of the ply, entrapped air bubbles have little distance to travel which could reduce the amount of time the pathway needs to stay open. When the resin viscosity decreases as temperature rises, the capillary effect of the NPN systems encourages full resin infusion into the interlaminar region. Therefore, NPN + VBO manufacturing can be thought of as creating an OoA prepreg system with out of plane void evacuation channels made from NPNs that have inherent enhanced capillary properties which can encourage resin infusion and enable traditional autoclave prepreg systems to be cured VBO.

4.7 Conclusions

This chapter presented the usage of two polymer based commercially scaleable material systems as NPNs for use in a next generation composite manufacturing technique

where there is no applied pressure during cure using autoclave-grade composites, along with no large manufacturing process changes or prepreg material changes (resin, morphology, etc.). The first explored NPN system is EPNs where two different versions of polyamide are demonstrated to remove voids: PA 66 (Nylon 66) and PA XD10 (Lexter®) each with a differing nanofiber diameter and film thickness. The second is a bespoke PI aerogel in different film thicknesses. The EPN specimens were demonstrated to be effective at the 15 cm × 15 cm (6 in × 6 in) scale. With all NPN materials, µCT analysis was done to show void-free samples of VBO cured autoclave-grade prepreg with NPN interlayers. Short-beam strength was also evaluated for the EPN NPN systems showing no degradation of composite properties with the addition of the 1.5 gsm 8 µm PA XD10 and 4.5 gsm 23 µm PA 66 NPN interlayers. The higher short-beam strength values is thought to be from the increased resin-rich interlaminar region with thermoplastic filler. The PI aerogel material, in addition to showing interlaminar void elimination with the 20 µm thickness, revealed that with too large of an NPN layer (200 µm thick) intralaminar voids occur due to resin flow into the NPN from the plies. Microscopy showed that the interlaminar region is still thickened with the thinnest utilized NPN systems: the 20 µm thick PI aerogel and the 8 µm thick 4.5 gsm PA XD10 EPN both had interlaminar regions of 5 to 7 µm as opposed to 1 to 2 µm regions of specimens cured without the NPN. Lastly, the mechanics of the capillary effects are discussed as well as the NPN layer acting as a whole ply area breathable pathway that is half a ply thickness away from any point before resin infiltration. This next generation composite cure methodology has the potential to eliminate autoclaves from the manufacturing process, improving the economics of composite manufacturing and revolutionizing aerospace-grade composite manufacturing.

Chapter 5

Preliminary Investigations into Integrating NPNs in Geometrically Complex L-shaped Composites and Woven Fiber Prepeg to Enable VBO Curing of Autoclave-grade Prepreg

Composites can be clustered into three distinct classes: flat panels, complex geometries, and sandwich structures [82]. Complex geometries come in many shape varieties and are typically used as stiffeners, or to attach two flat panels together at different angles, and contain at least one bend or curve. In aerospace, the L-shape is used extensively for connecting the stiffener to the skin or the wing spar to the skin and is also one of the simplest complex geometries [8]. Prepreg composite materials can be categorized into two common morphologies, unidirectional and woven. Unidirectional (UD) prepreg consists of fibers that run in a single direction as in the IM7/8552 prepreg in Chapter 4. Woven fabrics consist of fiber tows that run in two orthogonal directions, which are threaded together in an alternating fashion [6]. Chapter 4 focused on utilizing a variety of NPN materials to remove voids from flat panels

manufactured with traditional autoclave-grade unidirectional prepreg in VBO conditions. In this chapter, the same void removal NPN technology with autoclave-grade unidirectional prepreg is investigated but expands its use into complex geometries with a focus on L-shape geometric structures. The complex geometry necessitated convection heating, as opposed to previously demonstrated conduction heating, for the VBO + NPN cures. Additionally investigated is the integration of the NPN technology made with woven fabric prepreg in flat panels. In the woven fabric investigations, aligned carbon nanotubes (A-CNTs) were utilized as an additional NPN material system. In the L-shape manufacturing investigation, the NPN technology established in Chapter 4 was able to suppress voids in the both the flat and curved regions of the L-shape geometry. However, with the woven fabric void content was reduced, but never fully eliminated.

5.1 Materials and Methods

This section gives the materials and methods for the L-shape layup, synthesis of A-CNTs and an extended hold cure cycle that was attempted in order to try to reduce voids in laminates with woven prepreg.

5.1.1 L-shape Layup

The same unidirectional (UD) Hexcel IM7/8552 prepreg system, as described in Section 4.2.1, was utilized for the L-shape study. The bagging materials used include: guaranteed nonporous Teflon (GNPT) (Airtech Release Ease 234 TFNP), breather (Airtech Release Ease 234 TFNP), and a 2.25 mm tall cork dam. GNPT was utilized as a base layer to prevent any resin that would bleed through the peel ply from attaching to the mold. A 1 mm thick high temperature resistant silicone rubber (SOFIALXC Silicone Rubber Sheet) caul plate was ultimately used and provided an even distributed pressure gradient on the laminate. The cork dam ensures edge breathability and the breather ensures vacuum is pulled from across the whole bag layup area, blocking a pinch in the bag from occurring which would limit a uniform

vacuum pull of the bagged area. Different tooling and heat sources from Chapter 4 were necessitated due to geometric constraints of the L-shape. A 6010 aluminum tool seen in Figure 5-1 (McMaster-Carr Multipurpose 6061 Aluminum 90° Angles 8982k781) had dimensions of 12.7 cm (5 in) in height and width, 30.48 cm (12 in) in length and 1.27 cm (0.5 in) thickness. The mold's inner radius was 1.27 cm (0.5 in). The multi-material manufacturing layup is seen in Figure 5-2. The heat source for the L-shape investigations was a convection-based oven (Thermo Scientific™ Heratherm™ Advanced Protocol Oven 51028126H) unlike the conduction-based hot plate presented in Chapter 4. The L-shape specimens were cured as the mold shape sat in a V-shape with the L-corner at the bottom to take advantage of the symmetrical shape ensuring equal gravitational force on the two sides of the L. The L-shape layup diagram and oven curing image can be seen in Figure 5-2.

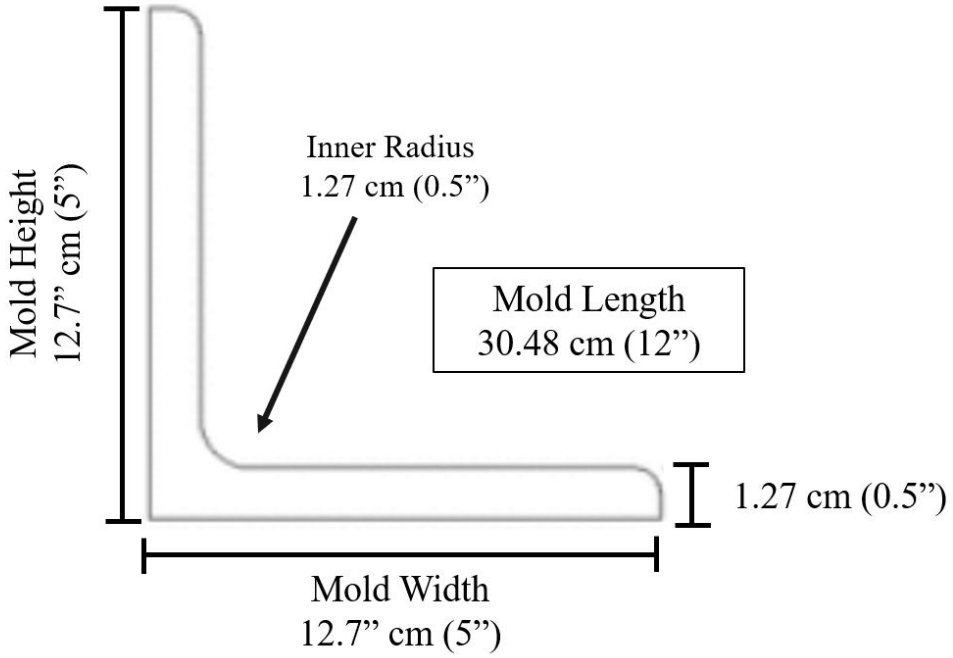

Figure 5-1: Diagram of L-shape mold dimensions. Image modified from [83].

The prepreg was cut into 2.54 cm × 7.62 cm (1 in × 3 in) strips before being inserted into the mold and firmly pressed down and the backing paper removed. The NPN layers were applied directly on top of the prepreg in the mold. The laminate was laid up with a stacking sequence of $[0°/90°]_{4S}$, seen in Figure 5-3, and cured according

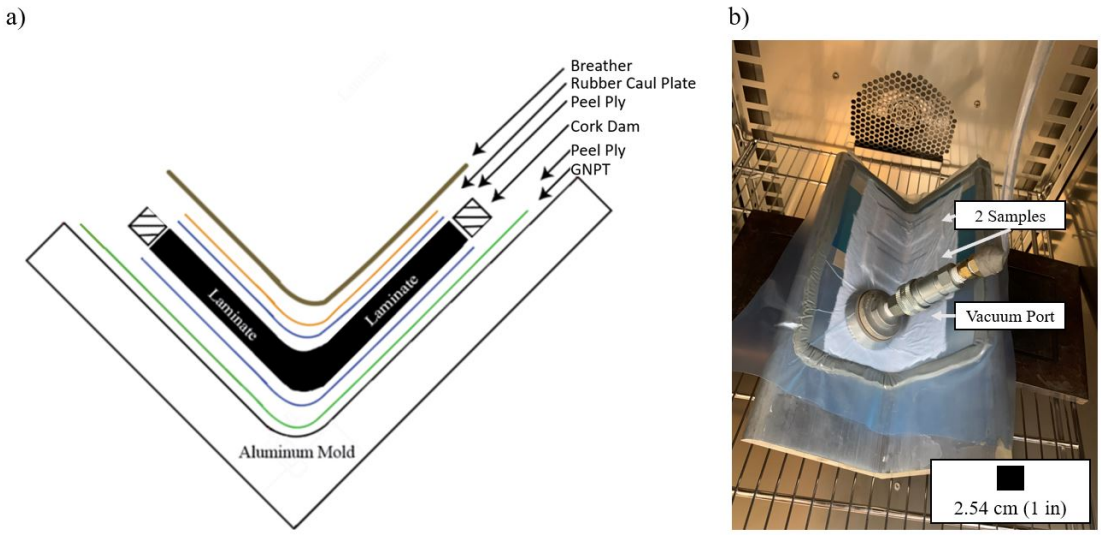

Figure 5-2: L-shape mold layup: a) layup diagram showing material and material stacking sequence, b) image of cure setup in oven prior to curing.

to the VBO standard cure cycle as documented in Section 4.2.1 and Figure 4-3. A 0° ply is defined to go across the mold width as depicted in Figure 5-3. When laying up the flat panel specimens (Chapter 4), a qualitative observation was noted that there is drapability improvements with the NPN interlayers due to the lack of contact between the resin of the two plies. This reduced tackiness due to the NPN acting as a non-tacky layer allows the plies to slide on each other and not cause fiber wrinkling or entrap air pockets during layup, and generally increased the ease of manufacture when laying up around the radius. Additionally, ply slippage is important for corner consolidation [63]. The observed reduction of ply-ply friction improves the ply slippage improving both ease of manufacture and laminate consolidation.

5.1.2 Aligned and Patterned CNT Synthesis and Transfer

A previously investigated NPN, aligned carbon nanotubes (A-CNTs) [10], was utilized in the woven fabric study with the thought that they could conform to the topographic changes in the fabric morphology due to their ability to buckle. This was investigated further with CNTs grown in a patterned format. The process for CNT manufacture was developed by Garcia et al [84]. The A-CNTs were grown via chemical vapor

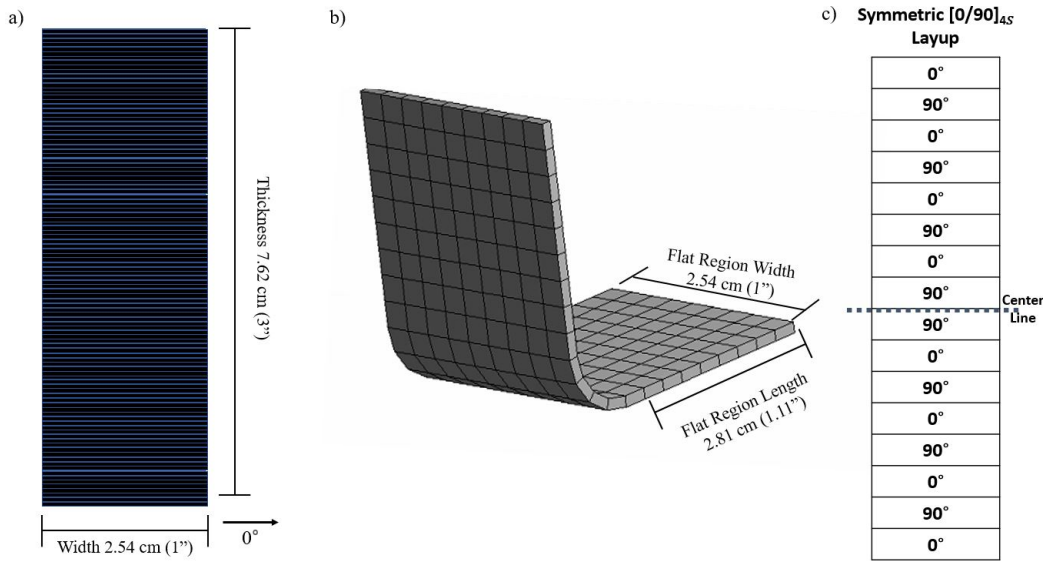

Figure 5-3: Ply and laminate diagrams for L-shape curing: a) ply dimensions, b) first ply laid up in L-shape mold, and c) L-shape geometry laminate stacking sequence.

deposition (CVD) in a 5.08 cm (2 inch) diameter quartz tube furnace (Linden/Blue M) at atmospheric pressure. 3.17 cm × 3.17 cm (1.25 in × 1.25 in) silicon (Si) wafers were precoated with an iron catalyst of Fe/Al_2O_3 by e-beam evaporation. The quartz tube reactor was first purged with an inert gas before a reducing atmosphere of H_2/He at 680°C for 15 minutes was applied. Following the reducing step, a reactant mixture of $H_2/He/H_2O/C_2H_4$ was then applied. The quartz tube setup can be viewed in Figure 5-4. This procedure grows CNTs with an average CNT density of $\sim$ 1% with inter CNT spacing of $\sim$ 60 nm. The CNTs outer diameters are $\sim$8 nm with 3 - 7 walls and inner diameters of $\sim$5 nm. The CNTs intrinsic density is $\sim$1.6 g/cm^3 [72]. The height of the CNTs was controlled by time of exposure to the carbon carrying gas (C_2H_4). Figure 5-5 shows CNTs grown with this process. After the growth process, a delamination step occurred where He was applied for 60 seconds to weaken the attachment between the A-CNT forest and the Si wafer aiding the ability of the CNT forest to be transferred to the laminate.

Patterned CNTs of aspect ratios (height to cross section) of 0.6 to 2.7 [85, 86] have been shown to enable buckling in wave like shapes. Patterned CNTs were investigated to see whether they too enabled void reduction or elimination while taking

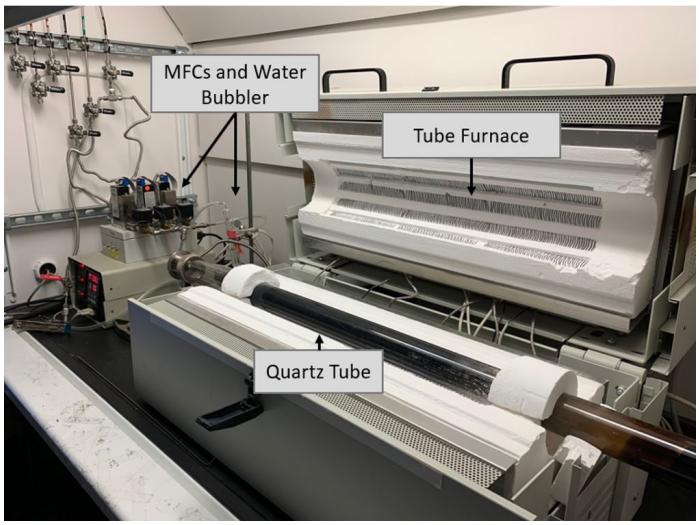

Figure 5-4: CNT synthesis furnace and 50.8 mm (2 in) diameter quartz tube. Tube is black due to carbon deposits built up over time.

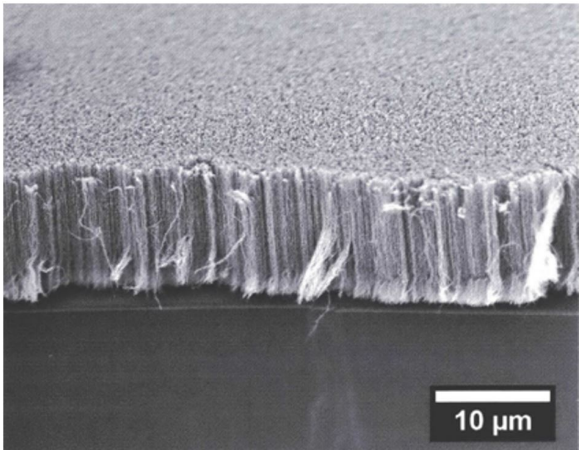

Figure 5-5: SEM image at 45° inclination of aligned carbon nanotube (A-CNT) array [10].

advantage of the favorable buckling qualities. The patterned A-CNTs were manufactured consistent to the process documented by Ni [87] and seen in Figure 5-6. The CVD growth process is the same as unpatterned wafers with the exception of a the Si wafer having the Fe/Al_2O_3 catalyst deposited in a patterned squares. The Si wafer was micro patterned with Fe/Al_2O_3 in 25 µm × 25 µm squares with gaps of 5 µm between them. To do so, the 500 nm thick SiO_2 coated Si wafer was dehydrated for 15 minutes at 115°C and cooled. Shiply 1805 positive photo resisit (Microposit, Dow Chemical Company) was deposited by spin coating for 60 seconds at 4000 rpm before

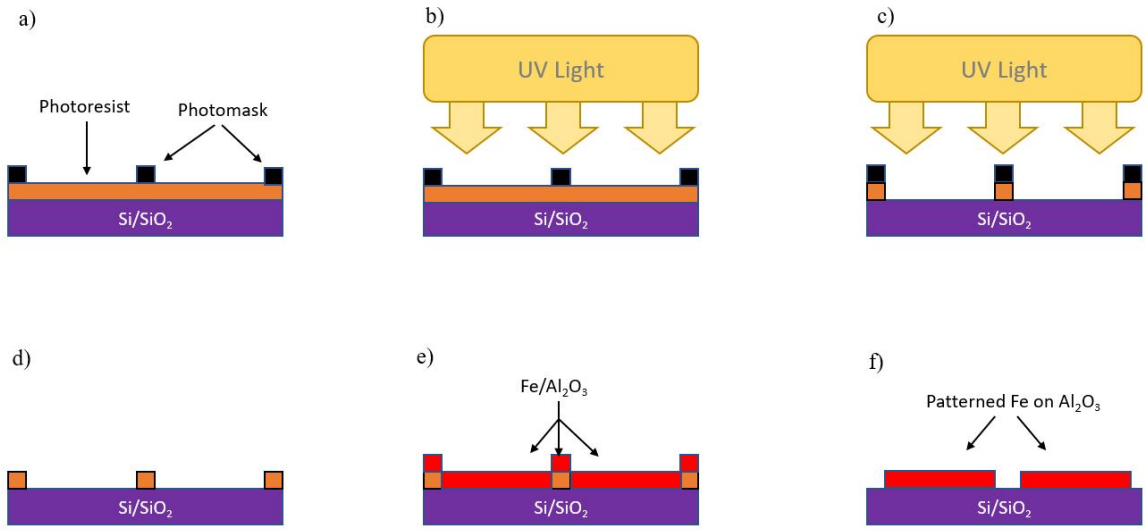

Figure 5-6: Patterning of Si wafer: a) Si wafer is spin-coated with a positive photoresist polymer (orange). A positive photomask (black) is placed on top. (b) UV light is introduced weakening the photo resist. c) A photo resist developer removes the photo resist from the unmasked area of the wafer. d) The photomask is removed. e) E-beam deposits 0.1 nm Fe/Al_2O_3 catalyst layer for A-CNT growth. f) Photoresist removed leaving desired catalyst and support pattern on wafer. Image modified from [87].

being baked at 115°C for 90 seconds. A positive photomask (Advanced Reproduction Corp) was placed on the wafer and exposed to 405 nm wavelength h-line UV light at a dosage of 40 mJ/cm^2. The exposed substrate was developed while swirling in a CD-26 (Microposit, Dow Chemical Company) photoresist developer for a few minutes, rinsed with de-ionized water, and blow dried with N_2. The catalyst layer of 0.1 nm of Fe/Al_2O_3 was deposited with a base pressure of 2×10^{-6} Torr. Patterned wafers were immersed in acetone and sonified for over 30 minutes, rinsed with isopropanol (ISP), and blown dried with N_2 to achieve lift off of the photo resist. The grown, patterned A-CNTs can be seen in Figure 5-7. The wafer patterning process was performed by Dr. Luiz Acauan and I am appreciative and grateful for his support.

After growth, the height of the A-CNTs was determined by measuring the z-axis travel between the focal planes of the Si wafer and the top of the CNT forest with an optical microscope [88]. The two edges of a wafer (forming the wafer's base) as well as three points (first quarter point, midpoint, third quarter point) along the center-line

of the wafer width, seen in Figure 5-7, were measured. The average height from the three points was taken. The accepted measured height was ±5 µm. This optical measurement method has a resolution of 2 µm.

The CNTs, after being grown on the Si wafer, are transferred to the prepreg plies using the following process: the laminate is laid up according to the desired stacking sequence. Once a desired CNT interface is encountered, the Si wafer is carefully flipped over, CNT side facing downwards, so the CNTs come in contact with the top ply. Gentle force is applied for 20 seconds. Then, the Si wafer is removed. Alignment of the CNTs are observed similar to [87, 89]. This transfer method is 95% effective for CNT transfer for forests over 50 µm as observed visually. If CNTs of less than 50 µm in height were utilized, there was incomplete transfer to woven material with a lack of transfer occurring between the tows of the weave. Only woven specimens where CNTs were taller than 50 µm are reported. The results of transfer can be seen in Figure 5-7 as well as the microscopy images of the patterned CNTs.

5.1.3 Extended Cure Cycle

The cure cycle is the process by which the gel state resin solidifies into its solid state. In a standard autoclave cure cycle, there are two holds. The first lower isothermal hold is used to reduce the resin viscosity to enable fiber wetting and to allow volatiles and entrapped air to escape [90]. The second stage occurs as temperature is ramped higher and held to complete the polymerization. The resin viscosity initially is reduced before increasing as the resin begins the cross-link process [90, 91]. While most specimens utilized the VBO standard cure cycle (Section 4.2.1), an extended cure cycle was utilized in the woven fabric-woven fabric interface (Woven-Woven) and unidirectional-woven fabric interface (UD-Woven) experiments with an extended first stage in the hope that the longer first hold time would further allow entrapped air particles to escape. While void content percentages ultimately decreased in the woven-woven study, it did not lead to void elimination from the laminate. For this extended cure cycle the following procedure was followed: Ramp to temperature of 110°C at 2° per minute with a hold time of 120 minutes (2 hr.), ramp to cure temperature of 180°C at

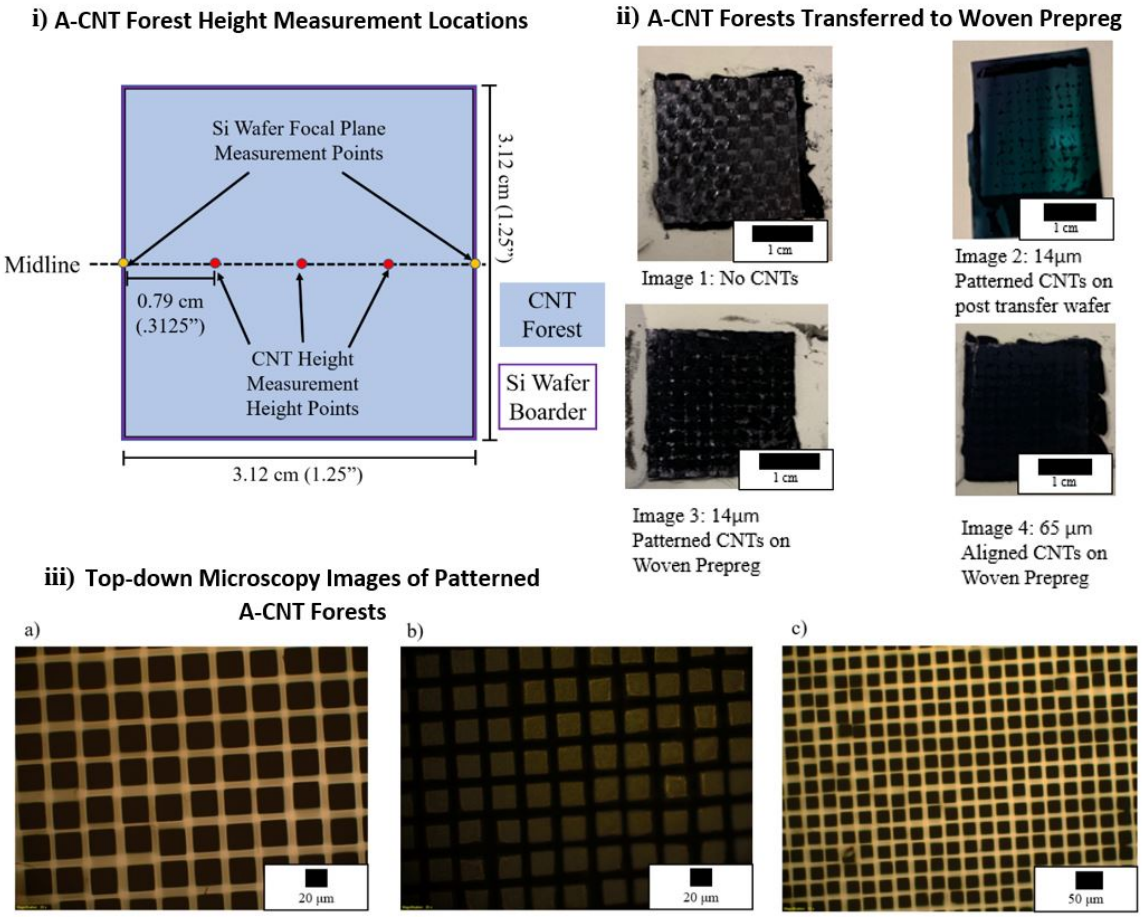

Figure 5-7: A-CNT post growth processing and imaging: i) CNT height measurement locations. ii) CNT transfer from wafer. Image 1 is of a ply interface before CNTs are applied. Image 2 shows the wafer post patterned 14 µm CNT transfer. The green color is the wafer and the black is the CNTs. Remnants of CNTs can be seen especially in the areas of the weave where there is no direct fiber contact with the wafer. Image 3 shows 14 µm tall CNTs post transfer on the woven prepreg. Image 4 shows 65 µm tall non patterned aligned CNTs post-transfer to the prepreg. Notice the matte black coloring from the complete transfer of CNTs due to the CNTs height. iii) Patterned CNTs under (a,c) light and b) dark microscopy. c) CNT pattern shows some non uniformity due to the ability of the CNT forests to delaminate from the wafer and shift position.

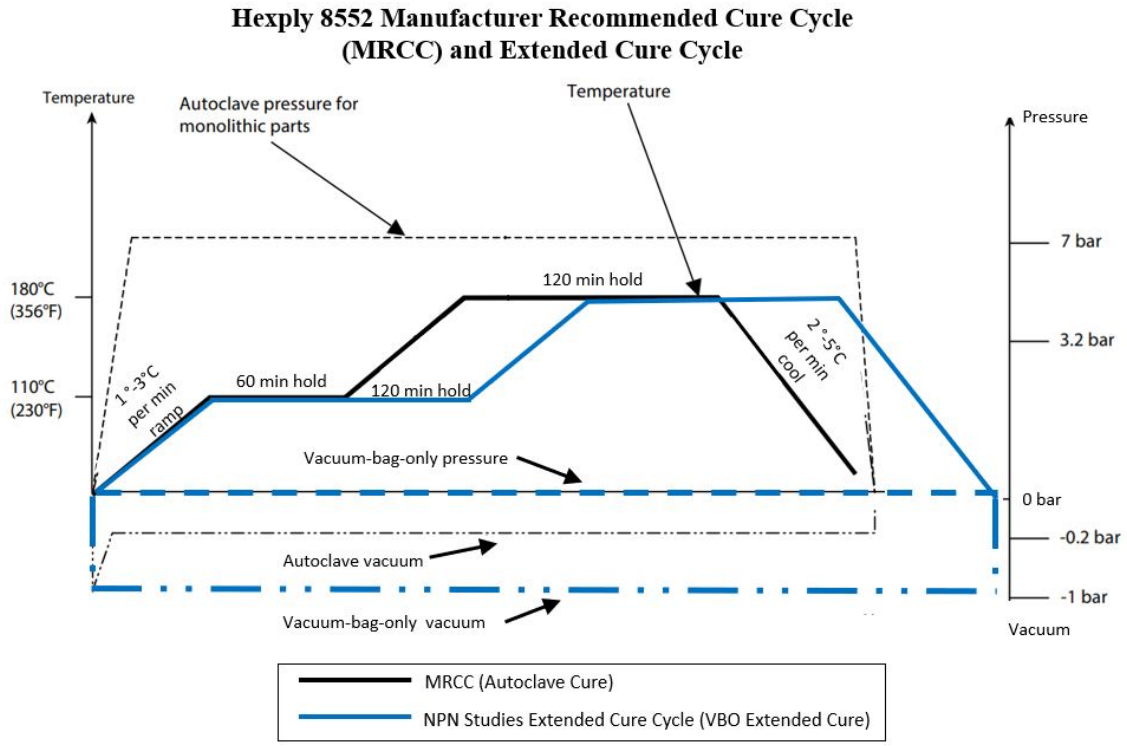

Figure 5-8: Hexply 8552 manufacturer recommended cure cycle (MRCC) for both UD and woven fabric materials [73], (black), and extended VBO cure cycle for some NPN studies in this work, where first temperature hold (solid blue line) is doubled to 120 minutes with -1 bar vacuum and no applied pressure (standard dashed blue line) throughout the cure.

2° per minute with a hold of 120 minutes (2 hr.), and cool at 2-5° per minute. Vacuum of -1 bar was pulled throughout the cure with no applied pressure. The cure cycle can be seen in Figure 5-8, comparing the manufacturer recommended cure cycle (MRCC) for an autoclave cure and the extended VBO cure. The NPN studies' standard (non-extended) cure cycle (VBO cure) utilized is the same from Section 4.2.1 and Figure 4-3.

5.2 NPN Integration into Geometric Complex L-shaped Composites for Vacuum-bag-only Curing of Autoclave-grade Prepreg

Composites manufactured in L-shape geometries have many use cases such as operating as stringers and enabling joining of flat plates in a T-configuration [8]. In these complex geometries, however, there have been unresolved challenges in void formation, fiber wrinkling, and thickness variation in the curved region of the laminate [8, 92]. This section focuses on the void elimination properties of NPNs and curing autoclave-grade prepreg in VBO conditions in the L-shape geometries.

The layup and integration of the specimens was completed according to Section 5.1.1 with a stacking sequence of $[0°/90°]_{4S}$. L-shape geometries can be observed after they are cured in Figure 5-9. The µCT imaging and void analysis was completed according to Section 4.2.3. Each sample was scanned in both the flat and curved section of the geometry midway through the laminate width at the midpoint of the curved and flat region. The approximate locations of the scan are seen in Figure 5-10. The NPN utilized in the L-shape investigations was the 4.5 gsm 23 µm PA 66 NPN described in Section [4.3]. In the first study, the NPN was applied to only the middle 5 interfaces and cured without a rubber mat caul plate. This middle 5 NPN interlayer stacking is similar to the flat cured specimen as seen in Figure 4-9c. µCT scans of the center of the laminate in the flat region and the curved region are seen in Figure 5-11.

In the flat region, the void content for the regions without NPN interlayers was 0.40 vol%. Similar to the work on flat plates in Chapter 4, no voids were identified in the region where NPN was applied. However, in the curved region this was not the case. In the curved region where NPN interlayers were placed, interlaminar voids were reduced but not eliminated, and intralaminar voids were also observed. The void content percentage where NPNs were placed as interlayers was 0.95 vol%. This is an improvement from the non-NPN region with a void content of 4.18 vol%.

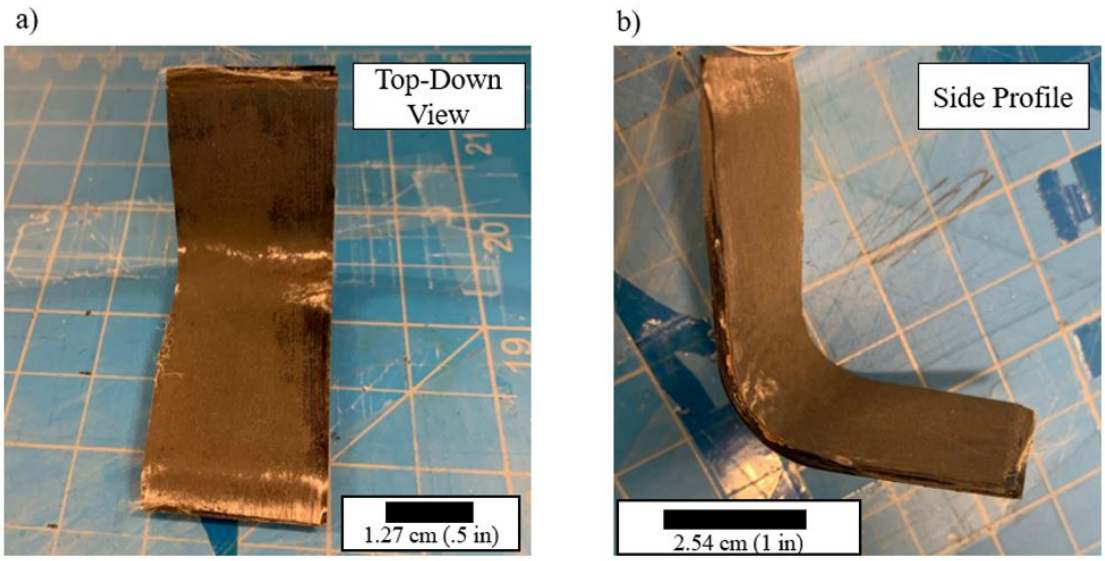

Figure 5-9: L-shape composite optical images after curing: a) top down view, b) side profile.

In both the flat and curved regions without NPN, voids were present. Upon further inspection, the region around the curve had a gloss like finish indicating a lack of full compaction as the the peel ply layer would cause there to be a more matte finish to occur if otherwise. Subsequently, a 1 mm thick silicone rubber mat was used. A 1 mm thick Al caul plate was used in Chapter 4 for the plate specimens. Rubber was used in the L-shape specimens as opposed to bent aluminum due to its pliability, which enabled it to conform to the laminate along the curve without needing to be precisely machined. The thickness of only 1 mm also helped in that regard. The addition of this a caul sheet or pressure intensifier is not uncommon and has been seen in previous studies [60, 61]. Layups were completed with no NPN applied to the interlaminar regions and 4.5 gsm 23 µm PA 66 NPN applied to all interfaces. Figures 5-12 and 5-13 show the results. In the flat region of the specimen with NPN, no discernible voids were found with a void percentage of 0.00 vol% compared to 1.13 vol% of the non-NPN specimen. In the curved section, the void percentage of the specimen with 4.5 gsm 23 µm PA 66 NPN was 0.00 vol% compared to 1.67 vol% with no NPN as shown in Figure 5-14. Two rare scattered interlaminar voids $\sim$ 5 µm

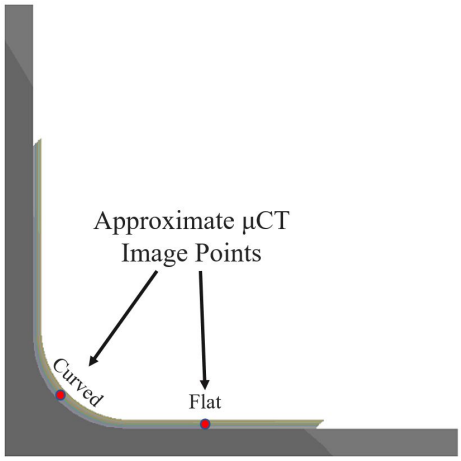

Figure 5-10: Approximate L-shape µCT scan points: in the midpoint of the curved and flat regions and midway through the laminate width.

in diameter along the center line of the NPN specimen were observed; however, the contribution to void content percentage were less than 0.01 vol%.

Microscopy confirmed this result in both of the flat region and the curved region as seen in Figure 5-15 and Figure 5-16. The microcopy images were taken mid-width of the specimen after being polished with 320, 400, 500, 800, and 1200 American grit sandpaper (P400, P800, P1200, P2400, P1000 European grit). In specimens with no NPN, both interlaminar and intralaminar voids were observed. The higher amount of darker regions optically observed showing voids in non-NPN samples conforms to the higher void percentage measured by µCT. With the NPN specimens, no voids were observed in either the curved or flat regions. There is a clear interlaminar region increase of 10-15 µm that can easily be seen in the middle interface between the 90° plies due to the 23 µm thick 4.5 gsm PA 66 NPN interlayer. Additionally, challenges such as fiber wrinkling were not observed due to the non-tacky and compliant NPN. This promising result shows the VBO curing can be utilized to make void-free composites when NPNs are placed in the interlaminar region in L-shape and other complex geometries that require curved geometries, albeit with a likely undesired increase in interlaminar thickness and laminate total thickness.

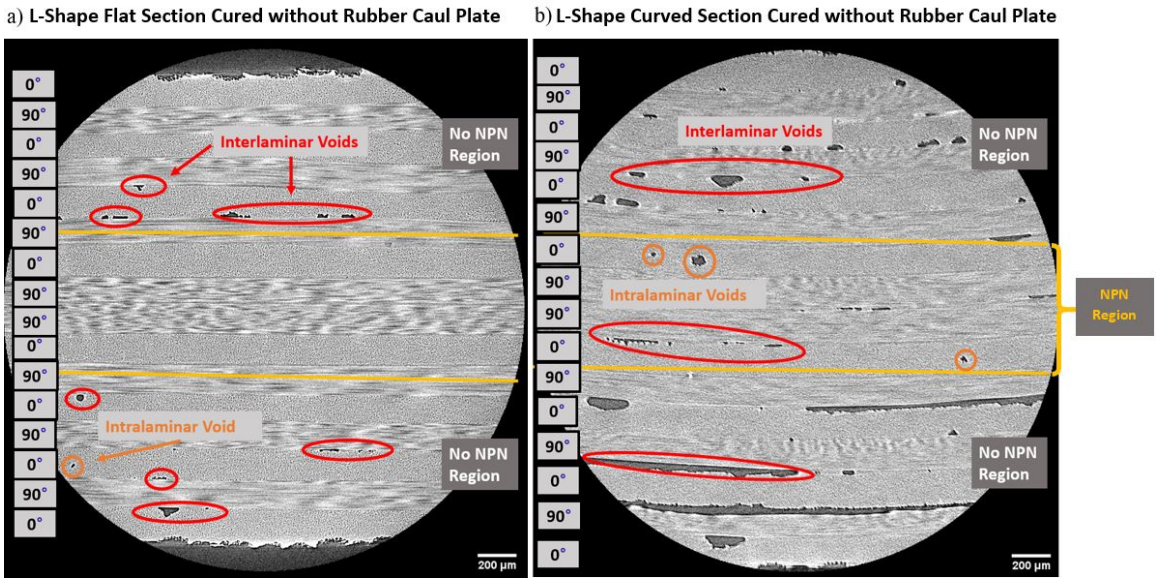

Figure 5-11: Representative µCT scans of a L-shape specimen with 4.5 gsm 23 µm PA 66 in the middle 5 interfaces cured without the 1 mm thick rubber caul plate; a) The flat area showed no voids in the NPN regions similar to flat plate results in Chapter 4; b) The curved area showed both interlaminar and intralaminer voids in the NPN region.

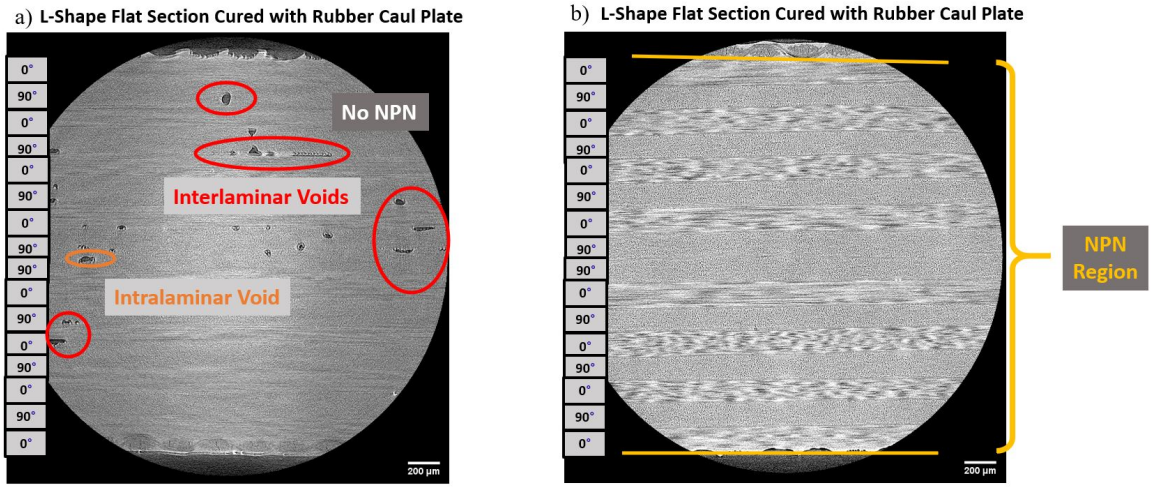

Figure 5-12: Flat section of L-shape specimen cured with 1 mm thick rubber caul plate; a) No NPNs were placed in the interlaminar regions and void content of 1.13 vol% was observed; b) 4.5 gsm 23 µm PA 66 interlayers were placed in all interlaminar regions (ply-ply interfaces) and void content of 0.00 vol% was observed.

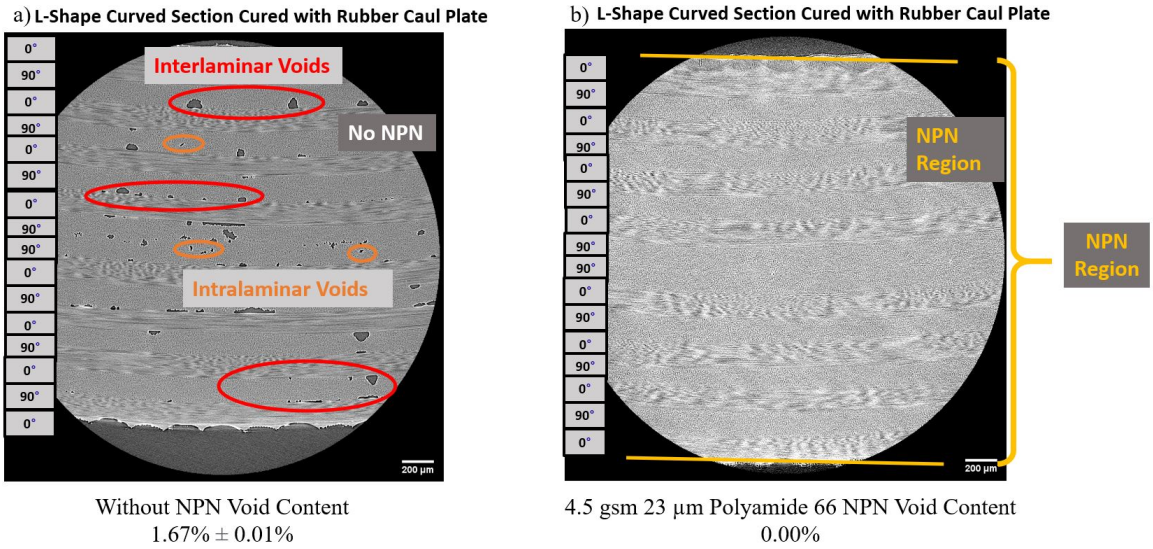

Figure 5-13: Curved section of L-shape specimen cured with 1 mm thick rubber caul plate: a) No NPNs were placed in the interlaminar regions and void content of 1.67 vol% was observed; b) 4.5 gsm 23 µm PA 66 interlayers were placed in all interlaminar regions (ply-ply interfaces) and void content of 0.00 vol% was observed. Two rare scattered interlaminar voids were observed $\sim$ 5 µm in diameter along the center line, however, the contribution to void content percentage was less than 0.01 vol%.

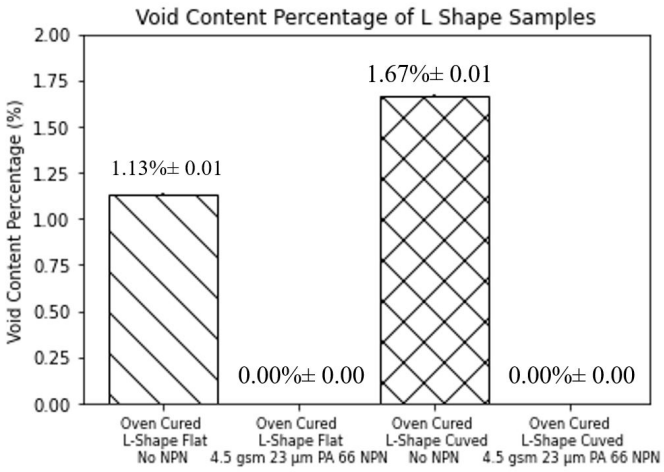

Figure 5-14: Void content percentage of L-shape samples.

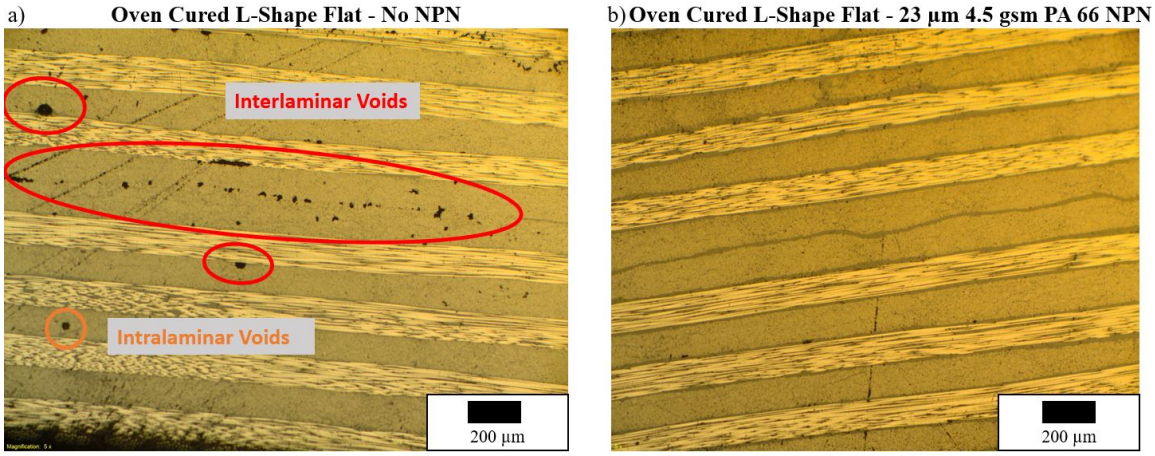

Figure 5-15: Representative microscopy images of the flat region of L-shape specimens: a) specimen without any NPN shows interlaminar and intralaminer voids; b) specimen with 4.5 gsm 23 µm PA 66 interlayers is void-free. There is a 10-15 µm increase in interlaminar thickness which can be easily seen in the middle interlaminar region.

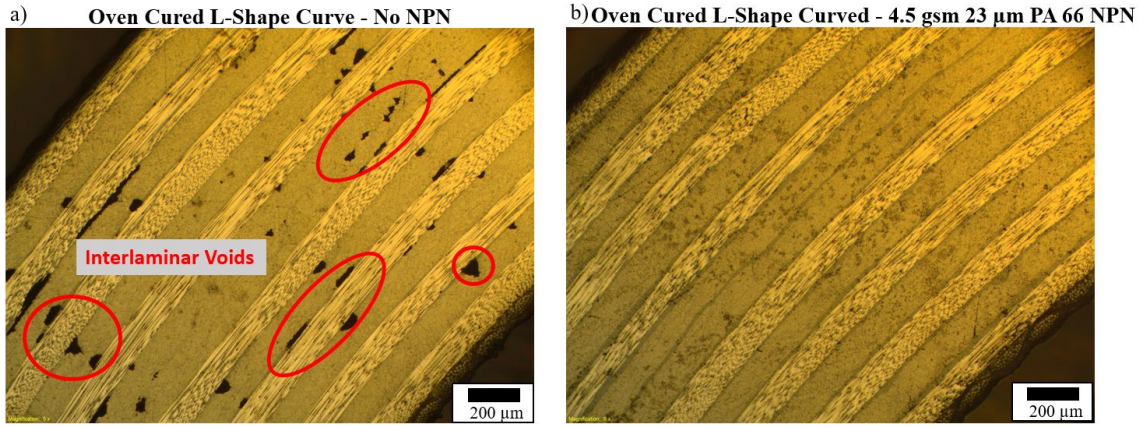

Figure 5-16: Representative microscopy images of the curved region of L-shape specimens: a) specimen without any NPN shows interlaminar and intralaminer voids; b) specimen with 4.5 gsm 23 µm PA 66 interlayers is void-free. There is a 10-15 µm increase in interlaminar thickness which can be easily seen in the middle interlaminar region

5.3 Preliminary Investigations into Autoclave-grade Woven Prepreg with NPN Interlaminar Integration for VBO Curing

Unidirectional (UD) plies have fibers aligned in one direction. They are strong in the fiber direction (longitudinal direction) where the fiber properties dominate and weak in the orthogonal direction (transverse direction) where the matrix properties dominate. Laminates can be engineered to have different mechanical couplings by alternating the direction of stacked plies. Additionally, UD plies have higher static strength, allow for increased fiber volume fractions and elastic properties compared to woven fabrics [6]. Woven fabrics, where fiber tows run in orthogonal directions and woven together, are used to create a fabric with more uniform in plane strength regardless of direction as seen in Figure 5-17. This has some drawbacks, such as lower fiber fraction due to the fibers not being as closely packed together and weaves preventing fibers from being straight, both affecting the static strength and stiffness negatively [6]. Woven fabrics tend to have similar transverse and longitudinal strength values and higher drapability due to the weave [93]. They are also more resistant to outer surface damage as, unlike UD prepreg, the fibers can not peel out or split when damage occurs as they are interwoven [94]. Woven fabrics are often utilized to create hybrid laminates with woven fabrics placed on the surface of a laminate to prevent delamination when holes are drilled, increase the abrasion resistance, and improve impact damage resistance [6]. The interfaces of UD-UD plies (Chapter 4), UD-woven fabric plies and woven fabric-woven fabric plies can be seen in Figure 5-18 and are important to be investigated for more universal application of VBO with NPN cures. Woven fabrics have been shown to be more challenging than UD plies for OoA prepreg. Ridgard noted that for void suppression, the dry pathways must persist for a significant time during the manufacturing process. To do so the cross sections need to be nearly completely non-impregnated in woven fabrics [3, 7].

The woven prepreg system utilized was IM7/8552 plain weave which had a warp

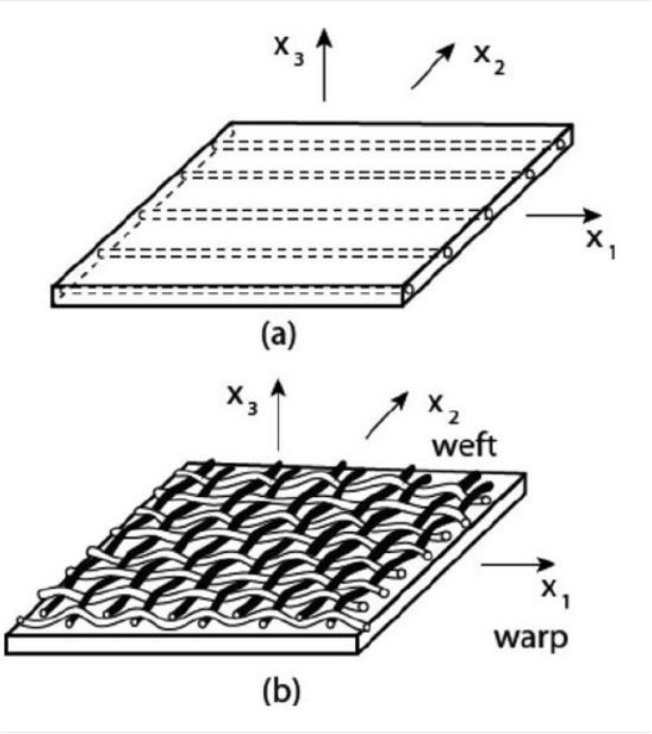

Figure 5-17: Diagram comparing: a) unidirectional ply and b) woven ply [6].

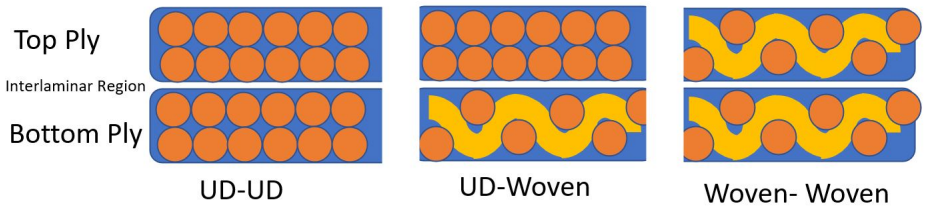

Figure 5-18: Diagram showing the different prepreg morphologies and interfaces of specimens tested.

to fill ratio of 50 to 50, a fiber volume percentage of 55.57 vol%, and a mass of 196 g/m^2. An optical image of the woven fabric can be seen in Figure 5-19 with the call out box showing a region where there are no fiber tows. The laminates were manufactured according to Section 4.2.1 but laid up in a 8-ply stacking sequence of $[0^{UD}/0^{Fabric}]_{2S}$ with the UD plies for the investigations of UD-woven interfaces and $[0^{F}]_{4S}$ for the investigations of woven-woven interfaces. Various methods of NPNs were applied using the VBO and extended VBO cures with mixed success. The specimens showed void reduction but not elimination. The UD-woven laminates achieved a void percentage of under 1 vol% with the 70-80 µm tall A-CNT NPNs. However,

after further investigation, large but rare void pockets still existed. For woven-woven laminates void percentage was never reduced to under 1 vol%. The A-CNT NPNs were manufactured according to Section 5.1.2.

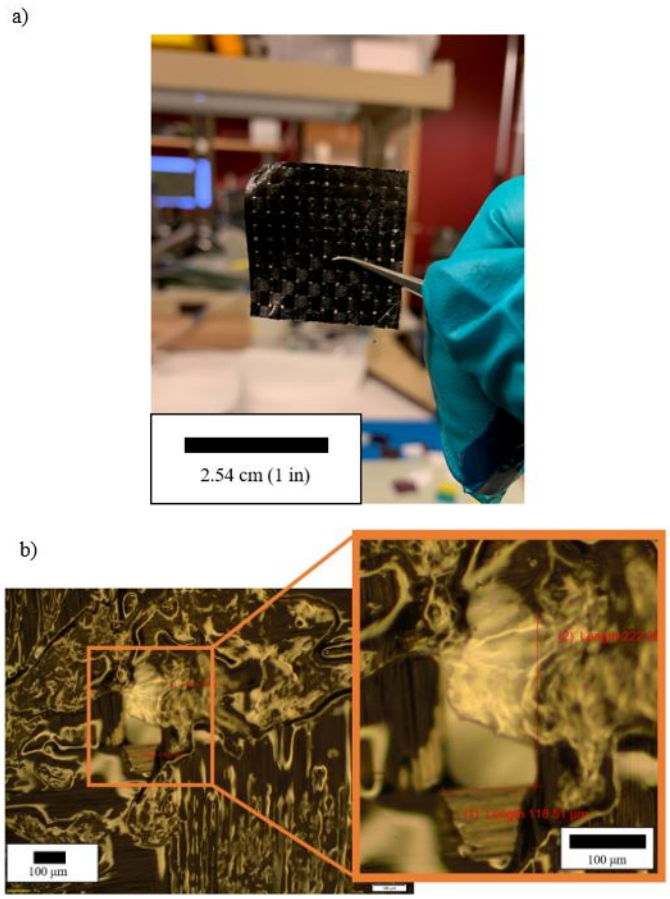

Figure 5-19: IM7/8552 woven prepreg characteristics: a) optical image of woven fabric ply; b) optical microscopy image of woven ply. The glossy area is the preimpreginated resin and the gap between the fibers tows as seen in the inset is one of the regions where voids still persist even after the integration of NPN.

5.3.1 NPN Integration at Unidirectional-Woven Ply Interfaces

Interfaces between UD and woven plies occur in hybrid laminates where oftentimes a woven ply is placed on the outer layer of the laminate for abrasion, surface, and impact resistance [6]. The natural morphology of the weave presents a larger challenge for void elimination with NPNs due to its varying interlaminar thickness. The µCT imaging and void analysis of the manufactured laminates was completed according to Section 4.2.3. The greatest success in void reduction in UD-woven fabric specimens were with 70 to 80 µm A-CNTs, in both patterned and non-patterned configurations, where void content was found to be less than 0.3 vol% as depicted in Figure 5-20 and Table 5.1. However, as Figure 5-21 depicts, there are still rare but large (>200 µm) voids seen in some slices and the laminates are not void-free. Additionally, A-CNTs with a height of 230 µm and the electrospun 4.5 gsm 23 µm PA 66, as described in Section 4.3, are utilized as NPN materials with a void content percentage of 2.03 vol% and 2.00 vol% respectively. While the introduction of NPN in the interlaminar region using VBO curing decreased void content from 3.62 vol%, more work needs to be done to ensure complete void removal. This result regardless might be might be promising for non-aerospace applications like wind and infrastructure.

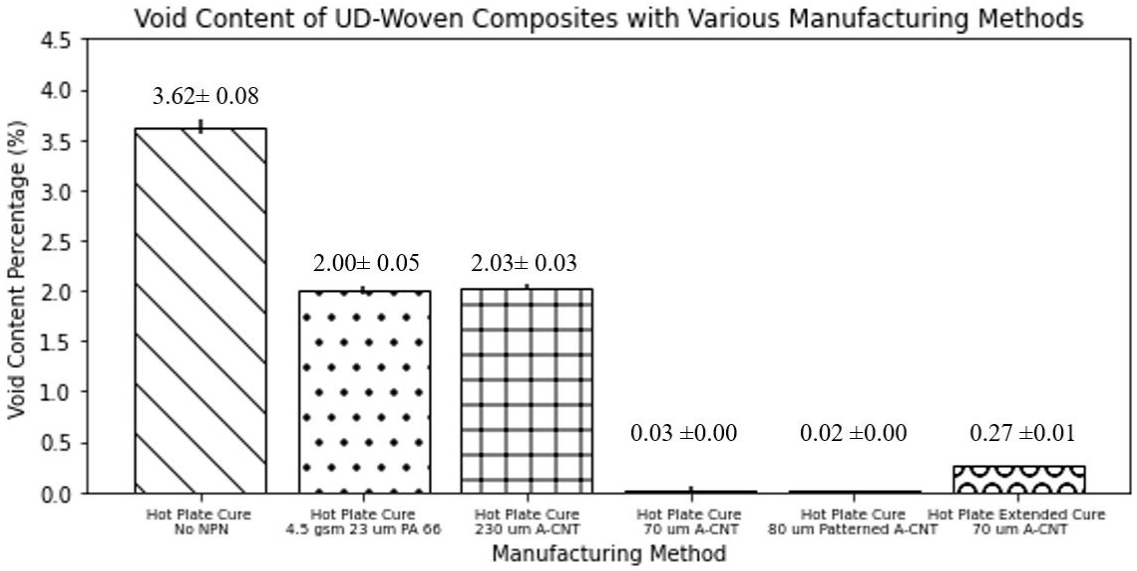

Figure 5-20: Void content of 8-ply IM7/8552 UD-woven fabric $[0^{UD}/0^{Fabric}]_{2S}$ laminates cured with various methods and NPN interlayers.

Table 5.1: Table of void content for 8-ply IM7/8552 UD-woven fabric $[0^{UD}/0^{Fabric}]_{2S}$ laminates cured with various methods and NPN interlayers.

Manufacturing Method	**Void Content (vol%)**	**Standard Error (+/-)**	**Percent Change from No NPN Specimen (%)**
Hot Plate Cure No NPN	3.62	0.08	0.0%
Hot Plate Cure 4.5 gsm 23 µm PA 66	2.00	0.05	-44.7%
Hot Plate Cure 230 µm A-CNT	2.03	0.02	-43.9%
Hot Plate Cure 70 µm A-CNT	0.03	0.00	-99.3%
Hot Plate Cure 80 µm Patterned A-CNT	0.02	0.00	-99.5%
Hot Plate Extended Cure 70 µm A-CNT	0.27	0.01	-92.5%

In specimens made with woven fabric, two void prone areas are identified as depicted in Figure 5-22. The first is described as an interweave void prone areas and occurs in between tows where there are no fibers. The second is what is described as corner void prone areas. As the tows typically have an elliptical, not rectangular,

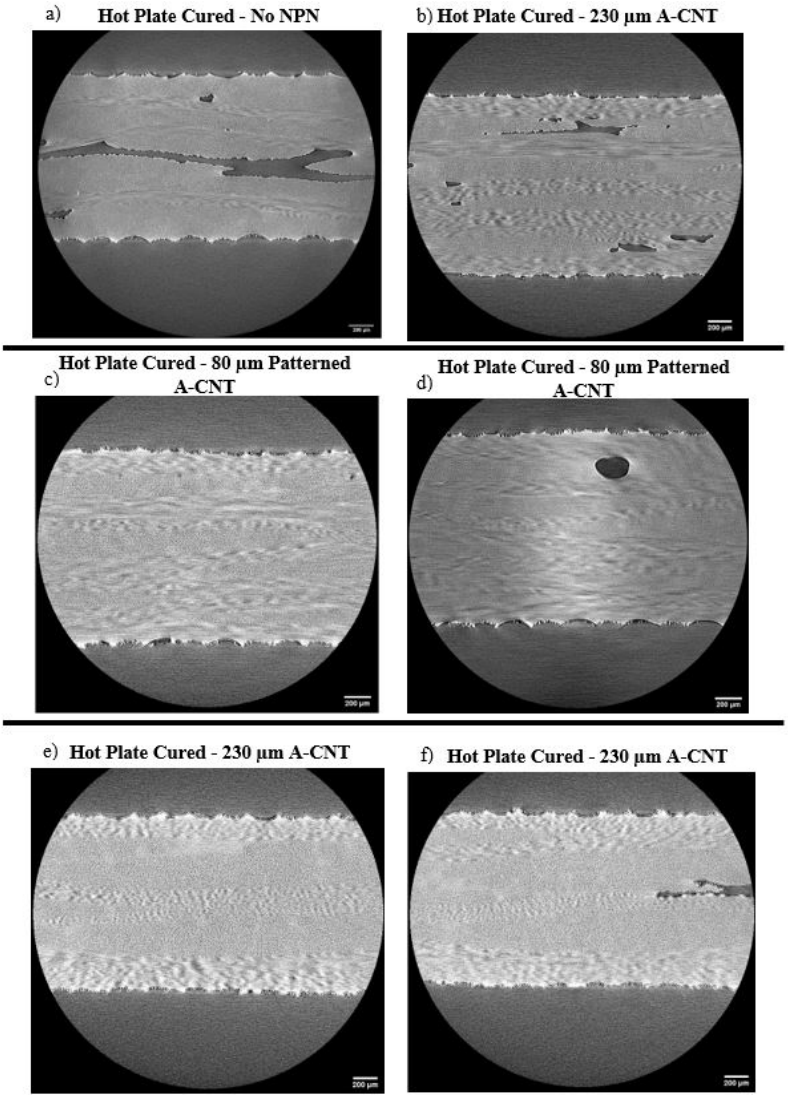

Figure 5-21: Representative µCT images of an 8-ply IM7/8552 hybrid laminates alternating between woven and unidirectional prepeg plies, $[0^{UD}/0^{Fabric}]_{2S}$, cured via hot plate with various NPNs at all ply interfaces showing: a) the baseline containing no NPN layers with a large elongated voids and an overall void content percentage of 3.62 vol%; b) 230 µm aligned CNT NPN with a void percentage of 2.03 vol%; (c-d) 80 µm patterned CNT NPN with a void percentage of 0.02 vol%; (e-f) 70 µm aligned CNT NPN with an extended cure cycle with a void percentage of 0.27 vol%. While most slices of the of the 80 µm patterned CNT and 70 µm aligned CNT NPN with an extended cure can be represented by c) and e) respectively, d) and f) show that the specimens are clearly not void-free and contains rare but large voids.

cross section, the tow perimeters have regions in the corners where there are no fibers and in these areas the corner voids occur and can follow the tow length. Illustrations on how they appear in the 2D slices of µCT are shown in Figure 5-23i, followed by representative µCT slices showing voids in both regions (Figure 5-23ii).

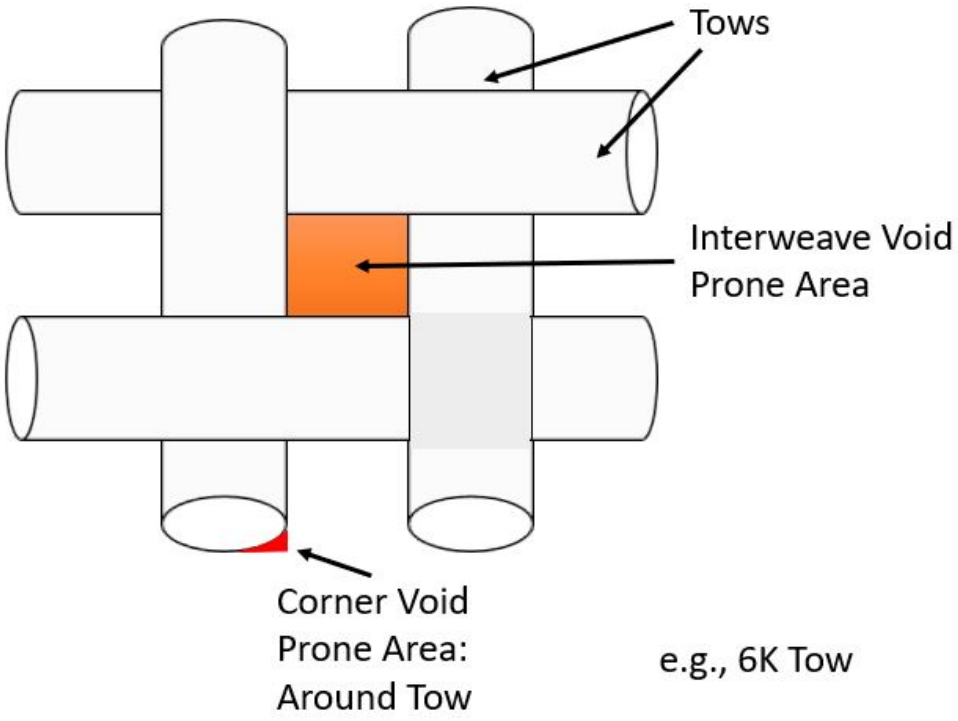

Figure 5-22: Identified void prone areas. Interweave void prone area (orange) occurs in areas where there are gaps between tows. Corner voids occur in the corner region of the elliptical tows and can generally follow a tow along its length.

Cross sectional optical microscopy was completed to investigate the voids that occurred in the woven plies. Figure 5-24 shows four images of a UD-Woven specimen with 70 µm A-CNT interlayers. The interlaminar thickness is ∼20 µm. There is some evidence of a lack of CNTs in the corner region and the interweave region which are the void heavy regions of the woven plies. Figure 5-24d shows that though the CNTs follow the interlaminar region, they fail to enter the corner region leaving a resin-rich region. This leads to the hypothesis that the voids in the woven fabric are not eliminated due to the lack of the penetration of NPN into the corner and interweave regions.

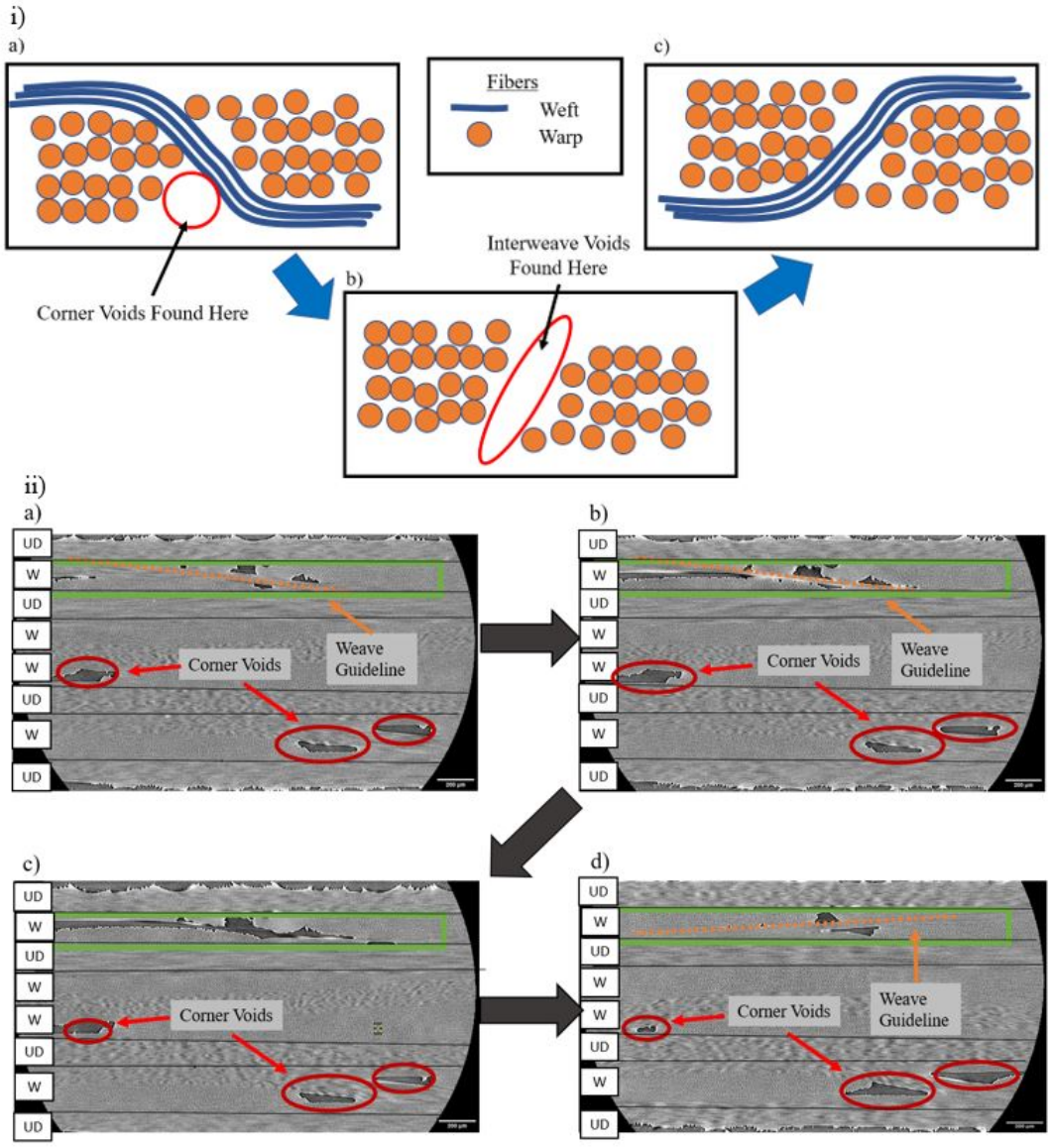

Figure 5-23: Representative images of void locations in UD-woven laminate interfaces: i) A diagram showing warp (orange) and weft (blue) fiber tows and how interweave voids appear on the slices as they progress (a to c) in a µCT scan where the weft fiber tows disappear. Due to the weave pattern the weft tows have the opposite slope when they reappear; and ii) Voids are shown in the µCT images of a UD-woven laminate with 230 µm CNT NPN interlayers. The red circles are corner voids. The interweave void progression can be seen in the green boxed woven ply. An orange guideline drawn to enable tracking of the weave slope flip (a to d).

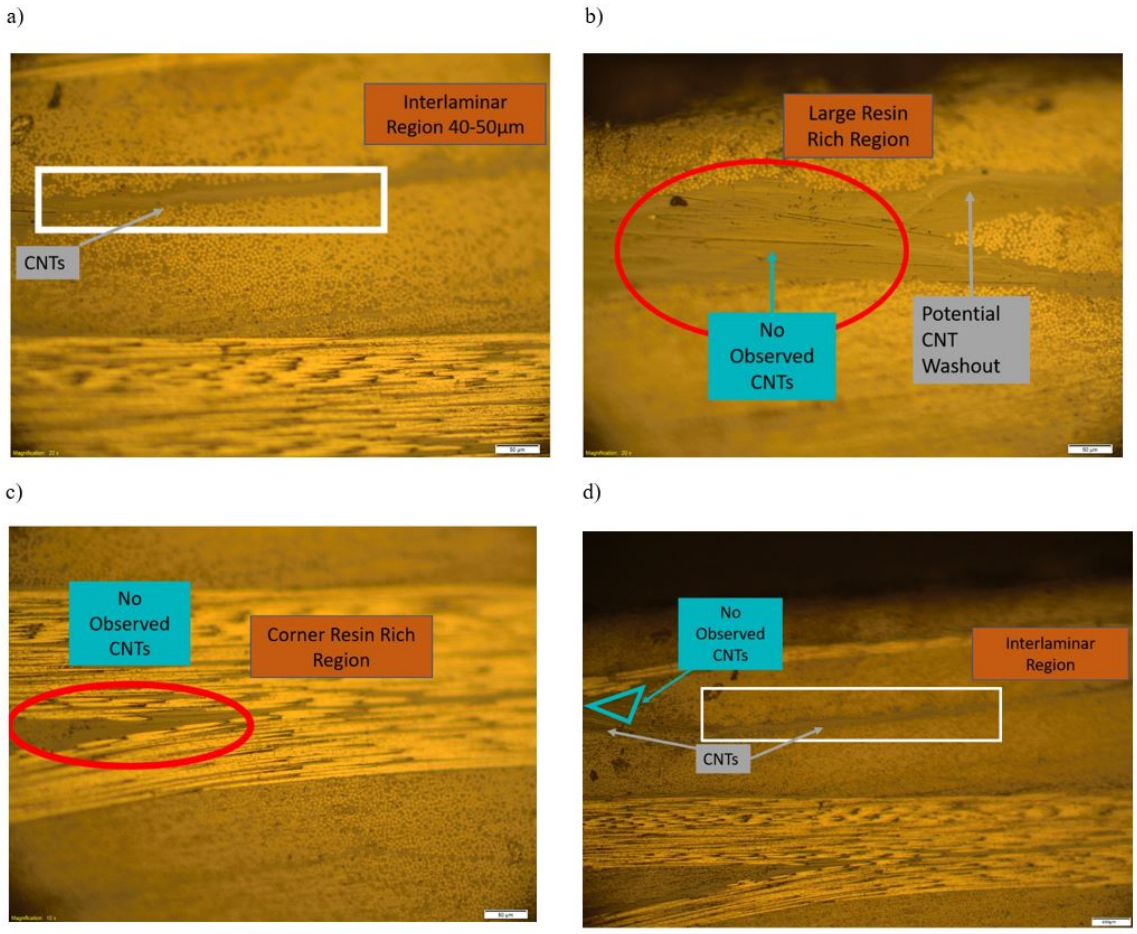

Figure 5-24: Cross sectional optical microscopy of interlaminar regions and resin-rich regions in samples of Woven-UD interfaces with 70 µm A-CNT interlayers: CNTs and interlaminar thickness of $\sim$ 20 µm, b) a large resin-rich interface where there is some evidence of no CNTs, c) corner region where there no CNTs are observed, d) CNTs in the interlaminar region follow the bottom ply and do not integrate into the corner region where there are no observed CNTs. The lack of CNTs in d) the corner region and b) the interweave resin-rich region is important as those areas are typically where voids have been found with µCT scans.

5.3.2 NPN Integration at Woven-Woven Ply Interfaces

VBO curing of $[0^{Fabric}]_{4S}$ laminates with NPNs integrated in the interlaminar region which has all Woven-Woven interfaces was investigated. Figure 5-25 and Table 5.2 show the various methods and NPN combinations. All VBO cures with applied NPN interlayers reduced void content compared to the VBO cure with no NPN interlayer which that had a void content percentage of 5.61 vol%. While void content was decreased with the integration of NPNs, voids were not fully eliminated. The laminates did not achieve aerospace-grade quality of a void percentage of under 1 vol% and voids were observed constantly throughout the µCT scans. Representative µCT images of three different specimens are shown in Figure 5-26. The voids occurred in the same regions in the woven plies as they did in the UD-woven specimens: corner regions and interweave areas. The lowest void content occurred in the specimen with 3 layers of 4.5 gsm 23 µm PA 66 placed in each interlaminar region and had a void content percentage of 1.65 vol%. A 4-ply laminate with 5 layered 4.5 gsm 23 µm PA 66 was also tested but it had a void content percentage of 4.27 vol%. Figure 5-27 shows the 8-ply laminate with 3 layers of 4.5 gsm 23 µm PA 66 and the 4-ply laminate with 5 layers of 4.5 gsm 23 µm PA 66 with the void content displayed in Figure 5-28. The increase in void content with additional NPN interlayers led to the conclusion that the continuous increase of EPN NPN material thicknesses would not lead to void removal in woven fabric plies, and NPN thickness has known detrimental effect of increasing interlaminar and laminate thickness.

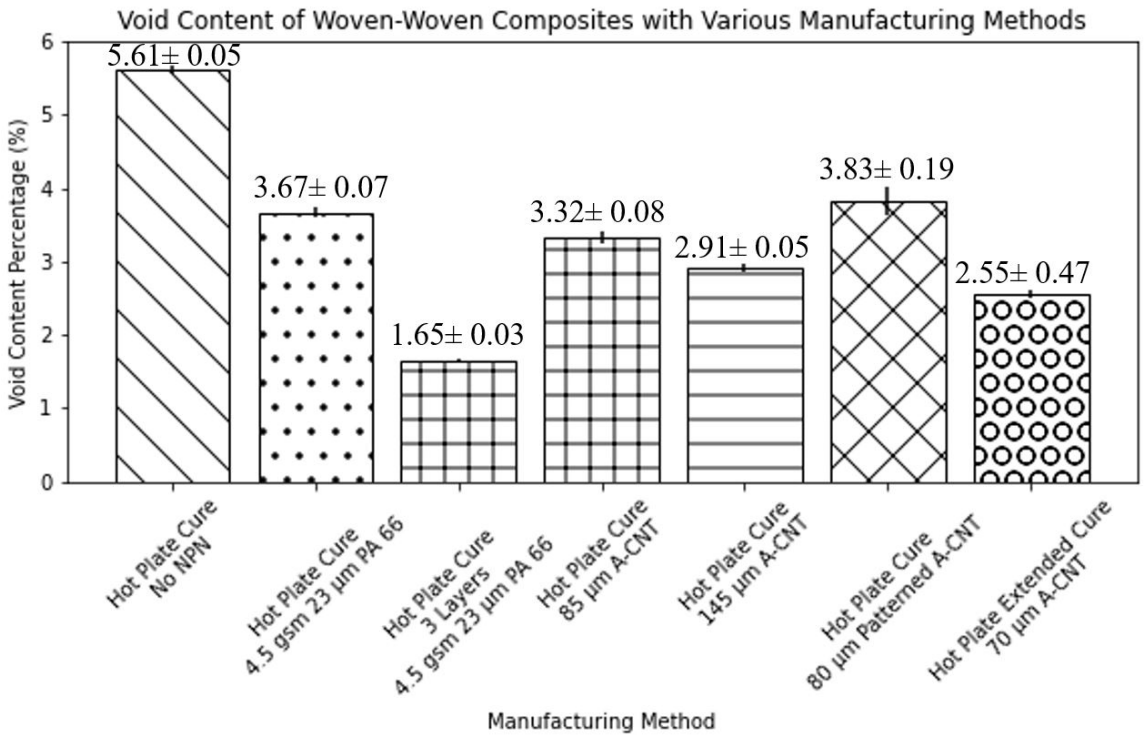

Figure 5-25: Void content of 8-ply IM7/8552 woven fabric $[0]_{4S}$ laminates cured with various methods and NPN interlayers.

Table 5.2: Void content of 8-ply IM7/8552 woven laminate fabric $[0]_{4S}$ laminates cured with various methods and NPN interlayers.

Manufacturing Method	**Void Content (vol%)**	**Standard Error (+/-)**	**Percent Change from No NPN Specimen (%)**
Hot Plate Cure No NPN	5.62	0.05	0.0%
Hot Plate Cure 4.5 gsm 23 µm PA 66	3.67	0.07	-34.7%
Hot Plate Cure 3 Layers 4.5 gsm 23 µm PA 66	1.65	0.03	-70.6%
Hot Plate Cure 85 µm A-CNT	3.32	0.08	-40.9%
Hot Plate Cure 145 µm A-CNT	2.92	0.05	-48.1%
Hot Plate Cure 80 µm Patterned A-CNT	3.83	0.19	-31.7%
Hot Plate Extended Cure 70 µm A-CNT	2.55	0.05	-54.6%

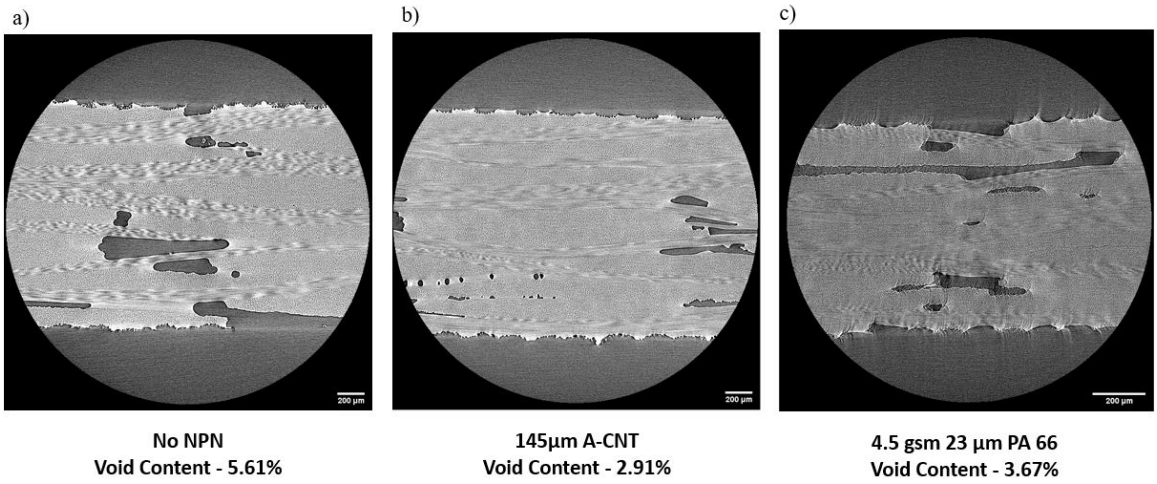

Figure 5-26: Representative µCT images of 8-ply IM7/8552 woven laminates, $[0^{Fabric}]_{4S}$, cured via hot plate with various NPNs at all ply interfaces showing: a) the baseline containing no NPN layers with a void percentage of 5.61 vol%; b) 140 µm aligned CNT NPN with a void percentage of 2.91 vol%; c) 4.5 gsm 23 µm PA 66 with a void percentage of 3.67 vol%.

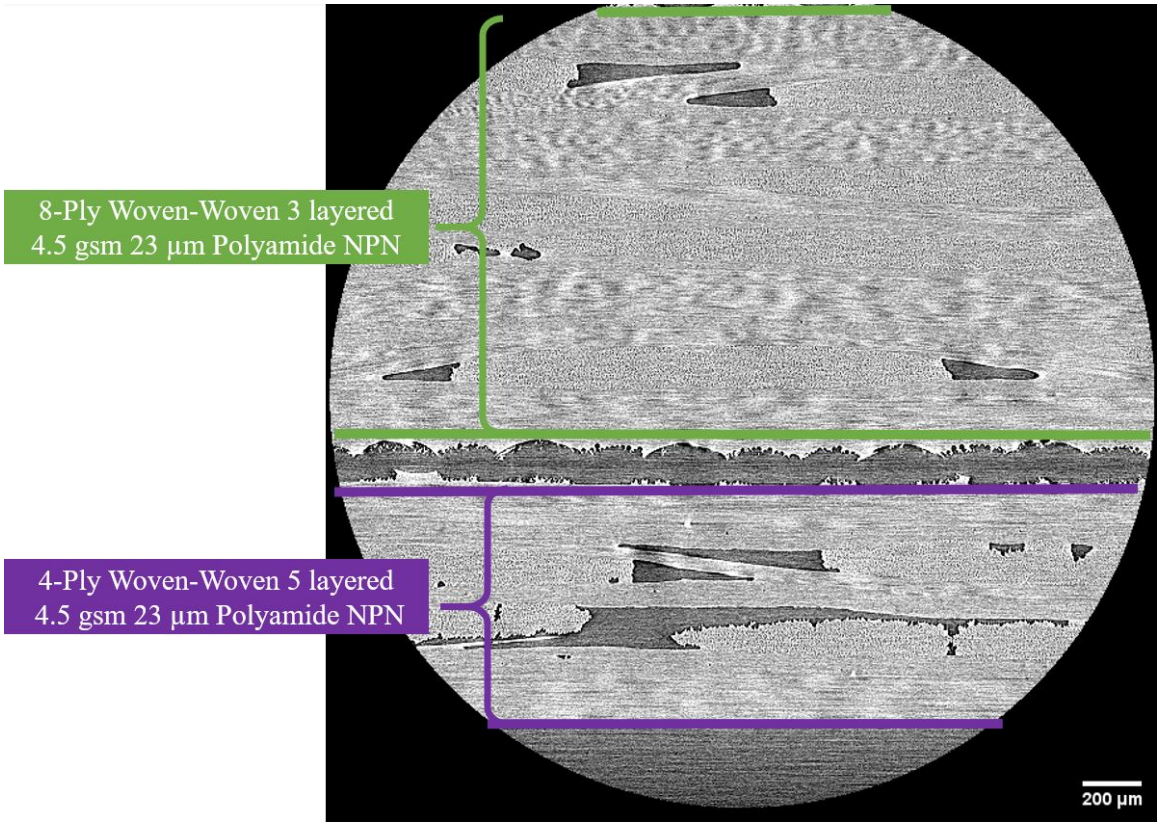

Figure 5-27: Void content of IM7/8552 woven fabric 8-ply $[0]_{4S}$ laminate (green) with 3 layers of 4.5gsm 23 µm PA 66 in each interface and 4-ply $[0]_{2S}$ laminate (purple) with 5 layers of 4.5gsm 23 µm PA 66 in each interlaminar region. The void content percentage of the 5 NPN layered 4-ply laminate is higher than the 3 NPN layered 8-ply laminate at 4.27 vol% and 1.65 vol% respectively.

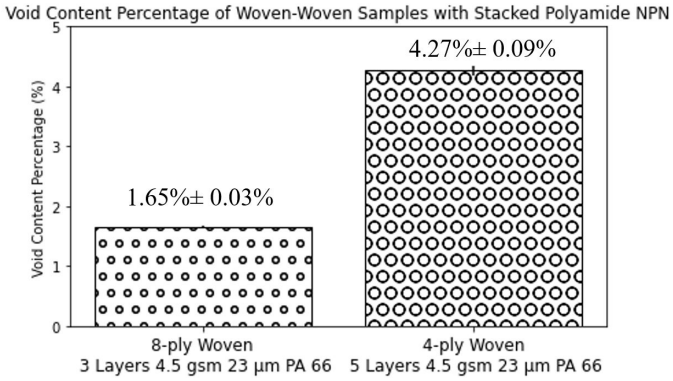

Figure 5-28: Void content percentage comparison of 8-ply $[0]_{4S}$ with 3 layers of 4.5 gsm 23 µm PA 66 in each interface and 4-ply $[0]_{2S}$ with 5 layers of 4.5 gsm 23 µm PA 66 in each interface.

5.4 Conclusions

This chapter presents preliminary investigations into expanding the next generation VBO curing with autoclave-grade prepreg materials into complex geometries and woven prepreg. Increased ply-ply slippage improved ease of manufacture of the complex shape while conveying laminate consolidation benefits. Additionally, A-CNTs and patterned A-CNT arrays were utilized as NPN materials. L-shape geometric laminates were manufactured representing complex geometries that require a curve or a bend expanding VBO + NPN cures into non-2D plate geometries. The L-shape manufacturing process additionally utilized a convection heat source (an oven) as opposed to previous conduction heat sources (hot plate, CNT heater) for VBO + NPN curing. Convection based OoA curing is common in industry and the L-shape specimens verify its compatibility with VBO + NPN cures. The electrospun 4.5 gsm 23 µm PA 66 NPN was utilized as the NPN interlayer material and when cured with a 1 mm thick rubber caul plate, voids were eliminated in both the flat and curved region of the L as observed by both µCT and microscopy. Studies with the woven fabric showed a significant void reduction but not void elimination with the NPN materials tested, though voids were reduced compared to the non-NPN specimens. In the specimens with UD-woven interfaces, voids were suppressed but never eliminated. The best results of the specimens tested had A-CNTs (patterned and non-patterned) with a height of 70-80 µm which had void percentages of under 0.3 vol%. However, upon closer inspection of the µCT scans, rare but large (>200 µm) voids still occurred. In the laminates made with only woven fabric, void content was reduced but never below the aerospace-grade level of 1 vol%, much less eliminated. Two regions were identified as void prone: interweave regions between tows, and corner regions around the perimeter of the elliptical tows. In a specimen with CNTs as the NPN material, no CNTs are observed with microscopy in the interweave and the corner regions leading to the hypothesis that the lack of NPN penetration during transfer in these regions lead to the lack of void reduction. The next generation composite cure methodology of VBO + NPNs for curing autoclave-grade prepreg was demonstrated in convection

cures and complex geometries successfully. While the integration of NPNs into the interlaminar regions of laminates with woven prepreg has been shown to reduce voids, it has not lead to complete void elimination yet and work in this area should continue in the future.

Chapter 6

Conclusions and Recommendations

This thesis investigates various nanomaterial systems (nanoporous network, or NPNs), which have nanoporous properties that when applied to the interlaminar region of a laminate made from traditional aerospace-grade autoclave prepreg, void-free composites can be achieved even when curing under vacuum-bag-only (VBO) conditions without an autoclave. The enabling mechanism acts as follows: the NPN is applied to the ply-ply interface of the laminate during layup as an interlayer creating a full laminate planar area breathable pathway for entrapped air, volatiles, and moisture to be removed via vacuum, which is only a maximum half ply distance away from any point. Then, during cure, as the resin viscosity decreases, the capillary pressure of the NPNs encourage resin infiltration of the interlaminar region, further eliminating voids. Due to the NPN's compressible nature and the vacuum pressure, the NPN-comprised interlayer is compressed and is observed to reduce in thickness. This is demonstrated with two separate commercially available polymer NPN material systems, in conductive and convective cure environments, and with the most common utilized complex geometry (i.e., L-shape), which demonstrates curved laminates to also be effectively manufactured via VBO cure. Unidirectional (UD) prepreg systems were investigated extensively and woven fabrics preliminarily. While UD prepreg showed complete void elimination in flat and L-shape geometries, woven fabrics only showed void reduction, not full elimination in flat panel geometries. A-CNTs and patterned A-CNTs were also investigated with the woven fabric prepreg.

The two alternative, commercially available NPN material systems were investigated and demonstrated void removal: electrospun polymer nanofiber (EPN) films and a polymer aerogel. Two variants of the EPN films were utilized: Polyamide (PA) 66 and PA XD10 which additionally had different fiber diameters and film thickness. Both variants of EPN films, when integrated into a UD laminates's interlaminar region, enabled void-free VBO manufactured composites. The polyimide aerogel additionally demonstrated the same void elimination properties with laminates cured in VBO conditions. Specimens with EPN films were scaled void-free to the 15 cm $\times$ 15 cm (6 in $\times$ 6 in) scale. Short beam shear (SBS) tests showed no degradation of interlaminar shear strength when the EPN NPNs were integrated. Microscopy of the interlaminar region showed increased interlaminar thickness (5-7 µm vs 1-2 µm) when even the thinnest obtained EPN NPN was integrated (1.5 gsm 8 µm PA XD10 and 20 µm polyimide (PI) aerogel). It is important to note that these material systems can be manufactured in thinner forms which would reduce the interlaminar region further.

In addition to their void reduction capabilities, the NPN materials, being applied as interlayers between two tacky resin coated plies, act as a lubricating layer increasing manufacturing ease. While noted for flat plate geometries, for curved shape geometries it takes on importance, not just for increased drapability in areas with small radii of curvature, but also for laminate consolidation as the ply-ply friction opposes the ply sliding necessary for full laminate consolidation [63]. The L-shapes manufactured with NPN in VBO conditions are not observed to have manufacturing defects such as fiber wrinkling, which are common in complex geometries. The results of this thesis show a diverse variety of scalable commercial (polymer) NPN material systems can be utilized to achieve void-free scaled composites cured VBO, even though they are autoclave-grade composites in various geometries, with no drop in interlaminar strength or thermophysical changes. The NPN can be applied to the prepreg directly pre-layup or as a layer during layup and is likely to be applied in an automated layup capable manner at industrial scale. Taken together, the demonstrated technology is an improvement over traditionally autoclave cured methods as it utilizes autoclave-

grade prepreg of which there is a diverse certified material selection, but it eliminates the capital and operational-intensive autoclave. It is an improvement over the higher material cost OoA grade prepreg material as it does not require resin chemistry modifications or prepreg morphology modifications which drives lengthy and expensive certification testing. The NPN + VBO system improves the economics of composite manufacturing and is transformative for aerospace-grade composite manufacturing.

6.1 Summary of Thesis Contributions

The thesis contributions are here summarized against the four stated thesis goals from Chapter 3:

1. Identify and demonstrate a variety of commercial (and therefore scalable) NPN material systems

Two different commercial NPN material systems were investigated: EPN films and a polymer aerogel material. SEM of the electrospun nanofiber material was taken and fiber diameter analysis completed. The nanofibers made out of PA 66 had a fiber diameter of 153 nm. The nanofibers made out of PA XD10 had a fiber diameter of 248 nm. Thickness measurement was taken by a micrometer and the 4.5 gsm PA 66 nanofiber mat had a thickness of 23 µm, while the 1.5 gsm PA XD10 nanofiber mat had a thickness of 8 µm. The thinnest PI aerogel's thickness was measured with SEM to have a thickness of 20 µm. Transfer methods for both the electrospun nanofibers and aerogel material to the laminate during layup were developed and implemented.

2. Demonstrate the removal and elimination of voids in composite laminates made up of traditional autoclave unidirectional (UD) prepreg systems using commercial NPNs cured under VBO conditions

The commercially available NPN systems (PA 66 EPN, PA XD10 EPN, and PI aerogel) showed that when integrated into the interlaminar region of UD prepreg laminates, voids were eliminated during the VBO cure cycle due to the breathability

and capillary forces. In the complex geometry, reduced ply-ply friction led to easier manufacturability and no observed fiber wrinkling. Interestingly, while there were both interlaminar and intralaminer voids in the L-shape laminate around the curve when no NPNs were used, with the 4.5 gsm 23 µm PA 66 NPN, integrated only in the interlaminar region, both inter- and intralaminer voids were eliminated. This is thought to be due to the enhanced laminate consolidation from the reduced ply-ply friction. Void-free composites were observed in µCT scans where void percentages of 0.0 vol% were observed as well as in dark field and light microscopy where no voids could be seen. Under the same conditions, and even within the same laminate, regions without the NPN had a void content percentage of typically around 1.5 vol%.

3. Confirm that there is no composite strength or quality degradation of the composite by using these NPN material systems, including evaluation of the interlaminar region to make sure there is not a large interlaminar increase which would reduce the fiber volume fraction of the composite, void content as it causes large mechanical performance shortcomings, and interlaminar shear strength as is is the most critical mechanical property to maintain for this NPN technology

Quality of the L-shape and plate geometry laminates were inspected by µCT, microscopy, and secondarily by SEM and no fiber wrinkling, delamination, or other major defect was observed. Evaluation of interlaminar shear stress was evaluated by SBS testing with samples from 15.24 cm × 15.24 cm (6 in × 6 in) laminates. A short-beam strength of 97.6 MPa was achieved for the specimen made with 1.5 gsm 8 µm PA XD10 and 104.1 MPa for specimens made with 4.5 gsm 23 µm PA 66. This compares to the autoclave baseline (with no NPN) which had a short-beam strength of 96.8 MPa [77], showing that short-beam strength was maintained. Microscopy of the interlaminar region was completed and there was an increase in thickness. The thinnest aerogel at 20 µm and the thinnest EPN film, 1.5 gsm 8 µm PA XD10 when integrated into laminates caused a laminate interlaminar thickness of 5-7 µm, the 200 µm aerogel of ∼40 µm, and the 4.5 gsm 23 µm PA 66 of 10-15 µm. These interlaminar

region thicknesses were an increase from specimens cured VBO without NPNs which had in interlaminar thickness of 1-2 µm.

4. Expand the applicability of NPNs to woven prepreg morphologies and geometries enabling complex shapes to enhance the applicability of the NPN technology

Voids were eliminated in an L-shape geometry when cured VBO when the 4.5 gsm 23 µm PA 66 EPN was integrated into the interlaminar regions of the laminate. No manufacturing defects were present when viewed under optical microscopy or µCT, either in the curved region or the flat region of the L-shape. While voids were significantly reduced with various NPNs integrated with woven fabric morphologies, they were never eliminated and more work is needed in this area. In the hybrid laminates with unidirectional ply to woven fabric interfaces (UD-woven), void content was reduced to below 0.3 vol% with A-CNTs and patterned A-CNTs; however, rare but large (>200 µm in extent) voids were observed.

6.2 Future Work

The work in this thesis has raised follow-on questions and future studies including:

- NPN material expansion: Even within the broad material categories investigated of electrospun polymer fibers and polymer aerogels, materials with various cost, capillary forces, melting points, and toughening properties are desired.

- NPN material thickness reduction: Find an NPN that continues the void elimination properties while also eliminating the interlaminar thickness increase.

- Reduced, limited, or eliminated vacuum pressure curing: Reduce

vacuum pressure while utilizing a high capillary force NPN to eliminate voids without manufacturing damage to sandwich or other fragile structures while gaining understanding on the NPN capillary pressure needed for various vacuum pressures.

• Mechanical strength tests of L-shape or other complex geometries: Preform mechanical strength tests to confirm mechanical strength is retained especially when undergoing cyclic loading.

• Woven fabric void elimination: Continue woven fabric investigation with a pure woven laminate or hybrid (UD-woven) laminate to achieve void elimination with different NPNs.

• Scaled technology demonstration: scale the NPN + VBO curing technology to production part scale including more complex geometries with 3D curvatures such as shells.

Bibliography

[1] L. Gorbatikh, B. L. Wardle, and S. V. Lomov, "Hierarchical lightweight composite materials for structural applications," *MRS Bulletin*, vol. 41, pp. 672–677, 9 2016.

[2] "Material property charts," *Granta Design*, 2021. `https://www.grantadesign.com/education/students/charts/`, last accessed on 05/10/2021.

[3] T. Centea, L. K. Grunenfelder, and S. R. Nutt, "A review of out-of-autoclave prepregs - Material properties, process phenomena, and manufacturing considerations," *Composites Part A: Applied Science and Manufacturing*, vol. 70, pp. 132–154, 2015.

[4] C. Ridgard, "Next generation out of autoclave systems," in *Proc SAMPE 2010 conf, Society for the Advancement of Material and Process Engineering*, (Seattle, WA), 2010.

[5] L. Farhang, *Void Evolution during Processing of Out-of-Autoclave Prepreg Laminates*. PhD thesis, University of British Columbia, 10 2004.

[6] B. Esp, *Excerpt from Practical Analysis of Aircraft Composites*. Grand Oak Publishing, 1st ed., 10 2017.

[7] C. Ridgard, "Out of autoclave composite technology for aerospace, defense and space structures," in *Proc SAMPE 2009 conf, Society for the Advancement of Material and Process Engineering*, (Baltimore, MD), 2009.

[8] M. H. Hassan, A. R. Othman, and S. Kamaruddin, "A review on the manufacturing defects of complex-shaped laminate in aircraft composite structures," *International Journal of Advanced Manufacturing Technology*, vol. 91, no. 9-12, pp. 4081–4094, 2017.

[9] M. Steele, T. Corden, and A. Gibbs, "The development of out-of-autoclave composite prepreg technology for aerospace applications," in *Proc SAMPE 2001 conferance, Society for the Advancement of Material and Process Engineering*, (Long Beach, CA), 2011.

[10] J. Lee, *Nanomaterial-enabled Manufacturing for Next-generation Multifunctional Advanced Composite Prepreg Laminate Architectures*. PhD thesis, Massachusetts Institute of Technology, 2018.

[11] D. Hull and T. W. Clyne, *An Introduction to Composite Materials*. Cambridge University Press, 8 1996.

[12] F. Campbell Jr, *Manufacturing Technology for Aerospace Structural Materials - 1st Edition*. Elsevier Science, 1st ed., 8 2006.

[13] "Composite curing autoclaves," *ASC Process Systems*, 2021. `http://www.aschome.com/index.php/en/products/autoclaves/autoclave-types/composites`, last accessed on 05/10/2021.

[14] D. Abliz, Y. Duan, L. Steuernagel, L. Xie, D. Li, and G. Ziegmann, "Curing methods for advanced polymer composites -A review," *Polymers and Polymer Composites*, vol. 21, pp. 341–348, 7 2013.

[15] B. Mas, J. P. Fernández-Blázquez, J. Duval, H. Bunyan, and J. J. Vilatela, "Thermoset curing through Joule heating of nanocarbons for composite manufacture, repair and soldering," *Carbon*, vol. 63, pp. 523–529, 11 2013.

[16] C. Joseph and C. Viney, "Electrical resistance curing of carbon-fibre/epoxy composites," *Composites Science and Technology*, vol. 60, pp. 315–319, 2000.

[17] R. A. Witik, F. Gaille, R. Teuscher, H. Ringwald, V. Michaud, and J. A. E. Månson, "Economic and environmental assessment of alternative production methods for composite aircraft components," *Journal of Cleaner Production*, vol. 29-30, pp. 91–102, 7 2012.

[18] L. K. Grunenfelder, T. Centea, P. Hubert, and S. R. Nutt, "Effect of room-temperature out-time on tow impregnation in an out-of-autoclave prepreg," *Composites Part A: Applied Science and Manufacturing*, vol. 45, pp. 119–126, 2 2013.

[19] G. Bond and J. Luner, "Design of experiments evaluation of processing parameters for non-autoclave composite Prepreg," in *SAMPE 2009 conf, Society for the Advancement of Material and Process Engineering*, (Baltimore, MD), 2009.

[20] T. Centea and P. Hubert, "Measuring the impregnation of an out-of-autoclave prepreg by micro-CT," *Composites Science and Technology*, vol. 71, pp. 593–599, 3 2011.

[21] H. Alshahrani and M. Hojjati, "A new test method for the characterization of the bending behavior of textile prepregs," *Composites Part A: Applied Science and Manufacturing*, vol. 97, pp. 128–140, 6 2017.

[22] J. Kratz, K. Hsiao, G. Fernlund, and P. Hubert, "Thermal models for MTM45-1 and Cycom 5320 out-of-autoclave prepreg resins," *Journal of Composite Materials*, vol. 47, pp. 341–352, 2 2013.

[23] D. Kim, T. Centea, and S. R. Nutt, "Out-time effects on cure kinetics and viscosity for an out-of-autoclave (OOA) prepreg: Modelling and monitoring," *Composites Science and Technology*, vol. 100, pp. 63–69, 8 2014.

[24] J. Boyd and R. Maskell, "Product design for low cost manufacturing of composites for aerospace applications," in *Proc SAMPE 2001 conf, Society for the Advancement of Material and Process Engineering*, (Long Beach, CA), 2001.

[25] A. R. A. Arafath, G. Fernlund, and A. Poursartip, "Gas transport in prepregs: model and permeability experiments," in *17th int conf compos mater, International Committee on Composite Materials*, (Edinburgh, Scotland), 2009.

[26] J. L. Kardos, M. P. Duduković, and R. Dave, "Void growth and resin transport during processing of thermosetting — Matrix composites," in *Epoxy Resins and Composites IV* (K. Dušek, ed.), (Berlin, Heidelberg), pp. 101–123, Springer Berlin Heidelberg, 1986.

[27] S. Lucas, S. Howard, and J. Senger, "Vacuum bag only processing: improving prepreg out-time and porosity for large composite structure," in *Proc SAMPE 2010 conf, Society for the Advancement of Material and Process Engineering,*, (Seattle, WA), 2010.

[28] K. Sutter, W. Kenner, L. Pelham, S. Miller, D. Polis, and T. Hou, "Comparison of autoclave and out-of-autoclave composites," in *Proc 42nd int SAMPE tech conf, Society for the Advancement of Material and Process Engineering*, (Salt Lake City, UT), 2010.

[29] M. Mehdikhani, L. Gorbatikh, I. Verpoest, and S. V. Lomov, "Voids in fiber-reinforced polymer composites: A review on their formation, characteristics, and effects on mechanical performance," *Journal of Composite Materials*, vol. 53, pp. 1579–1669, 5 2019.

[30] Y. Huang, J. Varna, and R. Talreja, "Statistical methodology for assessing manufacturing quality related to transverse cracking in cross ply laminates," *Composites Science and Technology*, vol. 95, pp. 100–106, 5 2014.

[31] H. Huang and R. Talreja, "Effects of void geometry on elastic properties of unidirectional fiber reinforced composites," *Composites Science and Technology*, vol. 65, pp. 1964–1981, 10 2005.

[32] H. Jeong, "Effects of voids on the mechanical strength and ultrasonic attenuation of laminated composites," *Journal of Composite Materials*, vol. 31, no. 3, pp. 276–292, 1997.

[33] A. E. Scott, I. Sinclair, S. M. Spearing, M. N. Mavrogordato, and W. Hepples, "Influence of voids on damage mechanisms in carbon/epoxy composites determined via high resolution computed tomography," *Composites Science and Technology*, vol. 90, pp. 147–153, 1 2014.

[34] J. M. Tang, W. I. Lee, and G. S. Springer, "Effects of cure pressure on resin flow, voids, and mechanical properties," *Journal of Composite Materials*, vol. 21, pp. 421–440, 7 1987.

[35] J. L. Kardos, M. P. Duduković, and R. Dave, "Void growth and resin transport during processing of thermosetting — matrix composites," *Advances in Polymer Science*, vol. 80, pp. 101–123, 1986.

[36] S. R. White and Y. K. Kim, "Staged curing of composite materials," *Composites Part A: Applied Science and Manufacturing*, vol. 27, pp. 219–227, 1 1996.

[37] S. Shim, J. Serferis, and W. Hudson, "Process induced void formation in a high performance structural composite system manufactured by autoclave lay-up processing," *Journal of Advanced Materials*, vol. 28, pp. 26–36, 7 1997.

[38] F. Y. Boey and S. W. Lye, "Void reduction in autoclave processing of thermoset composites. part 1: high pressure effects on void reduction," *Composites*, vol. 23, pp. 261–265, 7 1992.

[39] J. Lee, S. S. Kessler, and B. L. Wardle, "Void-free layered polymeric architectures via capillary-action of nanoporous films," *Advanced Materials Interfaces*, vol. 7, p. 1901427, 2 2020.

[40] S. Jiang, Y. Chen, G. Duan, C. Mei, A. Greiner, and S. Agarwal, "Electrospun nanofiber reinforced composites: A review," *Polymer Chemistry*, vol. 9, pp. 2685–2720, 5 2018.

[41] S. Ramakrishna, K. Fujihara, W. E. Teo, T. C. Lim, and Z. Ma, *An introduction to electrospinning and nanofibers*. World Scientific Publishing Co., 1 2005.

[42] A. L. Yarin, S. Koombhongse, and D. H. Reneker, "Taylor cone and jetting from liquid droplets in electrospinning of nanofibers," *Journal of Applied Physics*, vol. 90, pp. 4836–4846, 11 2001.

[43] R. Palazzetti and A. Zucchelli, "Electrospun nanofibers as reinforcement for composite laminates materials – A review," *Composite Structures*, vol. 182, pp. 711–727, 12 2017.

[44] V. Vijay Kumar, S. Ramakrishna, J. L. Kong Yoong, R. Esmaeely Neisiany, S. Surendran, and G. Balaganesan, "Electrospun nanofiber interleaving in fiber reinforced composites—recent trends," *Material Design & Processing Communications*, vol. 1, p. e24, 2 2019.

[45] J. Xue, T. Wu, Y. Dai, and Y. Xia, "Electrospinning and electrospun nanofibers: Methods, materials, and applications," *Chemical Reviews*, vol. 119, pp. 5298–5415, 4 2019.

[46] R. Palazzetti, A. Zucchelli, and I. Trendafilova, "The self-reinforcing effect of Nylon 6,6 nano-fibres on CFRP laminates subjected to low velocity impact," *Composite Structures*, vol. 106, pp. 661–671, 12 2013.

[47] G. W. Beckermann and K. L. Pickering, "Mode I and Mode II interlaminar fracture toughness of composite laminates interleaved with electrospun nanofibre veils," *Composites Part A: Applied Science and Manufacturing*, vol. 72, pp. 11–21, 5 2015.

[48] L. Daelemans, S. Van Der Heijden, I. De Baere, H. Rahier, W. Van Paepegem, and K. De Clerck, "Damage-resistant composites using electrospun nanofibers: A multiscale analysis of the toughening mechanisms," *ACS Applied Materials and Interfaces*, vol. 8, pp. 11806–11818, 5 2016.

[49] S. Karimi, M. P. Staiger, N. Buunk, A. Fessard, and N. Tucker, "Uniaxially aligned electrospun fibers for advanced nanocomposites based on a model PVOH-epoxy system," *Composites Part A: Applied Science and Manufacturing*, vol. 81, pp. 214–221, 2 2016.

[50] T. M. Brugo, G. Minak, A. Zucchelli, H. Saghafi, and M. Fotouhi, "An investigation on the fatigue based delamination of woven carbon-epoxy composite laminates reinforced with polyamide nanofibers," in *Procedia Engineering*, vol. 109, pp. 65–72, Elsevier Ltd, 1 2015.

[51] S. Salimian, A. Zadhoush, M. Naeimirad, R. Kotek, and S. Ramakrishna, "A review on aerogel: 3D nanoporous structured fillers in polymer-based nanocomposites," *Polymer Composites*, vol. 39, pp. 3383–3408, 10 2018.

[52] S. Thomas, G. Zaikov, and S. Valsaraj, *Recent Advances in Polymer Nanocomposites - 1st Edition - Sabu Thomas*. CRC Press, 1st ed., 3 2009.

[53] M. K. Williams', T. M. Smith', L. B. Roberson', F. Yang, . Gordon, and L. Nelson', "Flame retardant effects of aerogel and nanosilica on engineered polymers," 2010.

[54] A. A. Obaid, S. Anderson, J. W. Gillespie Jr, T. K. Vaidyanathan, and L. Studley, "Investigation of thermal and acoustic performance of aerogel-based glass fiber composites ," in *Annual Meeting of the Society of Advanced Manufacturing and Process Engineering*, (Long Beach, CA), 5 2005.

[55] T. H. Hsieh and Y. S. Huang, "The mechanical properties and delamination of carbon fiber-reinforced polymer laminates modified with carbon aerogel," *Journal of Materials Science*, vol. 52, pp. 3520–3534, 3 2017.

[56] R. K. Pandey and C. T. Sun, "Mechanisms of wrinkle formation during the processing of composite laminates," *Composites Science and Technology*, vol. 59, pp. 405–417, 2 1999.

[57] A. C. Loos and G. S. Springer, "Curing of Epoxy Matrix Composites," *Journal of Composite Materials*, vol. 17, pp. 135–169, 7 1983.

[58] Z. Sápi, R. Butler, and A. Rhead, "Filler materials in composite out-of-plane joints – a review," *Composite Structures*, vol. 207, pp. 787–800, 1 2019.

[59] P. Hubert and A. Poursartip, "Aspects of the compaction of composite angle laminates: An experimental investigation," *Journal of Composite Materials*, vol. 35, pp. 2–26, 1 2001.

[60] C. B. Xin, Y. Z. Gu, M. Li, J. Luo, Y. X. Li, and Z. G. Zhang, "Experimental and numerical study on the effect of rubber mold configuration on the compaction of composite angle laminates during autoclave processing," *Composites Part A: Applied Science and Manufacturing*, vol. 42, pp. 1353–1360, 10 2011.

[61] X. Wang, F. Xie, M. Li, and Z. Zhang, "Influence of tool assembly schemes and integral molding technologies on compaction of T-stiffened skins in autoclave process," *Journal of Reinforced Plastics and Composites*, vol. 29, pp. 1311–1322, 5 2010.

[62] M. Brillant, *Out-of-Autoclave Manufacturing of Complex Shape Composite Laminates*. PhD thesis, McGill University, 2010.

[63] A. Levy, J. Stadlin, and P. Hubert, "Corner consolidation in vacuum bag only processing of out-of-autoclave composite prepregs laminates," in *International SAMPE Technical Conference, Society for the Advancement of Material and Process Engineering*, (Seattle, WA), 2014.

[64] M. I. Naji and S. V. Hoa, "Curing of thick angle-bend thermoset composite part: curing cycle effect on thickness variation and fiber volume fraction," *Journal of Reinforced Plastics and Composites*, vol. 18, pp. 702–723, 8 1999.

[65] P. Hubert, *Aspects of flow and compaction of laminated composite shapes during cure*. PhD thesis, University of British Columbia, 8 1996.

[66] G. L. Hahn, "Accelerated insertion of materials – composites (aim-c) methodology," Tech. Rep. 2004P0020, Defense Technical Information Center, 2004.

[67] N. Matsumoto, N. Saegusa, J. Mitadera, A. Ohtani, and A. Nakai, "Method of producing complex shaped composites with xylylenediamine derived polyamide matrix," in *2018 SPE ACCE, Society of Plastics Engineers Automotive Composites Conference 'I&' Exhibition*, (Bethel, CT), 2018.

[68] M. Kurokawa, S. Hirose, and N. Matsumoto, "Polyamide resin," 7 2011. International patent application number: PCT/JP2011/066549.

[69] S. Mazumdar, *Composites Manufacturing: Materials, Product, and Process Engineering*. CRC Press, 1st ed., 2001.

[70] B. Lacovara, "Why out of autoclave processing is good for the composites industry," *Composites World*, 2013. `https://www.compositesworld.com/columns/why-out-of-autoclave-processing-is-good-for-the-composites-industry`, last accessed on 05/10/2021.

[71] L. Liu, B. M. Zhang, D. F. Wang, and Z. J. Wu, "Effects of cure cycles on void content and mechanical properties of composite laminates," *Composite Structures*, vol. 73, pp. 303–309, 6 2006.

[72] J. Lee, I. Y. Stein, S. S. Kessler, and B. L. Wardle, "Aligned carbon nanotube film enables thermally induced state transformations in layered polymeric materials," *ACS Applied Materials and Interfaces*, vol. 7, pp. 8900–8905, 4 2015.

[73] "Hexply ® 8552 epoxy matrix (180°c/356°f curing matrix) product data sheet," tech. rep., Hexcel, 2020. `https://www.hexcel.com/user_area/content_media/raw/HexPly_8552_eu_DataSheet.pdf`, last accessed on 05/10/2021.

[74] N. A. Hotaling, K. Bharti, H. Kriel, and C. G. Simon, "DiameterJ: A validated open source nanofiber diameter measurement tool," *Biomaterials*, vol. 61, pp. 327–338, 8 2015.

[75] J. Carruthers, "The short beam shear test for composite materials," 9 2019. `https://coventivecomposites.com/explainers/the-short-beam-shear-test-for-composite-materials`, last accessed on 05/10/2021.

[76] "Technical data sheet xantu.layr continuous nanofibre for composite toughening." Received from GP Marketing Consultants EU, 2020.

[77] J. Lee, L. H. Acauan, E. Kalfon-Cohen, S. S. Kessler, and B. L. Wardle, "Hierarchical nano-and micro-engineered interlaminar reinforcement of advanced aerospace grade composites with carbon nanotube arrays," in *AIAA Scitech 2021 Forum*, American Institute of Aeronautics and Astronautics Inc, AIAA, 2021.

[78] D. Lewis and B. L. Wardle, "Interlaminar shear strength investigation of aligned carbon nanotube-reinforced prepreg composite interfaces," in *56th AIAA/ASCE/AHS/ASC Structures, Structural Dynamics, and Materials (SDM) Conference 56th AIAA/ASCE/AHS/ASC Structures: American Institute of Aeronautics and Astronautics*, (Kissimmee, FL), 2015.

[79] P. Boisse, ed., *Advances in Composites Manufacturing and Process Design*. Woodhead Publishing, 1st ed., 2015.

[80] S. C. Amico and C. Lekakou, "Axial impregnation of a fiber bundle. Part 2: Theoretical analysis," *Polymer Composites*, vol. 23, pp. 264–273, 4 2002.

[81] S. Black, "Research on ooa processing continues," *CompositesWorld*, 2 2016. `https://www.compositesworld.com/articles/research-on-ooa-processing-continues`, last accessed on 05/10/2021.

[82] W. D. Callister Jr. and D. G. Rethwisch, *Materials Science and Engineering: An Introduction*. John Wiley & Sons, 6th ed., 2002.

[83] "Multipurpose 6061 aluminum 90 degree angle, with round edge, .5" thickness, 5" outside height," tech. rep., McMaster-Carr. https://www.mcmaster.com/8982K78/, last accessed on 05/10/2021.

[84] E. J. Garcia, B. L. Wardle, and A. John Hart, "Joining prepreg composite interfaces with aligned carbon nanotubes," *Composites Part A: Applied Science and Manufacturing*, vol. 39, pp. 1065–1070, 6 2008.

[85] M. R. Maschmann, G. J. Ehlert, S. Tawfick, A. J. Hart, and J. W. Baur, "Continuum analysis of carbon nanotube array buckling enabled by anisotropic elastic measurements and modeling," *Carbon*, vol. 66, pp. 377–386, 1 2014.

[86] S. B. Hutchens, L. J. Hall, and J. R. Greer, "In situ mechanical testing reveals periodic buckle nucleation and propagation in carbon nanotube bundles," *Advanced Functional Materials*, vol. 20, pp. 2338–2346, 7 2010.

[87] X. Ni, *Nanoengineered hierarchical advanced composites with nanofiber interlaminar reinforcement for enhanced laminate-level mechanical performance*. PhD thesis, Massachusetts Institute of Technology, 2 2020.

[88] D. Lewis, "Interlaminar reinforcement of carbon fiber composites from unidirectional prepreg utilizing aligned carbon nanotubes," Master's thesis, Massachusetts Institute of Technology, 2 2016.

[89] E. Kalfon-Cohen, R. Kopp, C. Furtado, X. Ni, A. Arteiro, G. Borstnar, M. N. Mavrogordato, I. Sinclair, S. M. Spearing, P. P. Camanho, and B. L. Wardle, "Synergetic effects of thin plies and aligned carbon nanotube interlaminar reinforcement in composite laminates," *Composites Science and Technology*, vol. 166, pp. 160–168, 9 2018.

[90] F. Campbell, "Curing: It's a Matter of Time (t), Temperature (T) and Pressure (P)," in *Manufacturing Processes for Advanced Composites*, pp. 175–221, Elsevier, 1 2004.

[91] P. Hubert, T. Centea, L. Grunefelder, S. Nutt, J. Kratz, and A. Levy, "Out-of-autoclave prepreg processing," in *Comprehensive Composite Materials II*, pp. 63–94, Elsevier, 1 2017.

[92] Y. Ma, T. Centea, G. Nilakantan, and S. R. Nutt, "Vacuum bag only processing of complex shapes : Effect of corner angle , material properties and processing conditions," in *Proc. of the American Society for Composites - 29th Technical Conference*, (San Diego, CA), 9 2014.

[93] G. Hatton, "Tech explained: Carbon fibre prepreg," *Racecar Engineering*, 2018. https://www.racecar-engineering.com/articles/tech-explained-carbon-fibre-prepreg/, last accessed on 05/10/2021.

[94] J. K. Kim and M. L. Sham, "Impact and delamination failure of woven-fabric composites," *Composites Science and Technology*, vol. 60, pp. 745–761, 4 2000.